Technische Universität München
TUM School of Medicine and Health

Development of mRNA and deficient Sendai Virus vector vaccine against Human Norovirus

Yazdan Samieipour

Vollständiger Abdruck der von der TUM School of Medicine and Health der Technischen Universität München zur Erlangung eines

Doctor of Philosophy (Ph.D.)

genehmigten Dissertation.

Vorsitz: Prof. Dr. Alessandra Moretti

Betreuerin: Prof. Dr. Ulrike Protzer

Prüfende der Dissertation:

1. Priv.-Doz. Dr. Jennifer Altomonte
2. Prof. Dr. Markus Gerhard

Die Dissertation wurde am 26.03.2024 bei der TUM School of Medicine and Health der Technischen Universität München eingereicht und durch die TUM School of Medicine and Health am 04.06.2024 angenommen.

Summary

Human Norovirus (HuNoV), accounting for 18% of global gastroenteritis and 58% of foodborne outbreaks, cause 19 to 21 million annual infections in the US, with notable fatalities and hospitalizations, especially among the elderly. Despite challenges like genetic diversity, vaccination against HuNoV s is deemed economically viable, potentially saving up to $2.1 billion over 48 months in the US. Transmission through contaminated food, water, and person-to-person contact complicates containment efforts. Infections appear with explosive outbreaks and diverse clinical manifestations, proving severe in infants, children, and the elderly. The unclear pathophysiology of HuNoV -induced diarrhoea and vomiting adds complexity. HuNoV immunity is often short-lived, with protection waning within a couple of years. This transient immunity makes people more susceptible to recurring HuNoV infections. The development of an effective HuNoV vaccine is challenging due to 1) the lack of suitable in vivo and in vitro infection models. 2) susceptibly of all age groups to multiple infections, 3) diverse strains of circulating HuNoV s 4) short time and limited cross-reactive protection immunity between different genogroups. The major (VP1) capsid protein can self-assemble into virus-like particles (VLPs), making it the most important candidate protein in vaccine development against HuNoV . VLP-based vaccines have various drawbacks, including a variable/low protein yield necessitating additional purification processes. Overall, overcoming these technological limitations makes the development of VLP-based vaccines difficult and poses a high economic burden

In the first part of the thesis, we focus on development of a replication deficient Sendai Virus (SeV) vector vaccine against HuNoV. The SeV vector is an attractive candidate due to its non-pathogenic nature in humans, wide replication in mammalian cells, and intranasal administration capability. This study explores the use of a replication-deficient SeV vector platform to develop a vaccine against HuNoV. The SeV vector was successfully engineered to express the HuNoV GII.4 VP1 capsid protein. In vitro, the vector expressed the target protein efficiently, and viral particles were purified, characterized, and validated. In vivo, intranasal and intramuscular administrations of the vector induced robust CD8 T-cell responses against HuNoV VP1. Heterologous prime-boost regimens with SeV and MVA viral vectors demonstrated enhanced CD8 responses. The vaccine also elicited significant IgG and IgA antibody responses, with intramuscular administration showing higher IgG levels. Mucosal immune responses were observed in lung homogenates following intranasal administration. The replication-deficient SeV vector induced a strong immunogenicity against HuNoV, offering promise for the development of effective vaccines. This study enhances our understanding of the immune responses elicited by this vaccine candidate and its potential as a valuable tool in HuNoV vaccine development.

In the second part of the thesis, we focus on the development of a mRNA vaccine encapsulated with Lipid Nanoparticles (LNP) against HuNoV. Over the past decade, technological advancements have made mRNA a viable tool in protein replacement and vaccine development. mRNA vaccines offer advantages like rapid production, inducing diverse immune responses, and avoiding DNA integration. Challenges include the need for optimization and proper delivery system. LNPs provide an efficient platform for delivery. Immunization with LNPs encapsulating unmodified and modified mRNA resulted in a robust T cell response, showing significant increases in virus-specific CD4+ and CD8+ T cells compared to control groups. mRNA encapsulated in LNPs, especially the modified version, induced higher levels of CD8+-IFNg+ and CD8+-IL2+ cells, suggesting the development of a virus specific CD8+ T cell memory. CD4+ T cell responses were significantly higher in both LNP-mRNA groups compared to the naked mRNA group. LNPs consistently outperformed naked mRNA and PBS in T cell response induction. Evaluation of IgG antibody responses revealed substantially higher titers in both LNP-mRNA groups compared to naked mRNA, emphasizing LNPs' effectiveness in enhancing humoral immune responses. The modified LNP-mRNA group exhibited the highest IgG Ab titer, suggesting mRNA modification further enhances the humoral immune response. Overall, the results highlight mRNA as an interesting vaccine candidate and LNPs as potent mRNA delivery tools, promoting both T cell and antibody responses effectively.

In conclusion, the comprehensive exploration of vaccine development against HuNoV in this thesis demonstrates significant progress in two distinct approaches. The replication-deficient SeV vector exhibits robust immunogenicity, eliciting strong CD8 T-cell and antibody responses, showcasing its potential as an effective vaccine candidate. Simultaneously, the mRNA vaccine encapsulated with LNPs proves highly promising, inducing enhanced T cell responses and substantial increases in IgG antibody titers. These advancements underscore the multifaceted strategies in the quest for a successful HuNoV vaccine, bringing us closer to comprehensive preventive measures against this important pathogen.

Zusammenfassung

Noroviren sind für 18 % der weltweiten Fälle von Gastroenteritis und 58 % der lebensmittelbedingten Krankheitsfälle verantwortlich. Sie verursachen in den USA jährlich 19 bis 21 Millionen Infektionen, die vor allem bei älteren Menschen zu Todesfällen und Krankenhausaufenthalten führen. Trotz Herausforderungen wie der genetischen Vielfalt von Noroviren wird eine Impfung als wirtschaftlich rentabel angesehen und könnte innerhalb von 48 Monaten Einsparungen von bis zu 2,1 Milliarden Dollar ermöglichen. Die Übertragung durch kontaminierte Lebensmittel, Wasser und direkten Kontakt erschwert die Eindämmung der Virenverbreitung. Hierbei sind explosionsartige Krankheitsausbrüche charakteristisch und manifestieren sich in unterschiedlichen klinischen Erscheinungsformen, die bei Säuglingen, Kindern und älteren Menschen schwerwiegend sein können. Die unklare Pathophysiologie der durch das HuNoV ausgelösten Diarrhöe und Erbrechens verkompliziert die Lage zusätzlich. Die Entwicklung von Impfstoffen stößt auf Hindernisse aufgrund der Antigenvariationen, der unterschiedlichen Immunreaktionen und der Notwendigkeit eines langanhaltenden Schutzes. Die Immunität gegen das HuNoV ist oft nur von kurzer Dauer, wobei der Schutz innerhalb weniger Jahre nachlässt. Eine vorübergehende Immunität kann die Menschen anfälliger für wiederkehrende HuNoV -Infektionen machen. Die Entwicklung eines wirksamen HuNoV -Impfstoffs ist eine Herausforderung, da 1) geeignete In-vivo- und In-vitro-Infektionsmodelle fehlen. 2) alle Altersgruppen anfällig für Mehrfachinfektionen sind, 3) Diverse Stämme von Noroviren zirkulieren 4) Kurzfristige und begrenzte kreuzreaktive Schutzimmunität zwischen verschiedenen Genotypen besteht. Das Hauptkapsidprotein (VP1), das von ORF2 kodiert wird, kann sich selbständig zu virusähnlichen Partikeln (VLPs) zusammensetzen und ist damit der wichtigste Kandidat in der Impfstoffentwicklung gegen HuNoV. VLP-basierte Impfstoffe haben verschiedene Nachteile, darunter eine variable/geringe Proteinausbeute und eine lange Expressionszeit in verschiedenen Expressionssystemen, was zusätzliche Reinigungsverfahren erforderlich macht. Verunreinigungen und Kontaminanten wie Verunreinigungen durch die Wirtszellen und Baculoviren stellen bei der Aufreinigung eine Herausforderung dar und erfordern die Entwicklung wirksamer Reinigungsverfahren, ohne die Immunogenität von VLP-basierten Impfstoffen zu beeinträchtigen, da diese aufgrund ihrer Empfindlichkeit gegenüber veränderten Bedingungen während der Herstellung und der nachgeschalteten Verarbeitung eine geringere Immunogenität aufweisen. Die Überwindung dieser technologischen Einschränkungen macht die Entwicklung von VLP-basierten Impfstoffen so schwierig und verbunden mit hohen wirtschaftlichen Belastungen.

Im ersten Teil dieser Arbeit liegt der Fokus auf der Entwicklung eines Impfstoffs gegen das humane HuNoV in einem replikations-defizienten Sendai-Vektor. Der SeV -Vektor ist ein attraktiver Kandidat, da er für den Menschen nicht pathogen ist, in Säugetierzellen gut repliziert

und intranasal verabreicht werden kann. In dieser Studie wird die Verwendung einer replikations-defizienten Sendai-Virus (SeV)-Vektorplattform gegen HuNoV in vivo untersucht. Der SeV -Vektor wurde erfolgreich zur Expression des HuNoV GII.4 VP1-Kapsidproteins entwickelt. In vitro exprimierte der Vektor das Zielprotein effizient und die viralen Partikel konnten gereinigt, charakterisiert und validiert werden. In vivo löste die intranasale und intramuskuläre Verabreichung des Vektors robuste CD8-T-Zell-Reaktionen gegen HuNoV VP1 aus. Heterologe Prime-Boost-Schemata mit SeV - und MVA-Virusvektoren zeigten verstärkte CD8-Reaktionen. Der Impfstoff löste auch signifikante IgG- und IgA-Antikörperreaktionen aus, wobei die intramuskuläre Verabreichung höhere IgG-Werte ergab. Nach intranasaler Verabreichung wurden in Lungenhomogenaten Immunreaktionen in der Mukosa beobachtet. Die replikations-defiziente SeV -Vektorplattform weist eine starke Immunogenität gegen HuNoV auf, was für die Entwicklung wirksamer Impfstoffe vielversprechend ist. Diese Studie verbessert unser Verständnis der durch diesen Impfstoffkandidaten ausgelösten Immunreaktionen und seines Potenzials als wertvolles Instrument für die Entwicklung von HuNoV -Impfstoffen.

Der zweite Teil der Arbeit konzentriert sich auf die Entwicklung eines mit Lipid-Nanopartikeln verkapselten mRNA-Impfstoffs gegen das humane HuNoV. In den letzten zehn Jahren haben technologische Fortschritte mRNA Wirkstoffe zu einem brauchbaren Werkzeug für den Ersatz von Protein basierten Applikationen und in der Entwicklung von Impfstoffen gemacht. mRNA-Impfstoffe bieten Vorteile wie die schnelle Produktion, die Auslösung verschiedener Immunreaktionen und die Vermeidung der Integration von DNA. Zu den Herausforderungen gehören die Notwendigkeit der Optimierung und ein geeignetes Verabreichungssystem. LNPs bieten eine sichere Plattform für die Verabreichung. Die Immunisierung mit LNPs, die unmodifizierte und modifizierte mRNA einkapseln, führte zu einer robusten T-Zell-Antwort, die im Vergleich zu Kontrollgruppen einen signifikanten Anstieg der virusspezifischen CD4+ und CD8+ T-Zellen zeigte. LNPs, insbesondere die modifizierte Version, induzierten höhere Mengen an CD8+-IFNg+ und CD8+-IL2+ Zellen, was auf ein verstärktes CD8+ T-Zell Gedächtnis hindeutet. Die Reaktion der CD4+ T-Zellen war in beiden LNP-mRNA-Gruppen signifikant höher als in der Gruppe mit nur mRNA. Die Werte der Gruppen mit LNPs übertrafen durchweg die derer mit nur mRNA und PBS bei der Induktion von T-Zell-Reaktionen. Die Auswertung der IgG-Antikörperreaktionen ergab wesentlich höhere Titer in beiden LNP-mRNA-Gruppen im Vergleich zur reinen mRNA, was die Wirksamkeit der LNPs bei der Verstärkung der humoralen Immunreaktionen unterstreicht. Die modifizierte LNP-mRNA-Gruppe wies die höchsten IgG-Antikörper-Titer auf, was darauf hindeutet, dass die mRNA-Modifikation die humorale Immunantwort noch weiter verstärkt. Insgesamt unterstreichen diese Ergebnisse, dass LNPs als wirksame mRNA-Transportmittel sowohl die T-Zell- als auch die Antikörperreaktion effektiv fördern.

Zusammenfassend lässt sich sagen, dass die Erforschung der Impfstoffentwicklung gegen das humane HuNoV in dieser Arbeit bedeutende Fortschritte in zwei verschiedenen Ansätzen zeigt. Der replikations-defiziente SeV -Vektor weist eine robuste Immunogenität auf, insbesondere bei der Auslösung starker CD8-T-Zell- und Antikörperreaktionen, was sein Potenzial als wirksamer Impfstoffkandidat unterstreicht. Gleichzeitig erweist sich der mit LNPs verkapselte mRNA-Impfstoff als sehr vielversprechend, da er eine verstärkte T-Zell-Antwort und einen erheblichen Anstieg der IgG-Antikörpertiter bewirkt. Diese Fortschritte unterstreichen die vielfältigen Strategien bei der Suche nach einem erfolgreichen Impfstoff gegen das humane HuNoV und bringen uns umfassenden Präventivmaßnahmen gegen diesen weit verbreiteten Krankheitserreger näher.

List of Abbreviations and terms

Abbreviation	Full Name
HuNoV	Human Norovirus
NoV	Norovirus
VLPs	Virus-like particles
SeV	Sendai Virus
mRNA	Messenger RNA
LNPs	Lipid Nanoparticles
CD8	Cluster of Differentiation 8
CD4	Cluster of Differentiation 4
IgG	Immunoglobulin G
IgA	Immunoglobulin A
MVA	Modified Vaccinia Ankara
PCR	Polymerase Chain Reaction
ASDR	Age-standardized death rate
AAPCs	Average annual percent changes
CSF	Cerebrospinal fluid
ssRNA	Single-stranded RNA
UTR	Untranslated region
IFN	Interferon
IL-10	Interleukin-10
HBGA	Histo-Blood Group Antigens
GI	Genogroup I
GII	Genogroup II
Ig	Immunoglobulin
MAb	Monoclonal Antibody

Abbreviation	Full Name
TMV	Tobacco Mosaic Virus
IVT	In Vitro Transcribed
APCs	Antigen-Presenting Cells
RE	Restriction enzyme
TEM	Transmission Electron Microscopy
ELISA	Enzyme-Linked Immunosorbent Assay
GFP	Green Fluorescent Protein
MTT	3-(4,5-dimethylthiazol-2-yl)-2,5-diphenyltetrazolium bromide
TAE	Tris-Acetate-EDTA
UV	Ultraviolet
TBE	Tris-Borate-EDTA
dsRNA	Double-stranded RNA
cDNA	Complementary DNA
FCS	Fetal Calf Serum
DMEM	Dulbecco's Modified Eagle Medium
OD	Optical Density
DSPC	1,2-distearoyl-sn-glycero-3-phosphocholine
SM-102	Heptadecan-9-yl 8-((2-hydroxyethyl) (6-oxo-6-(undecyloxy)hexyl) amino) octanoate
DMG-PEG	1,2-dimyristoyl-rac-glycero-3-methoxypolyethylene glycol-2000
ETOH	Ethanol
SDS-PAGE	Sodium dodecyl sulfate-polyacrylamide gel electrophoresis
MOPS	3-(N-Morpholino) propane sulfonic acid
FITC	Fluorescein isothiocyanate
APC	Allophycocyanin
PeCy7	Phycoerythrin Cyanine 7

Abbreviation	Full Name
FSCs	Forward Scatter Channels
HEK293T cells	Human Embryonic Kidney 293T cells
DLS	Dynamic Light Scattering
VP1	Major capsid protein
ORF	Open reading frame
MuNoV	Murine Norovirus
NS	Non-structural protein
RdRp	RNA-dependent RNA polymerase
ARCA	Anti-Reverse Cap Analog
Ψ	Pseudo-UTP
PBS	Phosphate-buffered saline
SDS-PAGE gel	Sodium dodecyl sulfate-polyacrylamide gel electrophoresis
PAA/BisAA	Polyacrylamide/Bis-acrylamide
TEMED	N,N,N′,N′-Tetramethylethylenediamine
APS	Ammonium persulfate
WB	Western blot
FVD	Fixable Viability Dye
PE Ab	Phycoerythrin Antibody
Pacific Blue Ab	Pacific Blue Antibody
FITC Ab	Fluorescein Isothiocyanate Antibody
APC Ab	Allophycocyanin Antibody
PeCy7 Ab	Phycoerythrin Cyanine 7 Antibody
TNFα	Tumor Necrosis Factor alpha
mRNA	messenger RNA
N:P ratio	ratio of positively charged amino groups to negatively charged phosphate groups

Abbreviation	Full Name
MOPS Buffer	3-(N-Morpholino) propane sulfonic acid
Tris-HCl	Tris(hydroxymethyl)aminomethane hydrochloride
PDI	Polydispersity Index
RNase I	Ribonuclease I

1 Introduction

1.1 The disease burden and impact of HuNoV

Dr. John Zahorsky, a pediatrician, first identified HuNoV -induced gastroenteritis in newborns in 1929 when he characterized "Hyperemesis hiemis or winter vomiting illness" [1]. In 1972 the faecal samples from kids at an elementary school in Norwalk, Ohio, were shown to have a tiny, non-enveloped 27-nm icosahedral virus that was linked to the illness. This early account, where 50% of the kids and staff contracted the illness over a 2-day period, made clear the Norwalk virus' capacity to spread quickly as epidemics. HuNoV s are now understood to be the root cause of 18% of all gastroenteritis cases worldwide because to the development of broadly reactive PCR-based detection tests [2]. If only outbreaks caused by foodborne illness are taken into account, this ratio rises to 58% [3]. According to estimates HuNoV s cause 19 to 21 million acute infections annually in the US, leading to up to 800 fatalities and 71,000 hospitalizations [4]. Nowadays, HuNoV s are thought to be the second most prevalent cause of gastroenteritis-related deaths in the United States, with elderly people (>65 years of age) having the highest risk of developing fatal HuNoV infections [5]. Although there are many challenges to vaccination against HuNoV es, such as high genetic diversity and rapid evolution [6], there is general agreement that the case for HuNoV vaccination is economically viable. According to estimates, depending on the effectiveness, length of protection, and cost of the vaccine, a cost savings of up to $2.1 billion over a 48-month period could be realized [7]

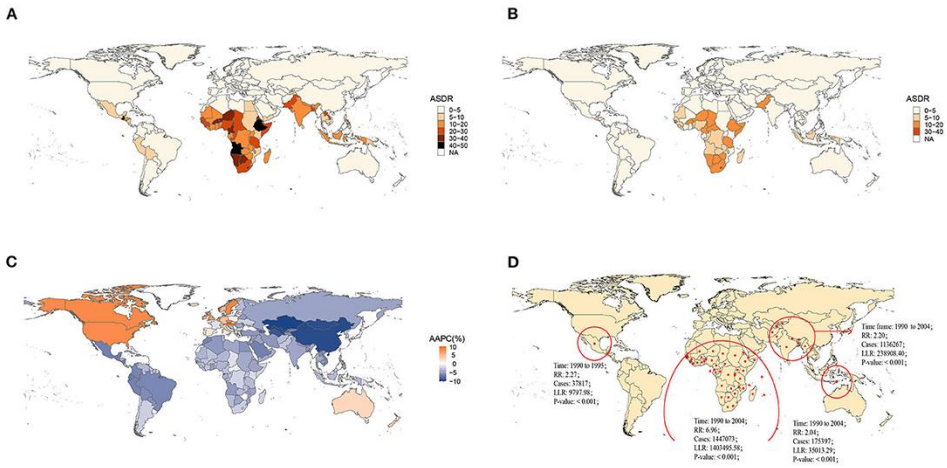

FIGURE 1. Global burden of HuNoV -associated diseases (NADs) in 1990 and 2019 with the annual percent change rate and spatial and temporal aggregation over the 30 years. (A) Age-standardized death rate (ASDR) in 1990; (B) ASDR in 2019; (C) average annual percent changes (AAPCs) from 1990 to 2019; (D) Spatial and temporal aggregation from 1990 to 2019 [8].

1.2 Pathogenesis of HuNoV infections in human

The HuNoV can spread by a variety of inoculations. First, they are quickly spread by the faecal-oral pathway when food, water, or fomites are contaminated. Foods like leafy greens and tender red fruits as well as shellfish raised in feces-contaminated harvest waters are frequently linked to HuNoV outbreaks [9]. Contamination by infected food workers is a significant point of HuNoV introduction into the food chain [10]. In addition to their resistance to standard disinfectants, HuNoV s are exceedingly stable and can remain contagious for weeks or months in the environment [11]. It can be challenging to stop the transmission of these newly named "ideal human pathogens" [12]. Second, they are easily disseminated from person to person, as evidenced by contact with an infected person, which is the main risk factor for infection [13]. Because of this, HuNoV s have a secondary attack rate that can range from 14% to 33% [14]. Third, vomitus aerosols can spread virus particles because they are contagious [15]. HuNoV infections also have extraordinarily high levels of virus shed in the stool and a protracted period of viral shedding following symptom resolution both of which contribute to the explosive nature of outbreaks [16].

HuNoV infections often progress quickly in healthy adults, with an incubation period of just 1-2 days followed by severe vomiting and diarrhea for a further 1-2 days. Together with them, malaise, stomach cramps, a low-grade fever, and nausea are all frequent symptoms. HuNoV infections in infants and young children can be more severe and persistent, lasting up to 6 weeks [17], while infections in the elderly can be quite severe and even fatal [18] Last but not least, there is proof that HuNoV s are a factor in traveler's diarrhea [19]. Uncertainty surrounds the pathophysiological underpinnings of HuNoV -induced diarrhea in humans. Nonetheless, there are histological alterations in the small intestine, including enlargement and blunting of the villi, even though the intestinal epithelium seems to stay intact during HuNoV infection [20]. With the exception of a notable increase in intraepithelial cytotoxic T lymphocytes seen in a small cohort of spontaneously infected individuals, intestinal inflammation is minimal [21]. Overall, the changes in secretory and/or absorptive mechanisms rather than structural damage to the intestinal wall may be the source of HuNoV -induced diarrhea in humans. High rates of vomiting episodes are a hallmark of HuNoV infections, but the underlying pathophysiology of this symptom is similarly unknown.

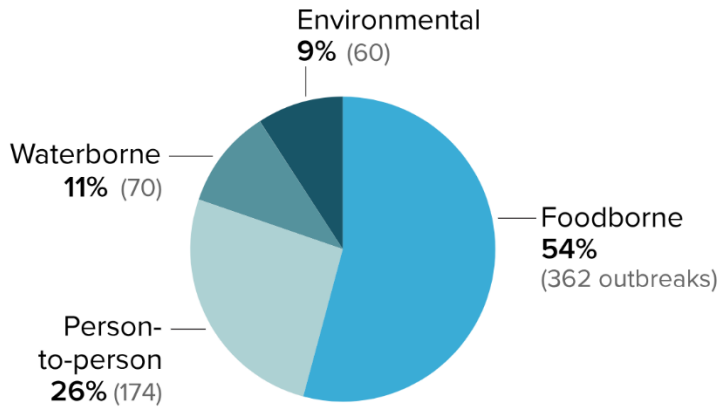

FIGURE 2. More than half of out- breaks of HuNoV over a 27-year periodwere linked to consuming food contaminated with the virus via vomit or feces. Direct contact with infected per- sons or with virus-coated environmental surfaces caused more than one third of outbreaks [22]

1.3 HuNoV tropism

The small intestine is thought to be the main location for HuNoV infection and replication, albeit this assumption is based more on clinical signs of infection than on scientific data. Although a ton of data militates against enterocyte infection, the cellular tropism of HuNoV s has not been identified. Several attempts to grow HuNoV s in epithelial cells in vitro have failed [23] and electron microscopic examination of intestinal biopsies taken from volunteers who had contracted HuNoV also produced negative results [24]. Studies have accumulated in recent years show that HuNoV s target intestinal immune cells. In vitro and in vivo, murine HuNoV s can infect macrophages, dendritic cells, and B cells [25, 26]. Lamina propria cells in a biopsy from an infected volunteer [27] lamina propria cells in human intestinal tissue sections incubated with an inactivated virus [28] intestinal dendritic cells and B cells in experimentally infected chimpanzees [29] and macrophage-like spleen and liver cells of immunodeficient mice [30] are all examples of places where HuNoV antigen has been found. Although it has not been shown that dendritic cells and macrophages may support HuNoV infection in vitro [27], it has been shown that low-level human B cell infection can occur [25] by intestinal bacteria that produce HBGAs (HBGA-expressing bacteria) [31]. During in vivo murine HuNoV infections, this activation by enteric bacteria was demonstrated by lower viral titres in mice given a cocktail of antibiotics to destroy their gut microbiota. As a result, HuNoV s are now part of a growing group of enteric viruses that have evolved to take advantage of enteric bacteria in order to increase their infectiousness [32]. Furthermore, contrary to the widely held belief that the attachment of HuNoV to HBGAs serves to enhance viral attachment to the intestinal wall, it may rather serve as a method for the viruses to bind to enteric bacteria that promote infection of receptive cells. HuNoV have been shown to spread outside the gastrointestinal tract. 15% of the patients in a healthy cohort of HuNoV -infected toddlers had viral RNA found in their

serum [33]. Additionally, two individuals who presented with encephalopathy had viral RNA found in their serum and CSF fluid [34]. Lastly, certain gnotobiotic pigs and calves that had been exposed to HuNoV showed signs of transitory viraemia [35]. HuNoV s might spread in a cell-associated way based on the known cell tropism of murine HuNoV s towards migrating macrophages and dendritic cells [26].

1.4 Molecular biology of HuNoV

Despite their importance, HuNoV s cannot be grown in immortalized cells, which has hampered our understanding of the HuNoV life cycle [36]. Notwithstanding these restrictions, substantial strides have been achieved in the previous ten years in our understanding of HuNoV biology. The Caliciviridae family of tiny positive sense RNA viruses, includes the five identified genera HuNoV , Vesivirus, Lagovirus, Sapovirus, and Nebovirus. Humans can develop gastroenteritis from members of the HuNoV and sapovirus genera, among others. Based on the sequence of the main capsid protein VP1, based on the latest update the HuNoV genus is currently divided into 10 genogroups and two non-assigned (NA) genogroups, with viruses in genogroups I, II, and IV inflicting gastroenteritis in humans. Genogroup II viruses (GII) are often more prevalent, and they have been largely responsible for recent significant epidemics. With the exception of murine HuNoV es, HuNoV s have small, 7.5 kbp-long genomes with only three open reading frames (ORFs). A virus-encoded protease (NS6) co- and post-translationally cleaves the big polyprotein produced by ORF1 to create six to Seven non-structural proteins. A subgenomic RNA created during viral replication is translated into ORFs 2 and 3 to form the major and minor capsid proteins VP1 and VP2, respectively. A protein implicated in the control of the innate immune response is encoded by a fourth ORF in murine HuNoV s [37]

1.5 HuNoV genome organization

The HuNoV genome is a small, positive-sense ssRNA molecule that varies in size within the genus from 7.3 to 7.5 kb. While the 3-prime end of the genomic RNA is polyadenylated, the 5 prime end is covalently joined to a virus-encoded protein called VPg. The untranslated regions (UTRs) at either end of HuNoV genomes are usually short; for example, the 59 and 39 UTRs of Murine Norovirus (MuNoV) are 5 and 78 nt, respectively, and the 39 UTR of HuNoV is normally 48 nt [38]. Except for MuNoV, which contains a fourth alternative ORF, the HuNoV genome is divided into three conserved ORFs. The only other member of the family Caliciviridae known to contain an analogous fourth ORF is human sapovirus [37]. All HuNoV s translate ORF1 as a large polyprotein, which the virus's encoded protease (NS6) then co- and post-translates to release at least six mature non-structural (NS) proteins, including NS6. The

other NS proteins are VPg (NS5), the suspected NTPase/RNA helicase (NS3), the viral RNA-dependent RNA polymerase (RdRp; NS7), NS1/2, and NS4 [39]. At the later phases of virus infection, cellular caspases activated by apoptosis and an unidentified cellular protease further process NS1/2. The major and minor capsid proteins, VP1 and VP2, are encoded by ORF2 and ORF3, which are translated from a subgenomic RNA, respectively. The subgenomic RNA is covalently bonded to VPg at the 59 UTR end and has a poly(A) tail at the 39 UTR end. It is identical to the final 2.4 kb of the genome [37, 40].

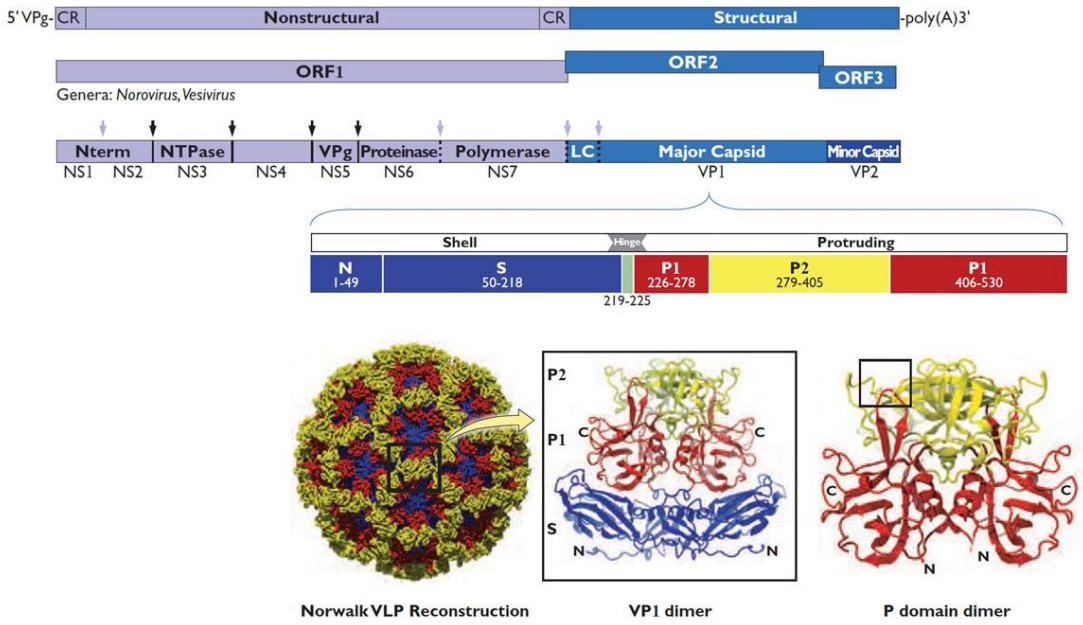

Figure 3. HuNoV genome organization and virus encoded nonstructural and structural proteins [41].

1.6 HuNoV immunology

Since HuNoV infections usually go away a few days after exposure, it is expected that innate immune responses will be crucial in regulating initial infections. In fact, experiments on animals lacking functional type I interferon signaling pathways that were infected with the murine MNoV have shown that type I interferon is essential necessary to avoid serious and even fatal infections. Furthermore, type I interferon regulates MNoV spread to peripheral organs [42, 43]. Consideration of interferon-based immunotherapy for treating norovirus infections is necessary given this need for type I interferon in suppressing MNoV infection. Exogenous type I interferon therapy inhibits the replication of the HuNoV and MNoV in this manner [44, 45], Moreover, reducing viral shedding in gnotobiotic pigs infected with a HuNoV with oral type I interferon therapy. Another top objective is to analyze the mediators responsible for interferon induction in response to norovirus infection, as well as the interferon-induced effectors that attack

noroviruses. Research in this field has shown that MDA5 can sense MNoV RNA, ISG15 exhibits antiviral activity against MNoVs, and both interferon regulatory factor 3 (IRF3) and IRF-7 contribute to the regulation of MNoV replication. IFN- may also prevent the replication of the MNoV when administered exogenously to cells [45]. Research has shown that IL-10, in addition to interferons, can reduce intestinal barrier breakdown and mucosal inflammation during MNoV infections. These findings might be connected to the discovery that intestinal bacteria promote norovirus infections. Lastly, there is evidence that the primary MNoV infections are controlled by adaptive immune responses, including B cells, antiviral antibodies, CD4+ T cells, and CD8+ T cells [46, 47].

Mucosal and serum antibody responses are brought on by noroviruses. B cells and antiviral antibodies are proven to be essential for preventing secondary norovirus infections in the animal model [46, 48]. The presence of virus-specific mucosal and serum IgA corresponds with protection against infection, further substantiating a role for protective antibody responses [16, 49] Both CD4+ and CD8+ T-cell responses are elicited by noroviruses, but only CD4+ T cells seem to be necessary for protection against re-challenges [48, 50]. Early volunteer studies showed that people do not develop immunity to a specific norovirus strain, which appears to be at odds with these findings that noroviruses might induce protective memory immunological responses [51, 52].

As norovirus genogroups differ genetically, there is conclusive evidence that protective immune responses are poor to nonexistent across norovirus genogroups [53]. A single cluster of genogroup II, genotype 4 (GII.4) norovirus strains has been responsible for the majority of recent HuNoV outbreaks, with new pandemic GII.4 strains emerging every two to three years [54, 55]. Herd immunity is supported as a driving mechanism in the evolution of HuNoV s by epidemiological data and the analysis of antibody cross-reactivity among the GII.4 pandemic strains [56]. It should be highlighted that compared to GII.4 strains, other HuNoV genotypes appear to be more genetically stable [57, 58]. In addition to the lack of cross-reactivity among protective immune responses to various norovirus strains There are noticeable differences in the robustness of protective immune responses even between closely related virus strains. At least for the dominant GII.4 norovirus strain, norovirus strains collectively are uneven in their induction of protective immune responses, and these responses are only effective during a homologous re-challenge [48]. The transitory character of immune defenses is another potential explanation for the recurring vulnerability to norovirus infections. Unlike many infections that promote lifelong immunity, noroviruses appear to cause protection to diminish quickly (within a few years). For instance, in a volunteer trial, participants were immune to a secondary challenge if they were exposed to it within 6 months of the original exposure, but protection had worn off by 2 years [52]. When mice are exposed to MNoVs again after a 6-

month period of protection, virus-specific antibody responses decline [48, 59]. Lastly, according to mathematical modeling, HuNoV immunity only lasts 4 to 9 years [60].

1.7 Challenges and achievements in HuNoV vaccine development

The development of a successful HuNoV vaccine potentially encounters various obstacles. Because circulating HuNoV s are antigenically diverse and constantly changing, a vaccination that does not elicit a broad immune response could restrict the longevity of protection. Immunizations that produce a strong immune response in adults may not be as effective in children due to differences in immune response to spontaneous HuNoV infection. Similarly, serious HuNoV disease consequences, including death, are more likely to affect the elderly and patients with immunocompromising disorders, two categories in which a patient's underlying immune function deficits may restrict the efficacy of the vaccination. Moreover, because results from epidemiologic research indicate that immunity following a natural HuNoV infection may only last for two months at most, it may be difficult to design a vaccine that offers a long enough length of protection to make immunization worthwhile [51].

Although no clinical study has evaluated the persistence of HuNoV immunity over this time, findings from more recent modeling studies using age-specific HuNoV prevalence data from the United Kingdom suggest that the probable duration of post-exposure HuNoV immunity may range from 4 to 9 years [60]. The outcome utilized to measure efficacy (e.g., the formation of a detectable infection, the development of diarrhea, or the development of clinically severe diarrhea necessitating clinical assessment) is also likely to have an impact on the length of a HuNoV vaccine's protective efficacy. HuNoV preclinical research on treatments has long been constrained by a lack of an in vitro culture system for HuNoV infection and by the lack of an accessible and applicable small animal model. The latter challenge has been overcome by recent developments. In the differentiated enterocytes of human intestinal enteroids, HuNoV s reproduce and create infectious offspring particles. Depending on the viral genotype, bile acids are either necessary for infection or facilitate it [61]. The successful inactivation of HuNoV by heat and radiation, as well as the elimination of HuNoV infectiousness by the addition of human serum containing HBGA-blocking antibodies, have both been demonstrated using this viral culture method. These initiatives are making it possible to create tests to see if antibodies produced by vaccination may reduce HuNoV infectivity in culture, which could speed up the transition of potential vaccines from preclinical to clinical testing [62, 63]

1.8 Candidate HuNoV vaccines in development

Currently, there is no licensed preventive vaccine available against HuNoV s (HuNoV). However, Several HuNoV vaccines are currently in the development stage. The following section provides descriptions of vaccines that are currently under development.

1.8.1 VLP vaccines

HuNoV VP1 proteins can self-assemble to create virus-like particles (VLPs) that are both morphologically and antigenically similar to native viruses, but lack viral genetic material [64]. Oral delivery of unadjuvanted GI was used in humans for the first time to provide a HuNoV VLP-based vaccination. There were no negative effects after receiving one HuNoV VLP; 83% of recipients showed a 4-fold increase in virus-specific serum IgG levels. [65] .These discoveries prompted the creation of a VLP vaccination adjuvanted with monophosphoryl lipid A and the mucoadhesin chitosan, designed for intranasal administration as 2 split doses given twice, three weeks apart. It was discovered that this vaccine induces HuNoV -specific IgG and IgA Memory B cells as well as HuNoV -specific IgG and IgA; no major vaccination-related side events occurred during the original Phase I, double blind, placebo-controlled study [66, 67]. In a randomized, double-blind, placebo-controlled evaluation the effectiveness of the intranasally administered vaccination in the prevention of infection and sickness, individuals were challenged with 10 human-infectious doses of the Norwalk virus after receiving 2 doses of the vaccine or a placebo. Receiving the vaccination reduced the risk of gastroenteritis by 32% overall (37% vs. 69%; P = 0.006). In contrast to placebo recipients, vaccine recipients who got gastroenteritis had a longer incubation period before symptoms appeared after being challenged (, 4.3 hours; P = 0.02); nevertheless, there was no difference in the overall length of symptoms among participants who were unwell and infected. With the second dosage in the vaccination arm vs placebo, local nasal symptoms like nasal discharge, stuffiness, itching, and sneezing were more frequent; nevertheless, there were no major or severe side events related to the vaccine [68].

The second strategy investigated was administering the VLP vaccination intramuscularly, which was selected for its simplicity of administration and ability to stimulate a more immediate and powerful immune response. Moreover, a GII.4 VLP component was added to the GI.1 VLPs to create a bivalent vaccination in response to the high prevalence of GII.4 HuNoV es. According to results from preclinical studies, combining a GII.4 "consensus" VLP with the GI.1 Norwalk VLP vaccine produced broadly reactive antibodies to heterologous GI.3, GII.1, GII.3,

and GIV.1 HuNoV . This vaccine was designed from the sequences of three different previously isolated GII.4 HuNoV strain variants [69].

The bivalent GI.1 and consensus GII.4 VLP vaccination was administered as a series of two intramuscular injections and adjuvanted with monophosphoryl lipid A and aluminum hydroxide [70]. The immunization resulted in the generation of GI.1- and GII.4-specific blood antibody responses that peaked at day 7 in a randomized, placebo-controlled clinical study of this vaccine; the majority of individuals experienced elevations in HBGA-blocking antibody levels. Moreover, vaccination produced plasmablasts, cells that secrete antibodies, and memory B cells unique to the HuNoV vaccine strains [71, 72]. No increased levels of HuNoV -specific antibodies were produced by dose escalation. After the first dosage of the vaccination, high levels of HBGA-blocking antibodies appeared in all age groups (18-49, 50-64, and 65-85 years), with minimal further boosting after the second dose. There were no reported severe vaccination-related side effects. Sera from the study participants' subjects were analyzed, and the results showed that vaccination could result in antibodies with widespread activity against GII.4 HuNoV es, including novel strains not included in the consensus sequence [73].

The effectiveness of the bivalent vaccine in defending against a GII.4 HuNoV s was evaluated through a challenge study. In that randomized, double-blinded, placebo-controlled trial, 63 participants received the HuNoV vaccine, and 64 participants received a placebo vaccine; of these, 56 and 53 participants, respectively, participated in the challenge phase, during which participants were exposed to 4400 reverse transcription polymerase chain reaction units of a GII.4 HuNoV variant that is not present in the consensus GII.4 sequence. Ig levels specific to HuNoV increased overall in vaccine recipients. None of the minor reductions in the occurrence of severe, moderate, and mild gastroenteritis that were associated with receiving the HuNoV vaccination as opposed to a placebo attained statistical significance. Furthermore, using a modified Vesikari score to assess the overall SeV erity of the illness, immunization was linked to reduced symptoms following HuNoV exposure. Among those who received the vaccination, neither the length of the HuNoV infection nor the time from challenge to symptom start was shortened. There were no documented serious negative events [74].

1.8.2 Plant-Expressing HuNoV VLPs

While the majority of the HuNoV VLPs mentioned above were created by recombinant baculoviruses in the insect cell line sf9, a plant expression method was also used for the creation of the HuNoV vaccine. For instance, HuNoV GII.4 VLPs were produced quickly and with a high yield in Nicotiana benthamiana leaves [75]. Moreover, transgenic potatoes were

used to make an oral GII.4 VLP vaccine, which resulted in 95% of volunteers consuming them having considerably more cells that secrete specific IgA, 20% of individuals having specific blood IgG, and 30% of subjects having specific stool IgA [76]. The plant-based HuNoV VLP vaccine was then created in tobacco (Nicotiana benthamiana) utilizing a productive transient expression method derived from the tobacco mosaic virus (TMV). Mice developed systemic and mucosal immune reactions as a result of the tobacco-derived HuNoV VLPs [77]. HuNoV GII is a tobacco (Nicotiana benthamiana) product. In mice who had been intranasally immunized, 4 VLP caused 56 days of VLP-specific blood IgG induction [78]. This research collectively suggest that plant-based technologies may one day be used to generate or safely distribute vaccines.

1.8.3 Vaccines Based on HuNoV P Particles

The two primary domains that make up the HuNoV capsid protein are the protrusion (P) domain, which makes up the virus's arch-like protruding domain, and the shell (S) domain, which forms the internal shell [79]. In yeast (*Pichia pastoris*) and *Escherichia coli* expression cultures, the P particle can be produced solely by the expression of the P domain [80, 81]. The P monomer is duplicated 24 times to generate the P particle. With a molecular mass of about 840 kDa and a diameter of about 20 nm, it demonstrated an octahedral symmetry. The P particle is very immunogenic, highly stable, and simple to create [81]. As a result, it has been suggested as a potential HuNoV vaccine.

Neonatal gnotobiotic pigs have been utilized as a model in one investigation to assess the effectiveness of HuNoV P particles and VLPs as protective agents. P particles significantly increased the number of activated CD4+ T cells in all tissues, interferon gamma-producing (IFN-+) CD8+ T cells in the duodenum, regulatory T cells (Tregs) in the blood, and transforming growth factor-producing (TGF-+) CD4+ CD25 FoxP3+ Tregs in the spleen when compared to VLPs [82].

In order to prevent numerous potential viral infections, HuNoV combined vaccines based on P particles have also been created in combination with immunogens generated from other viruses. It has been demonstrated that a vaccination that combines influenza virus M2e and HuNoV P particles causes protective antibodies against a lethal challenge with influenza virus PR8 (H1N1). Moreover, HuNoV VLPs and P particles could not bind to an HBGA when they were exposed to sera from inoculated mice [83]. When the RV VP8 was coupled with HuNoV P particles, similar fruitful outcomes were shown [84, 85]. The P particles, like VLPs, were immunogenic and had HBGA-binding capability [81], indicating their potential as a candidate for a HuNoV vaccine.

1.8.3 Adenovirus Vector-Based HuNoV VLP Vaccine

The Chinese Center for Disease Control and Prevention created a recombinant adenovirus vaccination that expressed HuNoV GII.4 VLPs. Recombinant adenovirus-expressed HuNoV GII.4 VLPs can induce particular cellular, humoral, and mucosal immune responses in mice when administered intravenously [86]. Purified HuNoV GII was used to enhance the animals after recombinant adenovirus was used to prime them. Heterogenous Adenovirus prime-VLPs boost vaccination is a more efficient way to induce immune responses against HuNoV , which may be another promising direction to improve the current HuNoV vaccine design. 4 VLPs showed stronger humoral, mucosal, and interferon- responses than those immunized with VLPs prime-recombinant adenovirus boost or VLPs alone. In order to evaluate the safety and immunogenicity of an oral HuNoV vaccine, a single-site, randomized, double-blind, placebo-controlled clinical trial was started. A non-replicating adenovirus-based vector encoding HuNoV GI.1 VLPs and a dsRNA adjuvant made up the tablet vaccination [87]. According to the findings, the oral HuNoV vaccine was well tolerated and produced significant immunological responses, including systemic and mucosal antibodies as well as memory IgA/IgG.

1.9 HuNoV vaccine Candidate in clinical trial

1.9.1 The Takeda HuNoV Vaccine

The TAK-214 produced by Takeda Pharmaceuticals International AG [88] is the most researched HuNoV vaccine candidate that was in clinical trials. Yerseke/2006a, Den Haag/2006b, and Houston/2002 variants of the GI.4 Norwalk virus (NV) strain and a consensus GII.4 sequence (GII.4c) generated from those three variants make up this adjuvanted VLP-based bivalent vaccination. The prevalent genotype responsible for the majority of HuNoV disease burden worldwide is GII.4 [89]. To increase its potential for protective immunity, the HuNoV antigens from both genotype I and genotype II have been included. Several phase 1 clinical trials were carried out, demonstrating strong immune responses to both vaccination antigen components in various formulations in healthy individuals as well as high safety and tolerability. Serum antibodies to the two VLP vaccine components persisted during a subsequent one-year follow-up investigation using memory probe vaccination [70, 90-92]. Three phase 2 clinical trials were conducted to evaluate the efficacy of the Takeda vaccine candidate after the phase 1 research. Two doses of an intranasally administered vaccine with

the adjuvants chitosan and monophosphoryl lipid A (MPLA) were shown to protect healthy persons against the challenge of homologous GI in a phase 2a study [68]. A four-fold increase in serum antibody titers was defined as an HuNoV -specific IgG seroresponse by 70% of vaccine recipients overall. The incidences of AGE ($p = 0.006$) and viral infection ($p = 0.05$) brought on by HuNoV challenge were dramatically reduced by vaccination. The bivalent vaccination adjuvanted with MPLA and aluminum salt was delivered intramuscularly for two doses in another phase 2a research [74], which decreased vomiting and/or diarrhea brought on by challenge with a GII. 4 Farmington Hills/2002 variant ($p = 0.054$).

1.9.2 The HuNoV Vaccine from Vaxart

A recombinant VP1-based HuNoV vaccine candidate is also in clinical testing. Based on its unique oral tablet technology, Vaxart Pharmaceutical Inc. developed the bivalent vaccination (VXA-NVV-104) [87, 93]. This vaccine has recombinant adenovirus-based vectors [94] that carry genes for noroviral VP1s, which are expressed locally in the epithelial cells of vaccine recipients' intestines to promote mucosal immunity. Moreover, the adenovirus vector has unique RNA-encoding regions that produce double-stranded RNAs as an adjuvant for the VP1 antigens' improved immunogenicity. As a bivalent vaccination with widespread efficacy, both the VP1-encoding genes of the GI.1 HuNoV strain and the GII.4 Sydney variation are included. In order to prevent HuNoV infection, this tablet vaccine is made to be taken orally and stimulate the mucosal immune response in the intestine. Because noroviral VP1s have a high propensity to spontaneously form VLPs and because the epithelial cells of the intestine are the natural host cells of HuNoV es, it is plausible to expect that the adenovirus-expressing VP1s self-assemble into noroviral VLPs in the epithelial cells of the intestine of vaccine recipients. A phase 1 clinical trial was conducted to examine an early monovalent vaccine formulation (VXA-G1.1-NN) that expressed the VP1 antigen of the GI.1 HuNoV strain [87]. The outcomes demonstrated the good tolerability of this oral vaccination. Vaccine recipients significantly increased their HBGA-blocking antibody titers after receiving a single dose of the vaccination ($p = 0.0003$). The vaccinees also produced fecal IgA, IgA+ memory B cells with gut-homing receptor [61] and mucosally primed circulating NV-specific antibody-secreting cells (ASCs). Vaxart has launched a new phase 1b HuNoV dose-ranging experiment in senior persons that will test the vaccine's safety, tolerability, immunogenicity, and effectiveness in healthy older adults between the ages of 55 and 80. (ClinicalTrials.gov identifier: NCT04854746).

1.9.3 The NVSI HuNoV Vaccine

The National Vaccine and Serum Institute of China's bivalent VLP-based vaccine produced in Hansenula polymorpha is the third HuNoV vaccine candidate that is undergoing clinical testing (ClinicalTrials.gov identifier: NCT04188691). It contains aluminum salt as the adjuvant and two recombinant VLPs that represent the GI.1 and GII.4 genotypes, respectively. 510 healthy people between the ages of 6 months and 59 years old were included in a phase 1 trial to assess the safety and immunogenicity of the vaccination. The vaccination was delivered intramuscularly in two or three doses. GI.1 and GII.4 HuNoV specific IgG antibody titers and their positive rates, as well as GI.1 and GII.4 HuNoV HBGA-blocking antibody titers and their positive rates, were included as outcome measures.

1.9.4 The Longkoma HuNoV Vaccine

This quadrivalent vaccination was created using a yeast expression system and consists of four aluminum salt-adjuvanted VP1 proteins that each represent the GI.1, GII.3, GII.4, or GII.17 genotypes (ClinicalTrials.gov identifier: NCT04563533). The vaccine was created in China by the Anhui Zhifei Longcom Biopharmaceutical Co. Ltd. and the Institut Pasteur of Shanghai in Hefei. Clinical trials in phases 1 and 2a were registered (ClinicalTrials.gov identifier: NCT04563533), with the goals of determining the ideal vaccination dose for future development, as well as the safety and tolerability of the vaccine at various doses as well as its immune response. 580 individuals will be enrolled in total, divided into 5 age groups (infants, toddlers, adolescents, adults, and elderly), ranging in age from 6 weeks to >60 years. The vaccine will be given intramuscularly, and adverse events, positive conversion rates, and a four-fold increase in HuNoV -specific IgA, IgG, and HBGA blocking antibodies after immunization will all be used as outcome measures.

1.10 SeV

In the 1950s, the mouse parainfluenza virus type 1 known as SeV was identified in Sendai, Japan [95]. The Japanese Society for Virology originally referred to the virus as "Hemagglutinating virus of Japan," but it is now known as "newborn viral pneumonitis (type Sendai)" [96]. SeV is now known to be a mouse-specific virus rather than a human one. SeV infections in mice were initially described by Fukumi et al. in 1954. [97] Although SeV is one of the main causes of pneumonia in some mouse strains, this infection can also be subclinical [98]. SeV 's restriction to certain hosts may be at least partially explained by the fact that it is

particularly sensitive to interferon-associated reactions in humans [99]. A benefit for the development of vaccines is that SeV develops to high titers in both chicken eggs and FDA-approved mammalian cell lines. SeV belongs to the Paramyxovirinae subfamily of the Respirovirus genus. SeV is an enclosed virus with a nonsegmented, negative-strand RNA genome, similar to other paramyxoviruses [100]. The SeV genome has six structural genes, a 3' leader sequence, a 5' trailer, and transcription start with nucleocapsid (N), followed by phosphoprotein (P), matrix (M), fusion (F), hemagglutinin-neuraminidase (HN), and big polymerase (L). It is interesting that leaky scanning, which results in the production of the proteins C', C, Y1 and Y2 [101, 102] and pseudotemplated insertion of nucleotides, also known as mRNA editing, which results in the production of the proteins V and W, both produce a number of extra proteins [103, 104]. A helical nucleocapsid at the center of the virion houses 2600 N, 300 P, and 50 L proteins in addition to the viral RNA genome. The SeV genome and antigenome must have an even multiple of six RNA nucleotides in order to replicate effectively [105-107]. As a result, the "rule of six" must be followed when cloning a foreign antigen insert into the SeV vector.

The M protein is the most prevalent protein in the virion, and it interacts with the host cell's plasma membrane, the F and HN envelope glycoproteins' cytoplasmic tails, the nucleocapsid, and itself to encourage the creation of viral particles [108]. The ectodomains of the F and HN proteins, which are type I and type II membrane proteins, project as spikes perpendicularly from the surface of the viral envelope [109]. When a virus enters a cell, the HN protein attaches to receptors on the plasma membrane's surface that are sialic acid-containing, causing the F protein to refold into a hairpin form at neutral pH and fuse the viral and host cell membranes. The HN protein annihilates its own receptors when the envelope glycoprotein moves to the cell surface in order to effectively release offspring virions and to stop virion aggragation or superinfection of previously infected cells. For SeV, the N gene is the first to be transcribed, and 90% of N mRNA transcripts that are started are finished. A viral gene junction, which consists of a gene start sequence, an intergenic region (GUU), and a gene end region, is located between each gene [110]. The viral RNA-dependent RNA polymerase is instructed to stop transcription at each gene junction, polyadenylate the nascent mRNA, and then restart transcription of the following gene. The precise frequency of reinitiating transcription, which is based on the nature of the transcript start sequence, is not known [111]. This causes a gradient of mRNA transcripts with the following abundance to be produced: N > P > M > F > HN > L. Thus, the amount that a foreign reporter gene or vaccination antigen is produced and the amount that SeV replication is inhibited depend on how far away from the starting 3 end of the genome the insert is positioned when it is inserted into the SeV genome [112, 113].

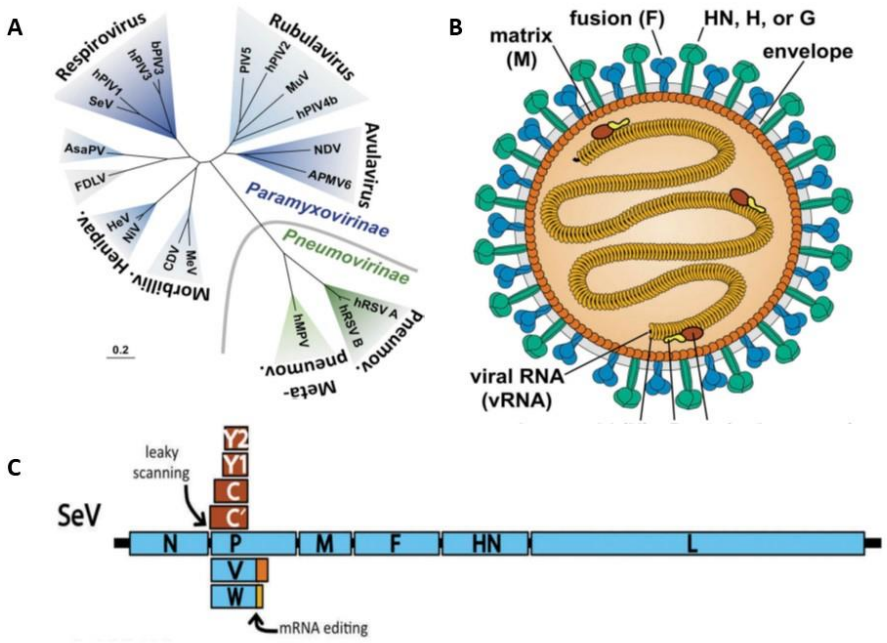

Figure 4. (A) Phylogenetic tree based on the F protein sequences of selected paramyxoviruses; (B) Structure of a paramyxovirus; (C) Schematic diagram of paramyxovirus genome [114]

1.10.1 SeV as a vaccine

SeV is particularly appealing as a human vaccination because it is a recognized mouse pathogen and has not been linked to any known human diseases. SeV is not an attenuated human virus, thus the worry that it would revert to its initial harmful nature is not a problem [115, 116]. SeV is especially appealing because mammalian cells can express endogenous antigens with posttranslational modifications that are similar to those of target antigens and neutralizing epitopes when SeV develops transiently within the cell [117]. Strong CD8+ T cell activation is also made possible by endogenous expression of antigens [118].

The majority of the viral vaccines we currently utilize are created using pathogen proteins or live, attenuated, or inactivated viruses. Due to their effectiveness and long-lasting immunity, live attenuated vaccines have proved particularly effective for the control or even elimination of illness. Yet, due to the possibility of genetic instability and lingering virulence, such vaccines and vaccine candidates are frequently questioned regarding their safety [119]. The drawbacks of live vaccines can be seen in the potential reversion of attenuating mutations, as was the case with the Sabin polio vaccine [120, 121] or in the difficulty of finding the ideal balance of attenuation, which, for example, makes the development of live-attenuated RSV vaccines challenging [115]. In order to achieve the best possible protection against infectious diseases, innovative vaccine techniques may be helpful. In recent years, viral vectors have become

effective and well-defined techniques with immunogenic properties [122] comparable to live attenuated vaccines. Live attenuated vectors still raise the same security issues, though. Hence, the ideal vaccination vector should combine the following traits: (i) replication deficiency & no persistence, (ii) genetic stability, (iii) no interaction with host cell genome, (iv) no pre-existing immunity, and (v)induction of specific humoral and cellular immunity [123].

1.11 mRNA vaccines

In place of traditional vaccine strategies, nucleic acid therapies have shown many potentials. In 1990, when reporter gene mRNAs were injected into mice and protein synthesis was discovered, the first report of the successful use of in vitro transcribed (IVT) mRNA in animals was published [124]. A second investigation in 1992 revealed that giving rats mRNA that encodes vasopressin in the hypothalamus could cause a physiological response [125]. These early, encouraging discoveries, however, did not result in a significant investment in the development of mRNA therapies, mostly because of worries about mRNA instability, high inherent immunogenicity, and ineffective in vivo transport. Instead, the field developed therapeutic strategies based on proteins and DNA [126, 127]. The growth of mRNA as a prospective therapeutic tool in the fields of protein replacement treatment and vaccine development over the past ten years has been made possible by significant technological advancements and research expenditure.

mRNA and its delivery method, both of which are necessary for the production of encoded antigens and the activation of adaptive immunity in the human body, make up the two main components of a conventional mRNA vaccine. First, the basic foundation for producing targeted immunity against a pathogen or tumor is provided by mRNA that encodes the required proteins or polypeptides. The antigens for infectious illness vaccines are often the surface proteins of pathogens. Strictly speaking, T7 RNA polymerase is typically used in in vitro transcription (IVT) to produce vaccine mRNA from a DNA template. For effective translation, mRNA also needs the 5 cap, 3 and 5 untranslated regions, nucleotide modifications, and poly(A) tail to be optimized [128].

When compared to other vaccines, mRNA vaccines provide a number of distinct advantages. First, due to the production of encoded antigens in host APCs, mRNA vaccines produce both antibody and CD8+ T cell responses, in contrast to inactivated pathogens, protein components, and peptide vaccines, which only stimulate antibody responses. Second, it is possible to produce mRNA vaccines more quickly[129]. As mRNA may theoretically encode any type of antigen, it is possible to produce mRNA vaccines against a variety of targets with minimum processing and formulation modifications. Rapid production is crucial for protecting against many types of worry and controlling pandemics that are forming quickly. Third, unlike protein-

or peptide-based vaccines, which typically call for the addition of adjuvants, mRNA and its delivery vehicles can promote powerful and long-lasting adaptive immune responses [128]. Fourth, as compared to DNA vaccines, mRNA vaccines' production of antigens encoded in them is speedier and more effective since mRNA can be functional in cytoplasm while DNA must enter the nucleus and be transcribed before proteins can be produced [130]. In comparison to DNA vaccinations, integration of mRNA into the host DNA genome is also far less likely. The transitory nature of mRNA also enables complete clearance after sufficient antigen expression, potentially reducing the strain on host homeostasis. The effectiveness of mRNA vaccines should be improved through mRNA and delivery system modification. Concerns about the safety of mRNA vaccines are also raised because there are more instances of adverse responses than there are with conventional inactivated vaccinations. Moreover, considerations like storage and antigen mutations should be made for upcoming mRNA vaccine development [131]. Between the translation of DNA encoding proteins and the synthesis of proteins by ribosomes in the cytoplasm, mRNA serves as an intermediary step.

Non-replicating mRNA and virally generated, self-amplifying RNA are the two main forms of RNA that are now being investigated as vaccines. The antigen of interest is encoded by conventional mRNA-based vaccines, which also contain 5 and 3 untranslated regions (UTRs). Nevertheless, self-amplifying RNAs encode both the antigen and the viral replication machinery, which allows for intracellular RNA amplification and profuse protein expression. Using a T7, T3, or Sp6 phage RNA polymerase, IVT mRNA is generated from a linear DNA template. A protein of interest's open reading frame, flanking UTRs, a 5 cap, and a poly(A) tail should all be present in the final product. Hence, the mRNA is modified to resemble fully mature mRNA molecules that normally exist in eukaryotic cells' cytoplasm [132, 133]. Naked mRNA is not effectively internalized and is promptly destroyed by extracellular Rnases [134]. As a result, a wide range of in vitro and in vivo transfection reagents have been created that make it easier for cells to absorb mRNA and keep it from being destroyed. The cellular translation apparatus creates protein after the mRNA transits to the cytoplasm, which then undergoes post-translational changes to produce. a protein with correct folding and functionality. For vaccines and protein replacement therapies that depend on the delivery of cytosolic or transmembrane proteins to the appropriate cellular compartments for optimal presentation or function, this aspect of mRNA pharmacology is very helpful. The danger of metabolite poisoning is eventually reduced by regular physiological processes that break down IVT mRNA [135].

1.11.1 Optimization of mRNA translation and stability

The coding sequence's flanking 5 and 3 UTR regions have a significant impact on the stability and translation of mRNA, both of which are crucial issues for vaccines. The half-life and expression of therapeutic mRNAs are significantly increased by these regulatory sequences, which can be obtained from viral or eukaryotic genes. It takes a 5’ cap structure for mRNA to produce proteins effectively [136-138]. By introducing synthetic cap or anti-reverse cap analogues or a vaccinia virus capping enzyme, different forms of 5 caps can be introduced during or after the transcription step. An ideal length of poly(A) must be added to mRNA either directly from the encoding DNA template or by employing poly(A) polymerase, as the poly(A) tail also plays a significant regulatory function in mRNA translation and stability [139-141]. Another method of sequence optimization that has been demonstrated to raise steady-state mRNA levels in vitro and protein expression in vivo is enrichment of G:C composition [142, 143].

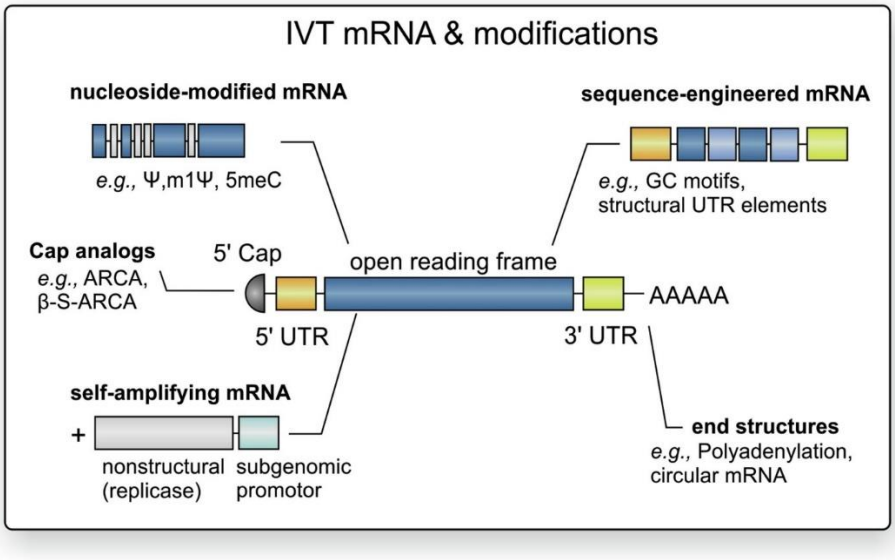

Fig 5. Structural elements of in vitro transcribed (IVT) mRNA. Each of these elements can be optimized and modified in order to modulate the stability, translation capacity, and immune-stimulatory profile of mRNA [144].

1.12 Lipid Nanoparticles (LNPs)

LNPs have proven useful as a platform for the delivery of RNA vaccines and treatments in recent years. Naked RNA is a hydrophilic negatively charged molecule. Macromolecule that is electrostatically attracted to the cellular membrane, preventing it from entering cells, and is quickly broken down by ubiquitous RNases. Hence, access to the interior of the cell requires a protective shell. Encapsulating RNA with lipid vesicles provides the chance to secretly cross the cellular membrane and released RNA to the cytosol because lipids make up the majority

of cellular membranes. The vesicles must first have a positively charged lipid that can attach to the negatively charged RNA in order to accomplish this [145]. Nevertheless, cytotoxicity can result from the electrostatic rupture of the negatively charged cellular membrane caused by the vesicles made of persistently cationic lipids. In response to the acidic endolysosomal pathways, the lipid structures then underwent further evolution to gain positive charge. The structural lipids and poly (ethylene glycol)-anchored lipids have been added to LNP composition to resemble the cell membrane and hide the positive charge (to prevent the LNPs from aggregation and undesired interactions with biological environments). The LNP-based method of delivering nucleic acids is secure and suitable for a range of therapeutic cargos. However, there is currently no one-size-fits-all treatment for every condition, thus LNP optimization research is ongoing [146].

1.12.1 LNP components

Ionizable and cationic lipids, cholesterol, phospholipids, and PEG lipids are frequently found in LNPs (50-100 nm in diameter), with ionizable lipid playing a significant role in preventing nucleic acid from being degraded by nucleases [147]. Moreover, helper lipids (such as phospholipids and cholesterol) support formulation stability and membrane fusion [148]; for siRNA to be effectively trapped within LNPs [149], a helper lipid content of between 30 and 40% is needed. The circulatory half-life and stability of PEG lipids, which are made up of a hydrophilic PEG polymer coupled to a hydrophobic lipid anchor, can be improved, inhibiting LNP clearance [150]. Particularly, it has been demonstrated that PEG lipids with low molecular weights reduce non-specific protein adsorption and restore the selective binding of receptor-targeting nanoparticles [151]. The particle size is also determined by the PEG lipid content [152].

LNPs are able to have micellar structures within the particle core, unlike liposomes. Moreover, compared to liposomes, LNPs had better kinetic stability and a stiffer shape; more homogeneous LNPs can be produced using a large-scale commercial production approach. At room temperature, LNPs can be classified as either solid nanoparticles or as nanostructured lipid carriers, which are composed of both solid and liquid lipids. The amine groups on ionizable lipids become protonated and positively charged at low pH, permitting assembly with negatively charged phosphate groups on nucleic acids. Curiously, ionizable LNPs have a near-neutral charge at physiological pH. To enable therapeutic delivery, the pH can be brought back to neutral or physiological levels after complexation. Ionizable LNPs have the ability to extravasate from the bloodstream to target tissues after being injected in vivo. Once on the cell surface, LNPs can adsorb and then enter the cell through endocytosis. Endosomal escape is

facilitated by positively charged ionizable lipids, which interact with the negatively charged endosomal lipid membrane to destabilize it and encourage nucleic acid release [153]. Because of variations in nucleic acid size and charge that may affect lipid packing and LNP structure, the manufacturing methods used to encapsulate nucleic acids (such as siRNA, mRNA, and pDNA) in LNP systems need to be fine-tuned in terms of molar ratio and lipid composition [154]. In order to recognize and bind to particular cell receptors, surface-attached ligands (such as transferrin and folate) can be conjugated to the surface of LNPs to create tailored LNPs.

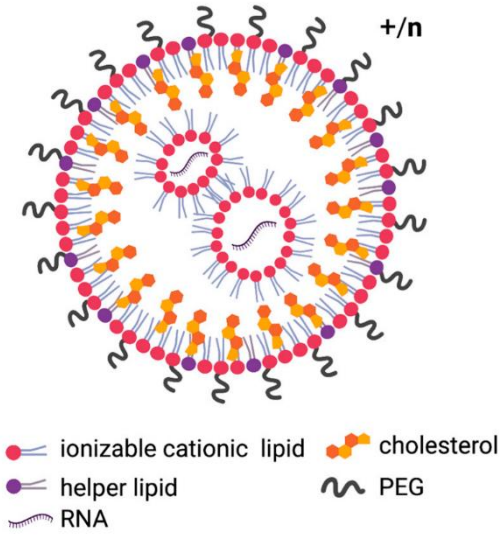

Figure 6. Schematic representation of structure and components of LNPs [155].

1.12.2 LNP preparation

The ability of self-assembly, or the spontaneous arrangement of lipid components into nanostructured entities based on intermolecular interactions, is what makes LNP preparation possible [156]. The electrostatic interaction of positively charged lipids and negatively charged nucleic acids leads to the production of LNP. After that, lipid components interact hydrophobically and by van der Waals forces to grow LNPs. Because of the variety in lipid chemistry, the special characteristics of nucleic acids, and the speed at which the two are combined, it is still difficult to characterize the early stages of self-assembly and the associated consequences on the final LNP features. Moreover, the homogeneity of the LNPs and the effectiveness of the nucleic acid loading are at least two additional ways that LNP manufacturing techniques impact the products of self-assembly. LNP can be prepared in a variety of ways, including by rehydrating the lipid film, extruding lipid vesicles, nanoprecipitation, and microfluidic mixing. Nevertheless, aqueous and lipid components are generally mixed quickly as part of the preparation process [157]. Nowadays, preclinical research prefers microfluidic technologies due to their high reproducibility. This technique is

now more widely available thanks to recent improvements in the production of microfluidic devices [158, 159]. Other methods to achieve even higher high-throughput LNP preparation include using parallel microfluidic paths or updated conventional techniques like pipet mixing and T-mixers [160, 161]. Although nucleic acids can be included without strictly using microfluidic mixing, it is generally advantageous to encapsulate hydrophilic moieties within the hydrophobic lipid core [162]. Overall, since the structure of the nanoparticles appears to be dictated by kinetic parameters of self-assembly, the type of the mixing process may have an impact on the loading effectiveness and internal organization of LNPs [163].

1.13 Aims of the study

The overall aim of the study was to evaluate alternative vaccine candidates to generate a human virus vaccine. Distinct aims were:

1) To generate recombinant replication deficient SeV (recSeV) viral vector encoding HNoV VP1 capsid protein as a vaccine candidate for intra-nasal and intra-muscular immunization
2) To evaluate immunogenicity of the recSeV /VP1in mice
3) To generate an mRNA-based vaccine against HuNoV GII.4 capsid protein
4) To establish a LNP delivery system for mRNA vaccine formulation
5) To evaluate specific immune responses against HuNoV VP1 after vaccination with naked and LNP-formulated mRNA vaccines

2 Results

2.1 Generation of SeV vaccine vector

2.1.1 Subgenomic replication deficient Sendai-VP1 vector construction

A subgenomic SeV (SeV) vector carrying the HuNoV capsid gene was constructed and utilized in conjunction with a full-genome SeV vector to create a replication-deficient SeV vector encoding the HuNoV GII.4 VP1 gene. The subgenomic vector has been modified by deleting the N-terminal 76 amino acids (the amino acids 2 to 77) of Phosphoprotein (Pdel). The manipulation of P gene makes the vector unable to replicate and synthesize new genomic templates in non-helper cell lines. As a result of the unique replication cycle and transcription characteristics of the SeV, there is a decrease in the abundance of mRNA transcripts from the 5' end to the 3' end of its genome (N > P > M > F > HN > L). This leads to a higher expression of the target foreign protein when the foreign reporter gene is cloned in closer proximity to the SeV genome. Therefore, to reach a high expression level of our gene of interest, the HuNoV GII.4 VP1 was cloned (considering the rule of six) right after the Pdel flanked by P gene stop signal, Intergenic sequence and start signal for transgene at the 5’ side and transgene stop signal, Intergenic sequence and M gene start signal at the 3’ side. For this aim, the subgenomic plasmid was linearized by *BssH*II restriction enzyme and the amplified VP1 gene (containing 2 *BssH*II site at 5’ & 3’ ends) was ligated into the vector as shown in Figure. 7 a,b.

2.1.2 Construction of replication deficient Sendai-VP1 vector

The full genome SeV vector is comprised of a 3' leader sequence, six structural genes (N, P, M, F, HN, L), and a 5' trailer, as shown in Figure. 7 c. Furthermore, an EGFP gene has been inserted downstream of the L gene, enabling the evaluation of the replication and expression efficiency of the viral vector through the observation of EGFP fluorescence. The expression of the SeV and HuNoV GII4 VP1 is controlled and started by a T7 promoter located at N gene 5’ upstream and stopped by a T7 terminator located at EGFP gene 3’ downstream. In order to make the final construct, both the subgenomic rd.SeV .VP1 vector and the full genome SeV vector were digested using *EcoR*I restriction enzyme and the target segment containg VP1 gene was ligated into the full genome vector resulting in a replication deficient SeV vector containing HUNOV GII4 VP1 gene (Figure. 7 d,e).

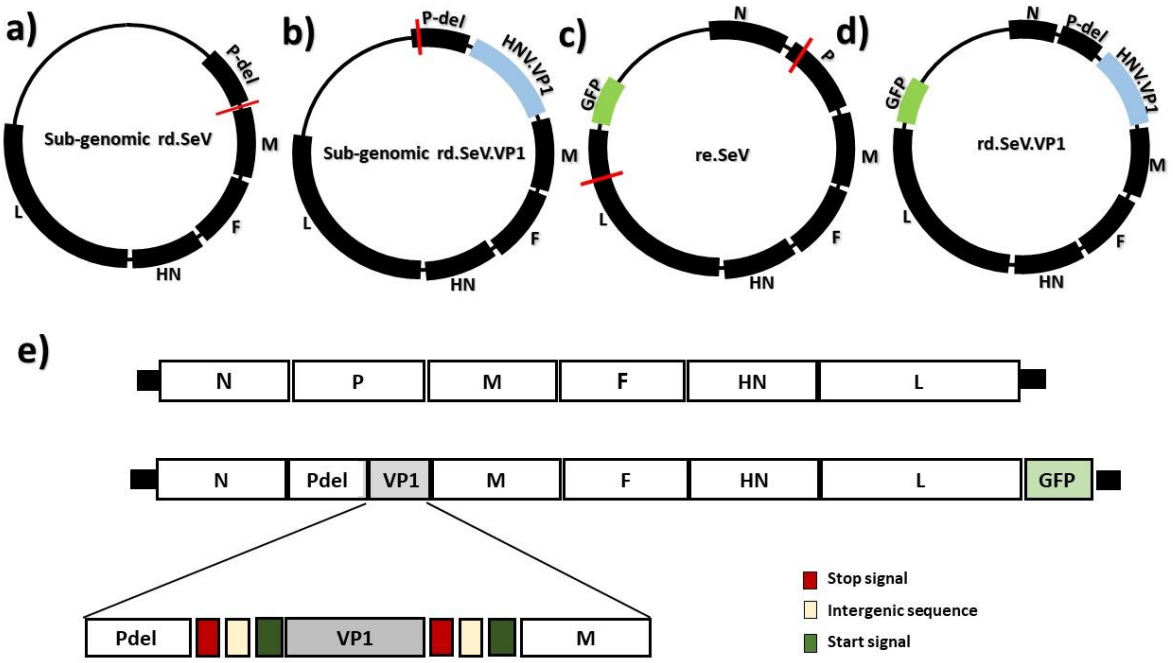

Fig 7. Schematic representation of Sendai Vectors and cloning steps. The HuNoV -VP1 gene was inserted into in *BssH*II restriction site of sub-genomic replication deficient (a) to generate the recombinant sub-genomic plasmid (b). The target region was cut at *Eco*RI restriction sites and inserted into the replication deficient SeV vector resulting in a recombinant replication deficient SeV vector harboring heterologous HUNOV -VP1 gene (c, d, e). The VP1 gene insertion comply with the rule of 6 concept and is cloned between the P and M genes flanked by a stop signal, intergenic sequence and a start signal at 5' & 3' sites.

2.2 SeV characterization

2.2.1 SeV rescue

BSRT7 cells were transfected with respective plasmids to recover the recombinant replication deficient SeV particles. BSR-T7 cells (0.5 × 106) were transfected with a plasmid mixture consisting of pTM-N (for SeV N gene), pTM-P (for SeV P gene), pTM-L (for SeV L gene), and a plasmid carrying the cDNA of the viral genome flanked by T7 promoter and terminator sequences so that the viral genomic sequence is transcribed by the T7 polymerase. As the vector encodes an eGFP gene, expression of proteins can be visualized and confirmed using fluorescent microscopy.

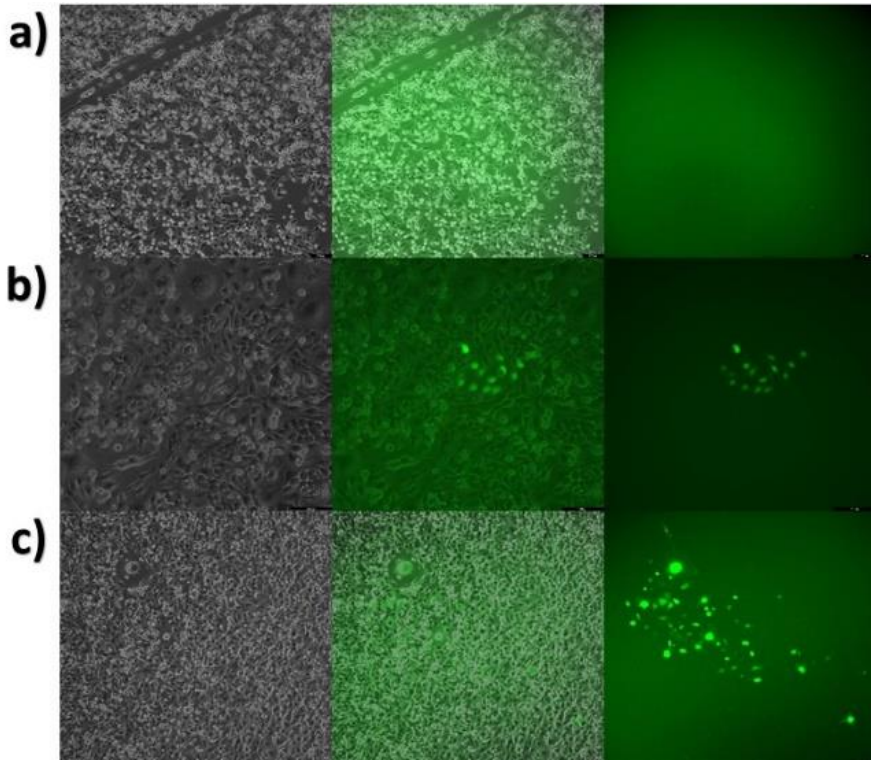

Fig 8. SeV rescue in BSRT7 cells. BSR-T7 cells (0.25 × 106) were transfected with SeV plasmid and, in parallel, with pTM-N (for SeV N gene), pTM-P (for SeV P gene), pTM-L. The development of eGFP-expressing cells was monitored for 12 days. Pictures show eGFP expression at day 0 as the starting daz of transfection (a), day 6 where the first signs of expression were seen (b), day 12 where the the transfection process was completed and the cell supernatants were collected for further propagation of the viral particles (c).

2.2.2 SeV propagation

The rescued recombinant SeV was propagated in the V3.10 helper cells expressing SeV P protein. The helper Vero cells were infected with rescued SeV and GFP expression was screened under flourescence microscope for six days to monitor the expression of eGFP as a representative of virus spread and propagation.

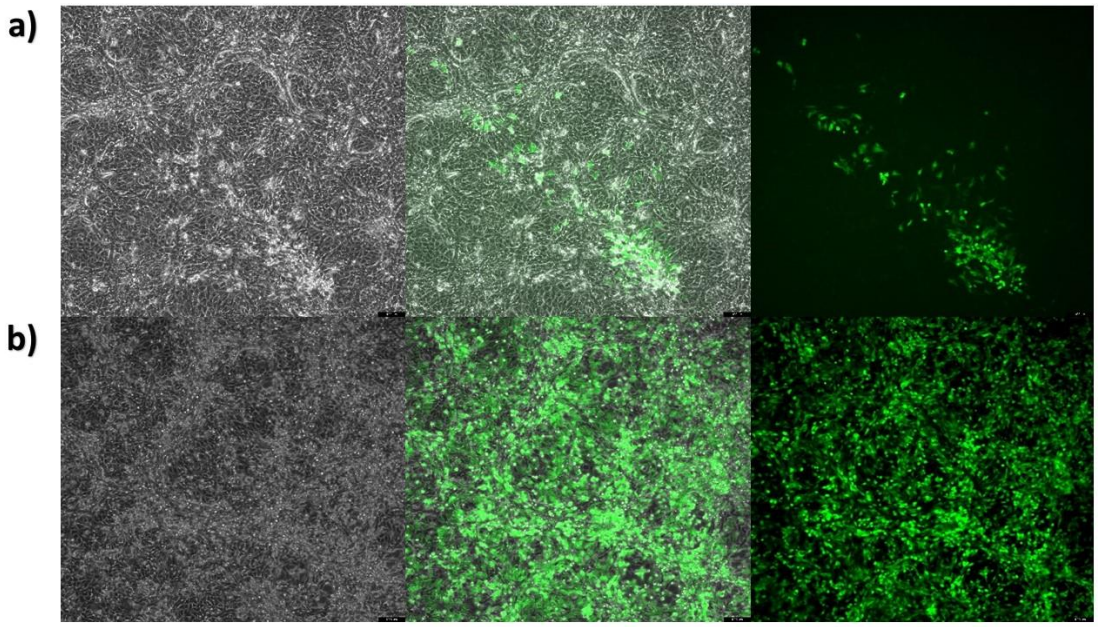

Fig 9. SeV propagation in helper-Vero cells. V3.10 helper cells were infected with replication deficient virus in order to produce enough viral particles to be purified for in vivo study. As a representation the eGFP expression status has been show at day 3 post infection (a) and 6 days post infection where more than 90 % of the cells became infected (b).

GFP expression was also evaluated in a non-helper cell line, wherein the rd.SeV vector demonstrated the ability to propagate, although at reduced levels. This is evident from the lower intensity of the GFP signal observed in the transfected cells, as shown in Figure 10.

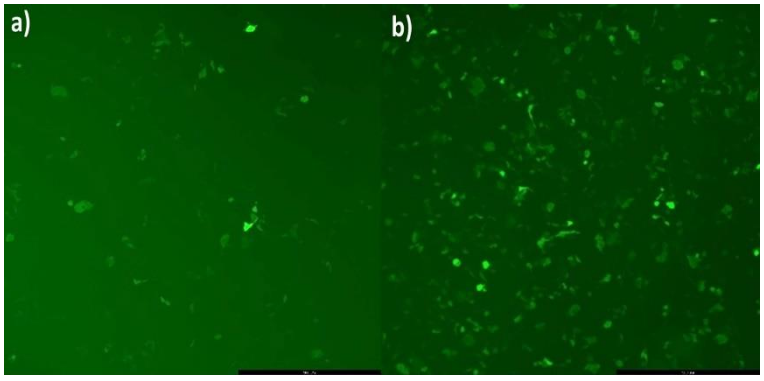

Fig 10. Infecting non-helper Vero cells with rescued SeV particles after 6 (a) and 12 days (b). This ensures the ability of the replication deficient SeV to express proteins which in fact mimics the function of the vector in in vivo environment.

2.2.3 Expression analysis of NoV VP1 in SeV -transfected cells

The expression of the hetrologous HuNoV VP1 gene was checked by Western blot to make sure the SeV viral vector is capable of expressing our gene of interest. The results showed

successful expression of NoV VP1 capsid protein in the infected V3.10 cells (Figure 11 a). To further validation, the SeV particles were purified using sucrose gradient method and were visualized by transmission electron microscopy (TEM). displayed intact SeV particles in our sample, exhibiting the expected size and shape (Figure 11b).

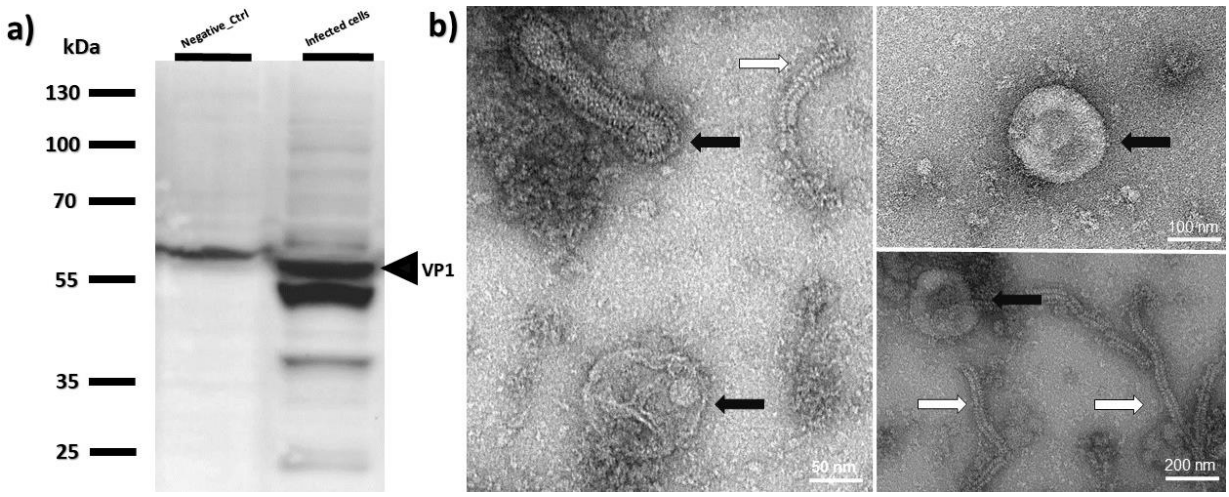

Fig 11. Expression of HuNoV VP1 and formation of Senai virus particles. The supernatant was loaded onto 35 % sucrose gradient & centrifuged. The SeV pellet was collected and stained to be used in WB and TEM. **a)** Western Blot imaging to screen the expression of HuNoV -VP1 protein in V3.10 cells infected with recSeV /VP1. The band below VP1 with a size of almost 55 kDa is the cleaved VP1 which is normally seen in WB for NoV capsid protein. **b)** Transmission Electron Microscopy imaging to screen the SeV particles. The black arrows depict the SeV viruses and the white arrows show the Nucleocapsid protein that has been released probably because of the breakage of viral particles under physical pressure of purification and centrifugation steps.

2.3 Immunogenicity of recSeV -VP1 in mice

To investigate the effectiveness of the replication-deficient vaccine candidate in inducing specific immunity to HuNoV VP1, a comprehensive analysis involving both homologous and heterologous prime-boost vaccinations utilizing the r.d-SeV -VP1 and MVA-VP1 vaccines was conducted. Six study groups of four female BALB/c mice at 6–8 weeks of age consisting of two low titer and high titer intranasally and intramuscular-immunized and two PBS groups were included. In each administration the low titer and high titer groups received 3×10^{8}/ml and 3.25×10^{10}/ml viral particles, respectively. Each group was inoculated three times, two weeks apart. Mice were sacrificed, ten days after the last administration, spleen, lung and blood samples were collected. The spleen was processed to isolate cells for T cell stimulation, involving steps such as smashing the spleen, washing, and incubating with ACK buffer, followed by stimulation with HuNoV GII.4 VP1 pooled peptides or positive controls. After stimulation, cells were stained with Fluorescently tagged antibodies for surface markers,

incubated, fixed, permeabilized, and then stained for intracellular cytokines. The cells were analyzed by the flow cytometry method. Antibody titers in vaccinated mice were measured via ELISA.

2.3.1 Homologous vaccination with rd.SeV .VP1 vaccine

In order to assess the specific T cell response efficiency triggered by the SeV viral vector, we isolated spleen cells from the vaccinated mice and subjected to in vitro stimulation using a mixture of HUNOV VP1-specific peptides following intracellular cytokine staining (ICS), identify NoV-specific cytokine-producing T cell population.

Our findings, summarized in Figure 12 a, revealed that both low-dose and high-dose intranasal administrations of SeV.VP1 were capable of eliciting CD8 responses specific to NoV in mice. Notably, the high-dose intranasal administration of SeV.VP1 exhibited an enhanced CD8 response as compared to the low-dose regimen, indicating a dose-dependent effect on the immune response. Moreover, we observed significantly higher NoV-specific CD8 responses with intramuscular injection resulted in higher compared to the intranasal route, regardless of the administered dose. The CD4 immune response showed also the same pattern.

The immunogenicity of the vaccine candidate was also assessed by measuring antibody levels against HuNoV VP1 in the mouse sera, where both intranasal (i.n.) and intramuscular (i.m.) administration routes were found to successfully elicited significant levels of NoV-specific antibodies (Figure 12 B). Comparing the two routes of administration, the i.m. route demonstrated a stronger IgG antibody response, surpassing the levels observed with both low and high doses of the i.n. route. This indicates that the i.m. administration route has a greater potential for inducing robust IgG antibody production in response to the vaccine.

2.3.2 Heterologous rd.SeV .VP1, recMVA.VP1 vaccination

To ensure a comprehensive analysis, we incorporated the MVA.VP1 vaccine vector into the study, serving two primary purposes. Firstly, the MVA.VP1 vector served as a control, allowing us to compare and evaluate the immunogenicity of the replication-deficient Sendai vector against a known benchmark. Secondly, the MVA.VP1 vector was employed as a booster in a heterologous prime-boost immunization strategy in conjunction with the recSeV /VP1 vaccine. This approach aimed to exploit the synergistic effects of different viral vectors, potentially enhancing the immune response. Notably, booster vaccination with MVA.VP1 vector significantly enhanced both CD8 and CD4 responses specific to NoV-VP1 when compared to the homologous vaccination with SeV VP1 or MVA.VP1 viral vectors.

The prime-boost regimen also demonstrated superior efficacy in inducing a higher NoV-specific antibody response compared to individual administrations of the viral vectors alone. This emphasized the synergistic effect of combining the two viral vectors in promoting a more potent and targeted NoV-specific antibody response (Fig 12 B). Anti-NoV IgG1 and IgG2a antibodies were also measured in the positive sera. IgG1 and IgG2a are associated with different types of immune responses. IgG1 is often linked to a Th2 (T-helper 2) response, which is involved in antibody-mediated immunity. IgG2a, on the other hand, is associated with a Th1 response, which is more focused on cellular immunity. Certain diseases, infections or vaccines may require a stronger Th1 or Th2 response, and monitoring IgG1 and IgG2a levels helps assess this balance. All the SeV vaccinated groups responses showed a tendency to IgG2a which is a representative of Th1 mediated response (Fig 12 C).

To determine whether the recSeV GII4, could stimulate specific mucosal immune response following i.n. administration, Lung- and intestinal homogenates were investigated for NoV-specific IgA level as the indicator for mucosal immunity to the virus. IgA level in intestinal- and lung homogenates were evaluated at a single dilution (1:10), and results were expressed as absorbance value at 450nm. A significant level of NoV-specific IgA response was detected in the lung homogenates ($p < 0.001$), whereas only a minor level of secreted NoV-specific IgA was detected in the intestinal homogenates of mice immunized with a high dose of the viral vector (Fig 12 D).

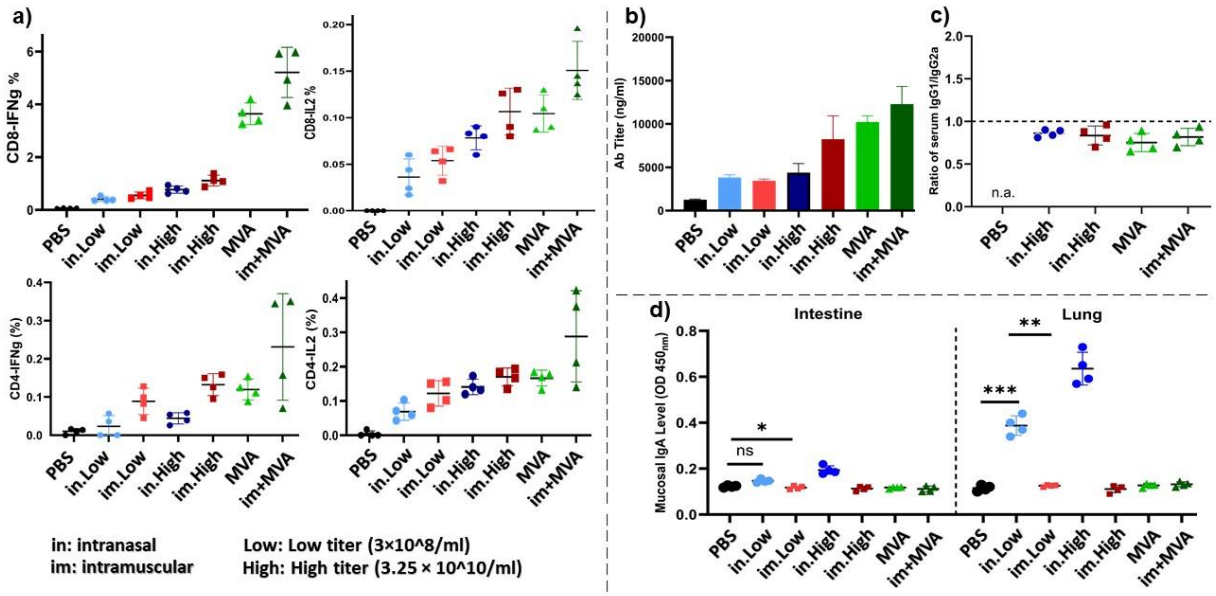

Figure 12. Evaluation of immune responses to recombinant replication deficient SeV vector. BALB/c mice were tested for NoV-specific immune responses in homologous and heterologous prime-boost vaccinations using recSeV.VP1 and MVA-VP1 viral vectors. In the homologous vaccination, mice were immunized either intranasally

or intramuscularly with both low and high virus titers, and in the heterologous vaccination following prime inoculation with recSeV.VP1, mice were injected with MVA.VP1, as a booster. The Splenocytes of the immunized mice were taken and stimulated with HuNoV GII.4 VP1 pooled peptides and stained for surface and intracellular markers. The measurements were performed using flowcytometry and ELISA techniques. After the last administration, immune responses were assessed in the mice: (a) specific CD8+ and CD4+ T-cell responses; (b) specific IgG Ab response; (c) serum IgG1 to IgG2a level ratio: (d) specific IgA response in the intestine and lung of the mice immunized with reSeV.VP1 intranasally.

2.4 Generation of mRNA vaccine

2.4.1 Construction of intermediate DNA plasmid for mRNA-production by in vitro transcription

A set HuNoV -targeting mRNA vaccines were generated using pcDNA3.1(-) DNA plasmids harboring NoV capsid gene downstream of the T7 promoter and employing *in vitro* transcription as detailed in the Material and Methods section. As shown in Figure 13, one pcDNA.VP1 plasmid was utilized as a template for the production of unmodified mRNA, while another DNA plasmid was used for the generation of modified mRNA in which the VP1 gene is flanked by a T7 promoter and a Xenopus β-globin 5´ UTR at the 5´ end and a Xenopus β-globin 3´ UTR. Plasmids encoding eGFP were served as a positive control in the process.

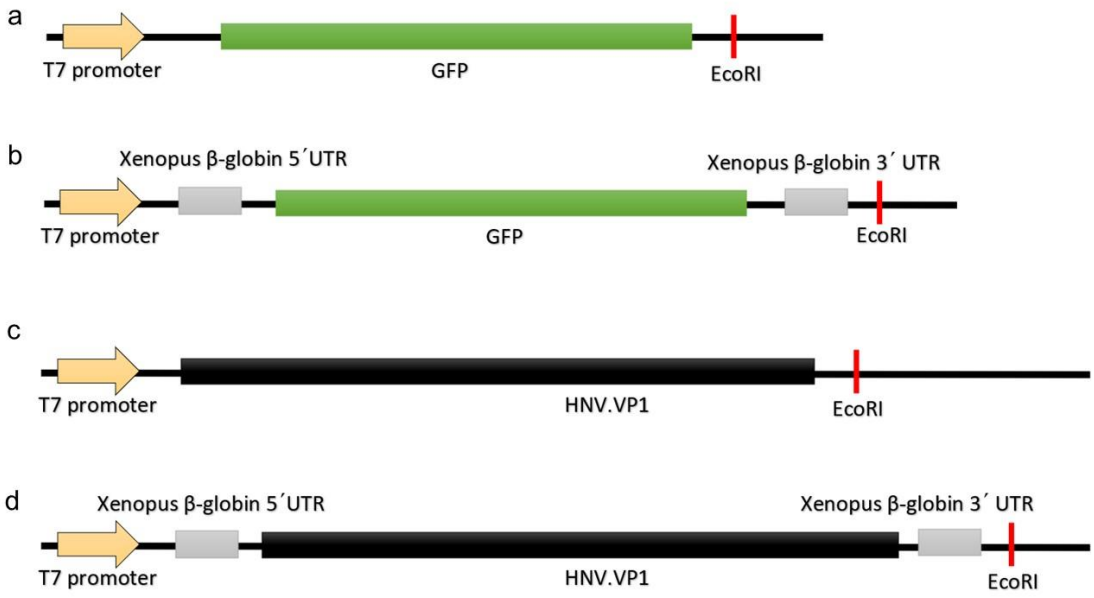

Fig 13. Schematic structure of Plasmid DNA construct for production of mRNA. Unmodified constructs of eGFP and VP1 genes (a, c), modified constructs (b, d).

2.4.2 in vitro production of mRNA constructs

In-vitro mRNA transcription was performed to synthesize the mRNAs, incorporating a 5´ Cap analog 3´-O-Me-7mG(ppp)G (ARCA), and a 3´ Poly-A tail. In the modified VP1 mRNA, 100 % substitution of UTP by Nucleoside modified mRNA Pseudo-UTP (Ψ) was also implemented. Figure 14, provides a schematic picture of unmodified and modified mRNA constructs.

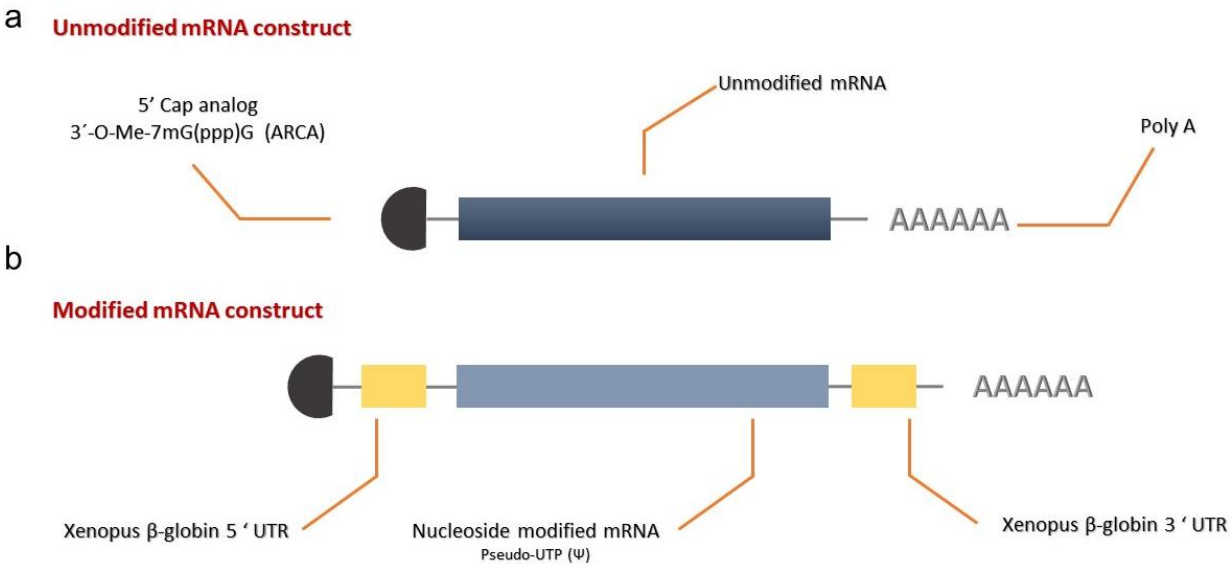

Fig 14. Schematic structure of in vitro synthesized mRNA constructs. Unmodified mRNA has only a 5 prime cap and a 3 prime poly A (a) but modified mRNA sequence is changed using 100 percent Pseudo-UTP (Ψ) modification and adding Xenopus β-globin UTRs (b).

After synthesizing the mRNA constructs, their size and integrity were assessed using denaturing gel electrophoresis method. As depicted in Figure 15, the produced mRNA showed a pure and intact band at the expected size. The concentration of the mRNAs was determined using Nanodrop and was within the range of 400 – 600 ng/µl.

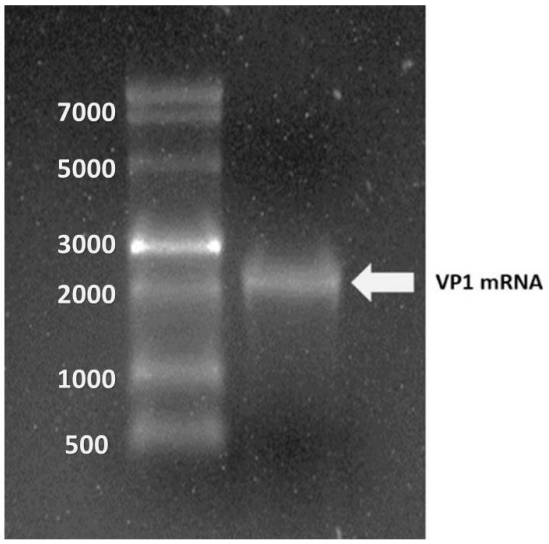

Fig 15. Gel electrophoresis of in vitro synthesized VP1 mRNA. As expected, the mRNA band appears in the range of 2K length.

2.4.3 In vitro characterization of mRNA constructs

To evaluate the capability and efficiency of mRNA constructs to be successfully translated in eukaryotic cells, we delivered them in to HEK293T cells using Lipofectamine 2000. As shown in Figure 16, both modified and unmodified GFP mRNA constructs were able to express GFP protein successfully.

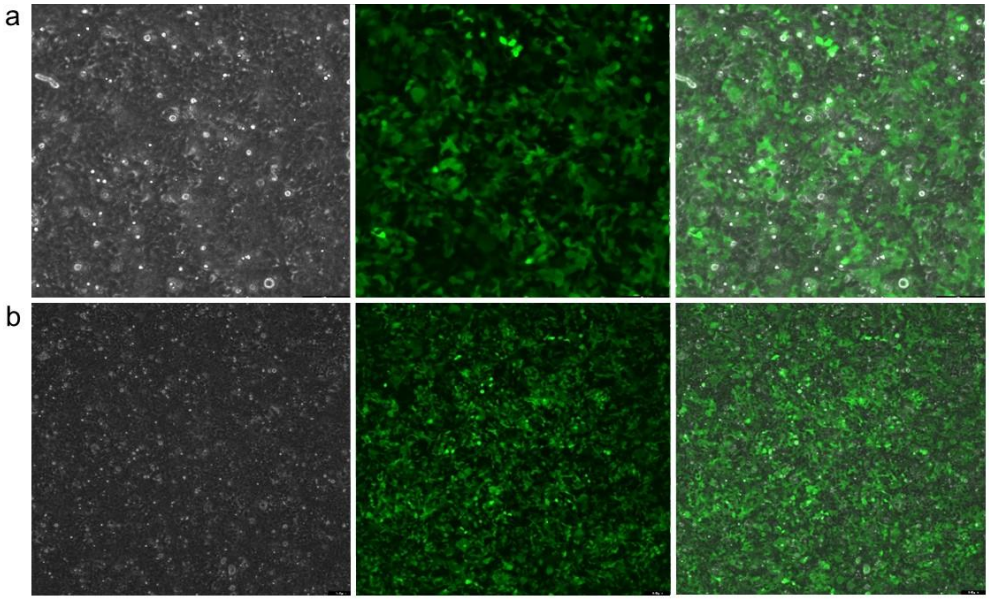

Fig 16. GFP mRNA transfection in HEK293T cells. Unmodified GFP mRNA transfection (a), Modified GFP mRNA transfection (b). The left images are phase contrast view, the middle images are fluorescent view, and the right images are overlay view. Both mRNA sample types were able to express the GFP gene which confirms the expected functionality of the mRNAs.

Subsequently, it was imperative to evaluate the capability and efficiency of VP1_mRNA constructs in VP1 expression *in vitro* using lipofectamine 2000. The VP1 expression was examined in the transfected HEK293T cells through Western blot 48 hours post-transfection, revealing the successful expression of NoV capsid protein with an approximate size of 56 KDa.

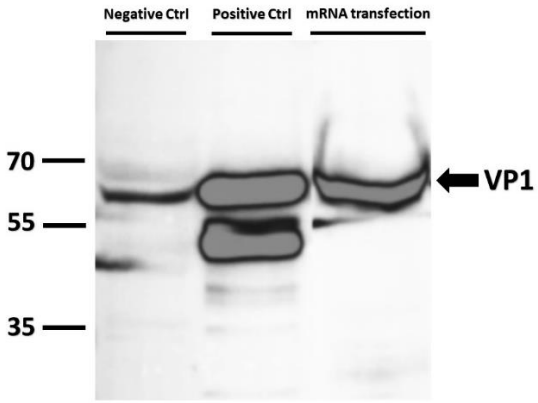

Fig 17. Expression of HuNoV VP1. Western blot imaging to screen the expression of HuNoV -VP1 protein in HEK293T cells transfected with in vitro synthesized mRNA constructs. The band below VP1 with a size of almost 55 kDa is the cleaved VP1 which is normally seen in WB for NoV capsid protein.

2.5 Lipid Nanoparticles (LNP) formulation of mRNA constructs

Once the quality and functionality of the in vitro synthesized mRNA constructs was evaluated and confirmed, mRNA constructs were encapsulated using LNP s (LNPs). The full and detailed preparation protocol is provided in section 4.2.26. Following the preparation of the GFP-mRNA LNP, we assessed size distribution and homogeneity of the sample using Dynamic Light Scattering (DLS) and Transmission Electron Microscopy. As shown in Figure 18 a, the autocorrelation function plot in DLS validated the high quality of data capturing within the sample. The y-intercept between 0.8 to 1, the exponential decay, and the zero baseline collectively confirm the data quality. The intensity size-distribution DLS plot shows the existing particle groups based on their hydrodynamic size. The presence of a single sharp peak in this plot (Figure 18 b) confirms the absence of additional particle populations, indicating the absence of aggregation and contamination within the sample. The PDI value below 0.2 also confirmed the homogeneity across the samples. The Z-Average value showed the mean size of 50 to 120 nm in our samples. In general, a size ranging from 10 to 150 nm is considered desirable for LNP intended for mRNA delivery *in vivo*. TEM imaging, depicted in Figure 18 C, also confirmed the presence of pure and undamaged LNPs in the samples, with sizes below 100 nm.

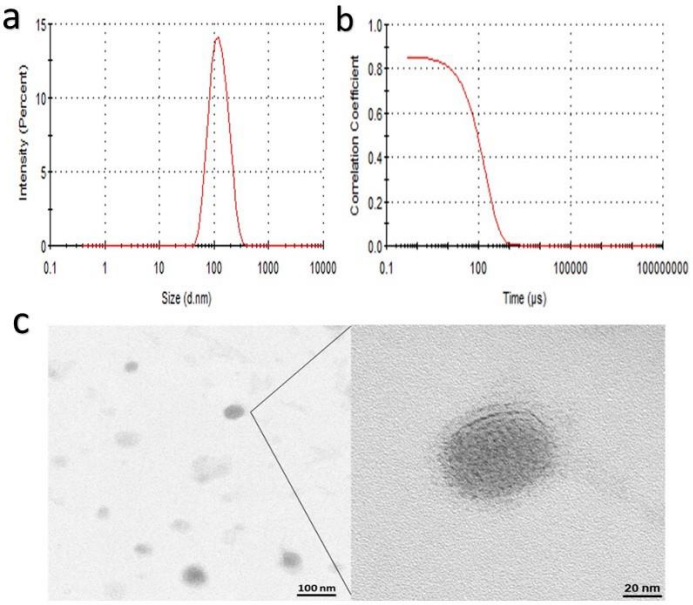

Fig 18. Physical characterization of LNP-mRNA particles. A single sharp peak in intensity size-distribution DLS plot confirms the homogeneity across the samples and the size range of nanoparticles with the the peak of 100 nm as the most abundant population size (a). The autocorrelation function plot validates the high quality of data capturing (b). The TEM shows the optimal homogeneity along with the sample and integrity and shape of the LNPs (c).

2.5.1 In vitro characterization of crude mRNA-loaded LNPs

Prior to purifying the mRNA-LNP samples, we checked the capability of crude LNPs to deliver the mRNA into Eukaryotic cells. Besides the GFP mRNA construct synthesized in our lab, a commercially obtained GFP mRNA control was included in the experiment (Fig 19). The HEK293T cells were transfected with the GFP mRNA-LNP samples and GFP expression was checked under fluorescence microscope. Monitoring GFP expression at different time points (Figure 20) revealed a gradual release of loaded mRNA from the LNP over time, reaching its peak within 48 hours.

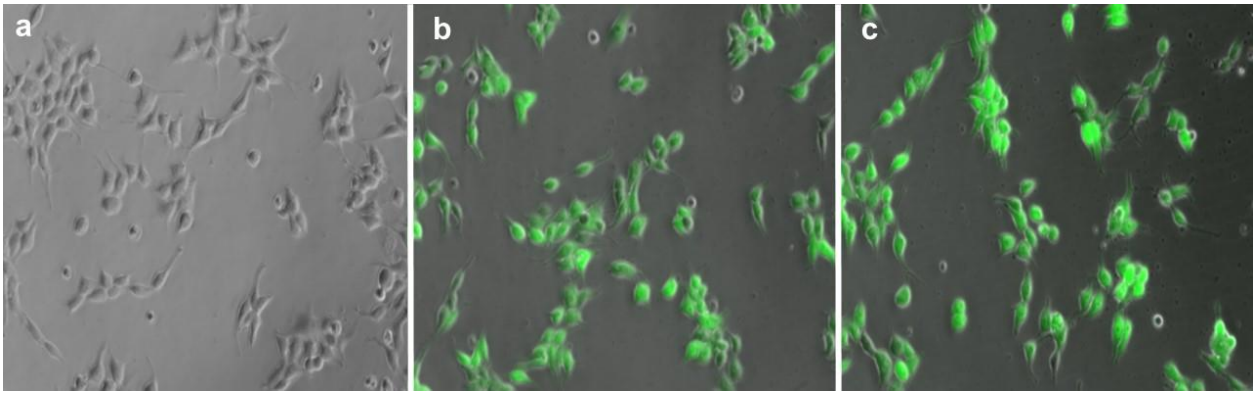

Fig 19. **Screening the expression efficiency of unpurified encapsulated mRNA constructs.** Transfection of 1µg mRNA in HEK cells (48 well plate format). Picture (b) shows the GFP expression of the encapsulated commercial mRNA. (c) shows the same concept but in the encapsulated in vitro synthesized mRNA group.

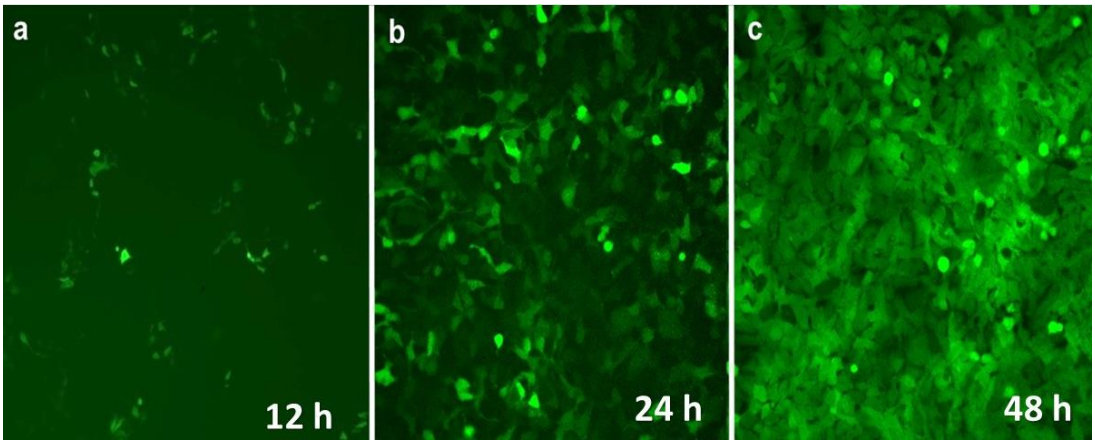

Fig 20. Screening the time dependency of protein expression after transfection of HEK293T cells with unpurified encapsulated mRNA constructs. Transfection of 1µg mRNA in HEK cells (48 well plate format). GFP expression was checked continuously for 2 days. the time points of 12 h(a), 24h (b) and 48h (c) are shown as representatives of time points. At 48 h post transfection almost 100 percent of the cells were green showing the optimal time for expression of protein in all cells.

To investigate whether transfection with LNP exhibits dose dependency, we transfected the cells with 125 ng, 250 ng, 500 ng, 1000 ng of mRNA then assessed the percentage of positive cells after 24 hours. Remarkably, all groups exhibited near 90 % positivity, regardless of the administered dose (Fig 21 a). The median fluorescence intensity (Figure 21 b) similarly did not show a meaningful difference among the three different dosages.

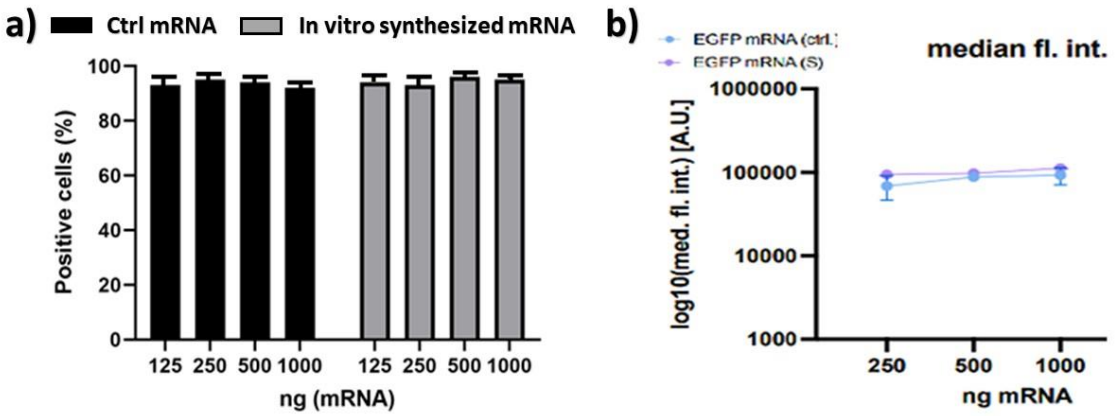

Fig 21. Screening the dose dependency of mRNA in transfection of HEK293T. A range of 125 to 1000 ng of mRNA was used t (48 well plate format) and no meaningful difference were seen in gene expression based on the percentage of positive cells (a) and median fluorescence intensity (b).

2.5.2 Encapsulation efficiency of crude mRNA in LNPs

It was also essential to check the encapsulation efficiency of mRNAs in the LNPs before purifying them. Encapsulation efficiency was determined using Quant-it™ RiboGreen RNA Assay-Kit. An untreated and a Triton X-100 treated version for each sample were prepared. In the untreated LNP samples, RiboGreen can only bind to free mRNA as it cannot penetrate the LNPs. In the Triton X-100 treated samples, the LNPs are destroyed by the detergent so the result here will be the total mRNA in the sample. By forming the ratio of untreated over treated samples and subtracting the result from 1 (1 - (untreated/treated)), we obtain the encapsulation efficiency. The experiment was performed using a starting mRNA material of 45 µg. The aim is to check before purification, how many percent of the mRNAs would be encapsulated. As shown in table X 33 µg of the whole mRNA was encapsulated, showing an encapsulation efficiency of 73%.

Table 1. Encapsulation efficiency of crude mRNA-LNP samples

	starting mRNA	**Free mRNA (ng/µl)**	**Encapsulated mRNA**	**Encapsulation efficiency**
Crude mRNA-LNP	**45 µg**	**9 µg**	**33 µg**	**73 %**

2.5.3 Purification and In vitro characterization of mRNA-loaded LNPs

As already discussed, we employed two different LNP purification methods: a) Dialysis membrane tubes, and b) Amicon ultra filter tubes. Before advancing to *in-vivo* studies, it was necessary to check the efficiency of both methods to recover prepared mRNA-LNP particles. The factor of freezing and thawing was also included in the experiment to check any negative effect of this process on LNPs. HEK293T cells were transfected with 1 µg of filter-purified (F), dialyzed (D), and their freeze-thawed versions (F_F, D_F). As shown in Figure 22, GFP expression was detected in all four conditions, confirming the functionality of recovered mRNA-LNPs from the purification methods

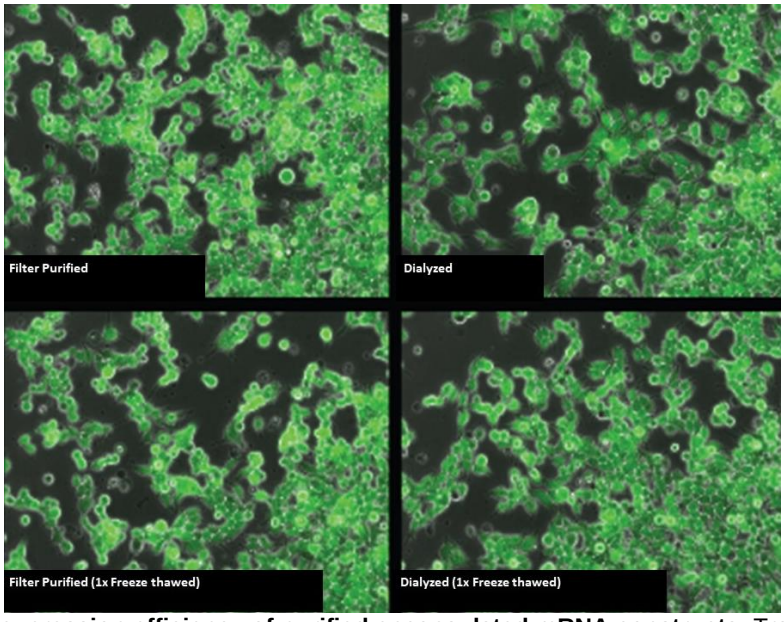

Fig 22. Screening the expression efficiency of purified encapsulated mRNA constructs. Transfection of 1µg mRNA in HEK cells (48 well plate format). Filter purified (left) and dialyzed (right) mRNA groups were compared. The samples went under a round of freeze thawing to asses if the process affects the expression negatively. In all of the conditions GFP expression was successful.

The percentage of GFP-positive cells and fluorescence intensity were measured in all conditions. Although no meaningful difference was detected in terms of the positive cell percentage, the was a subtle difference in intensity between conditions (Figure 23 a). As depicted in Figure 23 b, the freeze-thawing process has reduced the intensity in both filter-purified and dialyzed samples, suggesting a minor impact. Furthermore, the dialyzed samples (D, D_F) exhibited a higher intensity, indicating better quality and functionality compared to the filter-purified samples.

To check the expression efficiency of the modified and unmodified GII.4-VP1 mRNA-LNP samples, we conducted transfection in HEK293T cells and performed Western blot. Both mRNA constructs demonstrated successful expression of the NoV GII.4 VP1 protein.

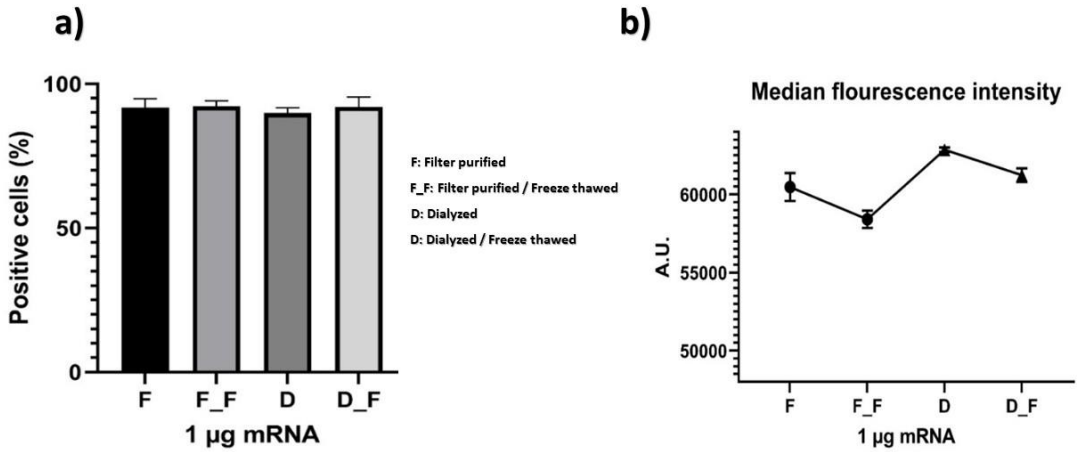

Fig 23. Screening the efficiency of LNP purification methods. 1000 ng of mRNA was used to transfect the HEK293 t cells (48 well plate format). Although no meaningful difference was seen in gene expression based on the percentage of positive cells (a) but the median fluorescence intensity plot weighs slightly towards the dialyzed samples (b).

Similar to the crude mRNA-loaded LNPs, we also assessed the encapsulation efficacy of the purified LNPs using Quant-it™ RiboGreen RNA Assay-Kit. The dialyzed samples showed a higher encapsulation efficiency compared to the filter-purified samples. In fact, the dialysis method yielded and recovered almost 20% more LNP-encapsulated mRNA. Although both purification methods successfully purified and recovered sufficient LNP-encapsulated mRNA, the dialysis method demonstrated superior performance and was selected as the final purification method for preparing our mRNA vaccine for *in-vivo* study.

Table 2. Encapsulation efficiency of purified mRNA-LNP samples

	starting mRNA	**Free mRNA (ng/µl)**	**Encapsulated mRNA**	**Encapsulation efficiency**
F	**150 µg**	**84 µg**	**66 µg**	**44 %**
F_F	**150 µg**	**91 µg**	**59 µg**	**39 %**
D	**150 µg**	**48 µg**	**102 µg**	**68 %**
D_F	**150 µg**	**56 µg**	**94 µg**	**62 %**

2.5.4 Cytotoxicity assay

The MTT assay was employed to assess the cytotoxicity effects of mRNA-loaded LNPs on HEK293T cells. The absorbance values obtained from the assay provides insights into cell viability and the potential toxic effects of the LNPs at different concentrations. As shown in Figure 23, at all the different doses, cell viability ranged between 90-95 %. These data indicated that the mRNA-LNP formula possesses an acceptable and safe profile in the term of cytotoxicity.

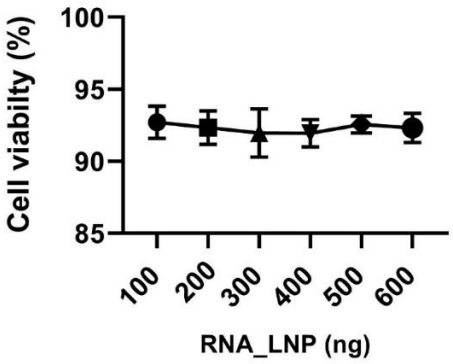

Fig 23. Cytotoxity evaluation of mRNA-LNP constructs. Different doses of mRNA were used to transfect the HEK293 t cells (48 well plate format) and after 24 h the MTT assay was performed. In all of the doses cell viability of almost 93% was confirmed.

2.6 Immunogenicity of mRNA vaccine in mice

To assess the efficacy of the mRNA vaccine candidates in inducing specific immunity to HuNoV GII.4 capsid protein, a comprehensive analysis was conducted, involving both naked and LNP-coated mRNA vaccines. The results demonstrated robust T cell responses in mice immunized with LNPs encapsulating unmodified or modified mRNAs, as evidenced by a significant increase in NoV-specific $CD4^+$ and $CD8^+$ T cells in splenocytes from vaccinated mice compared to the PBS and naked mRNA control groups, as summarized in Figure 24 a.

When analyzing the induction of $CD8^+$ T cell responses, the results demonstrated distinct differences among the vaccine groups. In contrast to the naked mRNA group, the groups receiving LNP-mRNA (unmodified and modified) exhibited significantly higher levels of $CD8^+$-$IFNg^+$ cells. The mean percentages of positive cells were 1.9% for LNPs loaded with unmodified-mRNA and 2.2% for modified mRNA-loaded LNPs. Moreover, the induction of $CD8^+$-$IL2^+$ cells, demonstrated similar trends. While the naked mRNA group showed a slight increase with a mean percentage of 0.013% positive cell, both LNP-mRNA groups exhibited

substantial induction of $CD8^+$-$IL2^+$ cells compared to the naked mRNA and PBS groups. These data suggest that LNP-formulated mRNAs enhance the development of NoV-specific $CD8^+$ T cell response which may contribute to long-lasting immune responses against NoV capsid protein.

Additionally, the study evaluated the induction of NoV-specific $CD4^+$ T cell responses to the vaccine candidates. The results showed marginal induction of $CD4^+$-$IFNg^+$ and $CD4^+$-$IL2^+$ cells in the mice immunized with the naked mRNA. In contrast, both LNP-mRNA groups displayed significantly higher levels of $CD4^+$-$IFNg^+$ and $CD4^+$-$IL2^+$ immune responses. This indicates that LNP formulation of mRNA vaccines effectively enhance CD4+ T cell responses to the target casid protein, further supporting their immunogenicity. Comparing the results among the different groups, LNPs consistently outperformed naked mRNA and PBS in terms of T cell response induction. Both LNP-mRNA formulations, unmodified and modified, demonstrated superior immunogenicity in inducing $CD8^+$ T cells immune responses compared to the naked mRNA and PBS. Furthermore, LNPs displayed a similar pattern in $CD4^+$ T cell responses. Overall, these results demonstrate the efficacy of LNPs as mRNA delivery tools for vaccine development. The significant increases in virus-specific $CD4^+$ and $CD8^+$ T cell responses, including the induction of IFN-γ and IL-2 producing cells, highlight the potential of LNP-encapsulated mRNA as a vaccine platform targeting the HuNoV GII.4 VP1 antigen. The superior immunogenicity observed in the LNP-formulated modified mRNA group suggests that mRNA modification within the LNPs may further enhance immune responses to the target antigen.

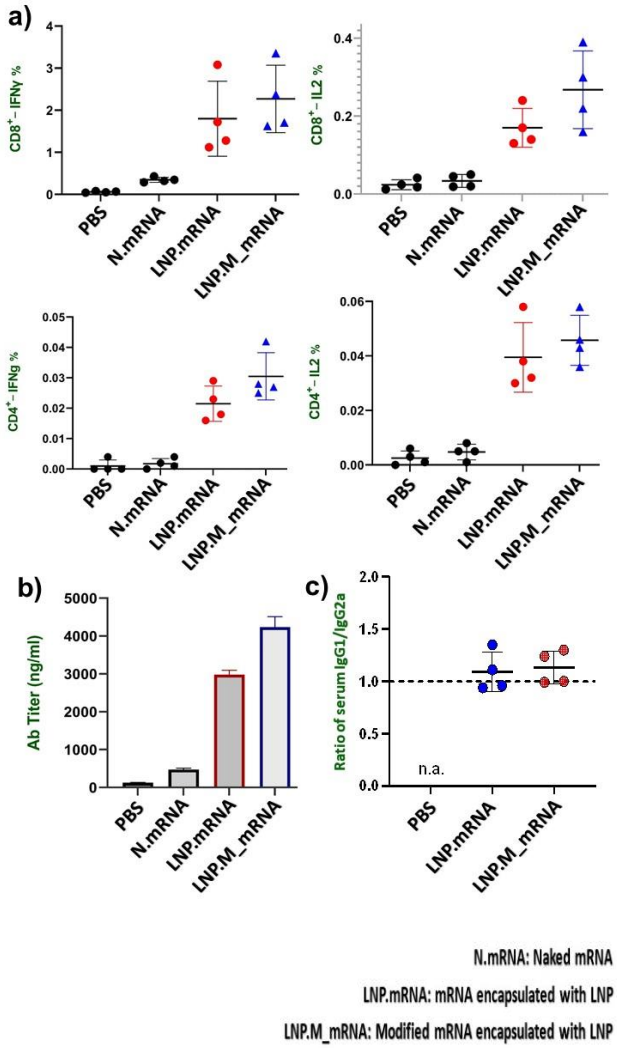

Figure 24. Evaluation of immune responses to mRNA vaccine. HuNoV -specific immune responses were tested in BALB/c mice immunized with LNP encapsulated mRNA vaccines. The encapsulated mRNA groups consisted of the normal/unmodified mRNA (LNP.mRNA) group and Modified mRNA (LNP.M_mRNA) group which went under 100% substitution of Uracil by Pseudouridine. The Naked mRNA group was considered as a control to compare the effect of the delivery system. The Splenocytes of the immunized mice were taken and stimulated with HuNoV GII.4 VP1 pooled peptides and stained for surface and intracellular markers. The measurements were performed using flowcytometry and ELISA techniques. After the last administration, immune responses were assessed in the mice: (a) specific CD8+ and CD4+ T-cell responses; (b) specific IgG Ab response; (c) serum IgG1 to IgG2a level ratio.

In addition to assessing the T cell response, we evaluated antibody (Ab) response in the vaccinated mice. The results revealed distinct differences among the groups. Compared to the PBS group, mice immunized with the naked mRNA displayed higher IgG Ab titer, with a mean value of 810 ng/ml. However, the groups receiving LNP-formulated mRNA (unmodified and modified) demonstrated substantially higher IgG Ab titers compared to both the naked mRNA and PBS groups with the mean Ab titer of 2988 ng/ml (for unmodified) and 4215 ng/ml (for modified), as shown in Figure 24 b. These findings indicate that LNPs, irrespective of

modification status, significantly enhance the induction of IgG antibody production. The substantial increase in IgG Ab titers observed in the LNP-mRNA groups suggests a robust humoral immune response against HuNoV GII.4. Furthermore, the higher IgG Ab titer in the LNP-modified mRNA group compared to the LNP-unmodified mRNA group indicates the potential of mRNA modification to further enhance humoral immune response to the target antigen. Comparing IgG Ab responses among the different groups, LNPs consistently outperformed naked mRNA and PBS in terms of antibody production. Both LNP-mRNA formulations, unmodified and modified, exhibited significantly higher IgG Ab titers compared to the naked mRNA and PBS. These findings highlight the superior immunogenicity of LNPs as mRNA delivery tools for stimulating robust humoral immune responses. Interestingly, vaccinated mice developed slightly higher IgG1 responsiveness than IgG2a to the NoV capsid protein, as shown in Figure 24.c. This suggests a tendency toward the induction of more Th2 responses than Th1 by the mRNA vaccines.

In summary, these findings provide further evidence of the enhanced immunogenicity of LNP-formulated mRNAs in promoting the production of antigen-specific antibodies. The significantly higher IgG Ab titers observed in the LNP-mRNA groups, particularly the LNP-modified mRNA group, underscore the potential of LNPs as a vaccine formulation platform for in vivo delivery of mRNA vaccine candidates against HuNoV.

3 Discussion

3.1 Generation of RecSeV Vector encoding HuNoV Capsid protein

The focus of the research is to generate recombinant SeV encoding HuNoV GII.4 capsid protein, with the aim of developing a potential vaccine candidate targeting the HuNoV GII.4 genotype. SeV holds significant promise as a candidate for human vaccination due to its unique attributes. It is recognized as a pathogen in mice, and importantly, it has not been associated with any known human diseases. Unlike some other vaccines, SeV is not based on an attenuated human virus, eliminating concerns about its potential to revert to a harmful state [112, 113]. What makes SeV particularly attractive is its ability to induce mammalian cells to express native antigens, complete with posttranslational modifications similar to the target antigens and their corresponding neutralizing epitopes during transient cellular development [114]. This feature also facilitates the robust activation of CD8+ T cells [115]. Most of the viral vaccines currently in use rely on pathogen proteins or live, attenuated, or inactivated viruses. Live attenuated vaccines have shown great efficacy in providing enduring immunity and in some cases, even eradicating diseases. However, they come with concerns about safety, primarily due to the potential for genetic instability and persistent virulence [116]. In the pursuit of achieving the highest level of protection against infectious diseases, innovative vaccine strategies hold promise.

The first step in development of the SeV vaccine involves modifying the construct to render it incapable of replication, aiming to create a safe and efficient platform for production of the HuNoV GII.4 capsid protein. Deficient SeV vector was generated by employing two key components: a subgenomic SeV vector and a full genome SeV vector. The subgenomic vector was modified by removing the N-terminal 76 amino acids of the Phosphoprotein, rendering it incapable of replication. The subgenomic plasmid was linearized, and the VP1 gene was inserted. This subgenomic vector was then combined with the full genome SeV vector, resulting in the replication-deficient SeV vector containing the HuNoV GII4 VP1 gene. The strategy capitalized on the unique transcription and replication features of the SeV, with closer proximity of the foreign reporter gene to the SeV genome leading to higher expression of the target foreign protein. This method has already been used by Marian Wiegand, where the primary goal of their study was to establish an innovative vaccine platform by harnessing a replication-deficient SeV vector, designed to express heterologous genes integrated into the viral genome. executing a multi-step process. They incorporated the ectodomain of the RSV fusion (F) protein and introduced the PIV3 fusion (F) and hemagglutinin-neuraminidase (HN)

genes into the vector genome. This resulted in the formation of a recombinant SeV genome, denoted as rc/rdPIRV, which adhered to the fundamental "rule of six" guidelines. This strategically engineered platform aimed to facilitate the development of vaccines against various viral pathogens by taking advantage of the unique properties of the SeV vector[123]. In their second study a a genome replication-deficient SeV (SeV) vector was constructed to target Respiratory Syncytial Virus (RSV). The construction strategy involved the precise insertion of the genetically stable RSV F-encoding gene into the vector by substituting the ectodomain of the SeV F gene with its RSV counterpart. This strategic modification yielded a chimeric vectored vaccine with the RSV F protein as an integral structural component, expressed on vaccine particles in its prefusion conformation. The procedure combined two existing Sendai vector constructs, prdPIRV and pSeV V31, involving *EcoR*I digestion to insert the RSV F gene fragment into the acceptor construct, ultimately resulting in the creation of the new pSeV 76 constructs. This approach laid the foundation for a replication-deficient SeV vector with potential applications in vaccine development [165].

As our research commenced towards the development of a robust vaccine against HuNoV, our primary objective was the comprehensive evaluation of the newly engineered SeV vaccine carrier. This investigation aimed to assess its efficacy, efficiency, and reliability across various dimensions. Specifically, we scrutinized the vector's replication capabilities, its gene expression proficiency, and the preservation of its structural integrity. The methodology for characterizing the SeV vector constructs *in vitro* involved Several key steps. First, the constructed recombinant vectors were subjected to Sanger sequencing to detect any potential mutations or inaccuracies. The sequencing covered the entire length of the recombinant rd-SeV -VP1 vector, confirming no mutations or sequence changes after cloning. Following this, the process of virus rescue and propagation was undertaken, where BSR-T7 cells were transfected with the recombinant rd.SeV .VP1 vector and helper plasmids encoding SeV N, P, and L proteins, monitored for successful expression using a fluorescence microscope. Virus propagation was achieved through infection of V3.10 helper cell lines and Subsequently virus purification. The collected supernatant was then loaded onto a 35% sucrose gradient and centrifuged to isolate the SeV pellet. Titration was conducted through a TCID-50 test, utilizing serial dilutions of the purified viruses and V3.10 cell infection to quantify live viral particles. SeV propagation was evaluated by overlaying the rescued virus on V3.10 cells (helper Vero cells). This assessment aimed to determine virus capability to express our target gene, HuNoV GII.4 VP1, which was screened by observing GFP expression under a fluorescence microscope. The vector's capability to propagate in non-helper cell lines was also examined. The expression of the HuNV.GII4 capsid protein was also confirmed by Western blotting. Additionally, electron microscopy was employed to confirm both the formation and integrity of the viral particles.

These results provide valuable insights into the capabilities of the SeV vector construct for vaccine development. Initial indications of protein expression were observed in BSRT7 cells after transfection with the corresponding plasmids. Notably, on day 6, we noted the onset of GFP expression in the infected cells, and by day 8, this expression had extended to neighboring cells, reaching almost 10 percent of positive cells. By day 12, GFP expression became more substantial, with approximately 20-30 percent of the cells exhibiting positivity. The observed expression pattern, driven by the GFP gene located at the end of the SeV genome, serves as a strong indicator of the SeV vector's proficiency in expressing both SeV and heterologous NoV capsid proteins. Furthermore, we explored the vector's capacity to express the heterologous gene by overlaying the rescued virus onto the helper Vero V3.10 cells. This *in vitro* assessment revealed that, remarkably, by day 6, nearly 100 percent of the cells exhibited GFP positivity. This robust expression in helper cells underscores the vector's potential to efficiently express the protein of interest. To further assess the vector's performance conditions mimicking *in vivo* administration to mice, we examined GFP expression in non-helper cells. Although the expression persisted, it was evident that non-helper cells yielded lower levels of expression and intensity. This signifies the vector's capacity to function at a diminished level under these conditions. To further substantiate the vector's potential, we examined the expression of the heterologous HuNoV VP1 gene via Western blot analysis. The detection of significant amounts of HUNOV -VP1 protein in the Western blot images reinforces the vector's competence in expressing our protein of interest. Moreover, virus particles were successfully purified using a sucrose gradient and screened through Transmission Electron Microscopy (TEM). The TEM images confirmed the presence of SeV particles in an intact form, exhibiting the anticipated size and shape. These results collectively highlight the robustness and reliability of the SeV vector construct, supporting its potential as a promising foundation for vaccine development against various viral pathogens. We found out that the engineered SeV, rendered incapable of replication, proved highly efficient in expressing the HuNoV GII4 VP1 gene. This was validated through careful analyses, including Western blotting and detailed observation using high-powered microscopes. These techniques revealed not only the successful expression of the gene but also the integrity of the virus particles. These data assure that this carrier could serve as a strong tool for delivering our target gene. This represents a solid starting point for advancing to the next steps in vaccine development.

In a similar study [165], a bivalent vaccine targeting human Parainfluenza Virus 3 (PIV3) and Respiratory Syncytial Virus (RSV) was generated using a SeV vector, termed rdPIRV. This vector successfully expressed the RSV F ectodomain encoding a soluble protein (sF), while replacing the SeV F and HN Open Reading Frames (ORFs) with their PIV3 counterparts. The resulting chimeric envelope proteins, F and HN from PIV3, served as antigens, both as

structural components of the viral vector particle and as proteins expressed within host cells. Safety measures were taken by rendering the Sendai vector replication-deficient, achieved by deleting the N-terminal 76 amino acids in the phosphoprotein (P) gene (Pdel). Through extensive sequencing and ten consecutive passages, the structural integrity and sequence stability of the vaccine vector were confirmed. To assess the replication deficiency and biodistribution of the vaccine vector, a series of experiments were conducted. Mice were intranasally inoculated with rdPIRV, and after three days, the presence of viral particles in various tissues and blood was determined. Notably, no viral particles of rdPIRV were detected in any of the examined animal tissues, demonstrating the vector's replication deficiency. In contrast, when a replication-competent SeV (SeV -E wt) expressing EGFP was used, viral particles were detected in the lungs but not in the blood. The study provided a solid foundation for the development of safe vaccines using this innovative viral vector platform, with a particular focus on its immunostimulatory potential. The results indicated that the deletion of amino acids 2–77 in the P gene effectively disabled the vector from generating progeny genomes in vivo, limiting the spread of replication-competent SeV to the respiratory tract. The animals exhibited no adverse effects, such as pain or weight loss, further emphasizing the safety profile of the vaccine vector.

3.2 Immunogenicity of recSeV -VP1 in mice

In the pursuit of developing a potent vaccine against HuNoV, a comprehensive investigation was essential to elucidate the immunological impact of the vaccine candidate. The principal objective of this phase of the study was to assess the vaccine's capacity to instigate a targeted immune response, with specific emphasis on T cell-mediated reactions. A diverse array of experimental techniques was employed to unravel the vaccine's proficiency in eliciting an immune response. The present study aimed to investigate the effectiveness of a replication-deficient vaccine candidate, r.d-SeV -VP1, in eliciting specific immunity to HuNoV VP1. The results reveal several key insights into the immune responses triggered by this vaccine, offering important implications for vaccine development and immunization strategies.

In this study, six groups of female BALB/c mice were subjected to immunization through both intranasal and intramuscular administration, involving low and high titer viral particle doses. Each group received three vaccinations, administered at two-week intervals, and mice were sacrificed ten days after the final vaccination. Spleen, lung, and blood samples were collected to evaluate the immune response. Splenocyte cells were prepared by isolating and processing spleen samples, followed by T cell stimulation with HuNoV GII.4 VP1 pooled peptides and control stimulants. The cells were assessed for cytokine production through intracellular

cytokine staining. The study encompassed both homologous and heterologous prime-boost vaccinations, which allowed for a thorough evaluation of the replication-deficient Sendai vector's immunogenicity. The findings suggest that r.d-SeV -VP1 has the capacity to stimulate robust $CD8^+$ responses specific to HuNoV VP1 in mice. These responses were characterized by the induction of IFN-γ and IL2 cytokines, highlighting the activation of T cell-mediated immunity. The dose-dependent effect observed in intranasal administration, with the high-dose regimen resulting in an enhanced $CD8^+$ response, emphasizes the importance of vaccine dosage in influencing the magnitude of the immune response.

Comparing different routes of administration, the study revealed that intramuscular injection of the vaccine candidates led to significantly higher NoV-specific $CD8^+$ responses compared to the intranasal route, regardless of the dose administered. This observation suggests that the choice of administration route plays a crucial role in shaping the magnitude and nature of the immune response. Furthermore, it underscores the importance of optimizing the delivery method for maximizing the vaccine's immunogenicity. To provide a more comprehensive assessment, the study incorporated a heterologous prime-boost strategy involving the MVA.VP1 vaccine vector. This approach served as a control for evaluating the immunogenicity of r.d-SeV -VP1 against a benchmark and explored the potential synergistic effects of different viral vectors in enhancing the immune response.

The results demonstrated that the combination of recSeV /VP1 and MVA.VP1 in a prime-boost regimen significantly augmented NoV-specific $CD8^+$ response. This suggests that the synergistic effects of multiple viral vectors can promote a more robust and effective immune response. This finding holds promise for the development of future vaccine strategies, where combining different vaccine platforms may enhance overall vaccine efficacy. The detailed analysis presented in this study provides strong evidence that the replication-deficient Sendai vector, r.d-SeV -VP1, possesses significant immunostimulatory properties. It induces robust $CD8^+$ responses specific to HuNoV VP1, emphasizing its potential as a promising candidate for the development of effective vaccines against HuNoV. The results also underscore the importance of dosage and administration route in vaccine design, highlighting the need for tailored immunization strategies. Moreover, the demonstration of synergistic effects through heterologous prime-boost regimens opens up new possibilities for designing more potent vaccines in the future. These findings contribute to our understanding of immune responses to novel vaccine candidates and their potential in combating infectious diseases like HuNoV.

A similar study [123] aimed to assess the vaccine's capacity to evoke PIV3- and RSV-specific T cell responses. The analysis began with an examination of IFN-γ and IL-5 cytokine production. The results demonstrated a substantial level of IFN-γ, signifying a robust Th1 response, while IL-5 remained undetectable. Remarkably, mice immunized with rcPIRV

exhibited higher IFN-γ production than their rdPIRV counterparts, underscoring the vaccine's impact on Th1 responses. Furthermore, the study explored the ability of rdPIRV immunization to elicit cytotoxic T cell responses against PIV3 and RSV. The findings illustrated specific cytolysis within splenocytes, particularly when exposed to target cells infected with PIV3 or RSV. Importantly, mice inoculated with rdPIRV or inactivated rdPIRV demonstrated similar CTL responses against PIV3, suggesting the capability of PIV3 antigens within the SeV envelope to induce cell-mediated immune responses. Conversely, inactivated rdPIRV-immunized individuals did not develop a CTL response against RSV due to the absence of antigen expression. In summary, the study showcased the broad immunostimulatory potential of replication-deficient Sendai vector-based vaccines, emphasizing the multifaceted pathways of antigen presentation and their influence on the immune response's magnitude and quality. Another study [165] aimed to determine whether the replication-deficient vaccine candidate could elicit a similar response. Spleen cells were isolated and in vitro stimulated with RSV-specific peptides and inactivated RSV to measure the expression of gamma interferon (IFN-γ) and interleukin 4 (IL-4) using enzyme-linked immunosorbent assay (ELISA). The results confirmed a clear stimulation of IFN-γ expression by the vaccine, with some surprising observations of low-level IFN-γ values in samples from SeV -GFP-immunized mice, indicating a possible contribution of the RSV antigen in the vaccine to IFN-γ expression. Additionally, IL-4 production was detected in splenocytes of SeV 76- and RSV-immunized mice, albeit at low levels, with no significant differences based on vaccine administration route. Furthermore, the study investigated the presence of RSV-specific cytotoxic T lymphocytes (CTLs), revealing the ability of SeV 76 to induce a robust cytotoxic T cell response, similar to live RSV. In contrast, neither the vector itself nor phosphate-buffered saline (PBS) induced any cytotoxic response against RSV-infected cells. These findings collectively underscore the capacity of the replication-deficient Sendai vector-based vaccine to effectively stimulate RSV-specific cellular immunity, offering promising insights into its immunogenic potential. These collective results reinforce the significance of the replication-deficient Sendai vector as a promising platform for developing effective vaccines against various infectious diseases and underscore the critical roles of dosage, administration route, and the synergistic effects of viral vectors in shaping immune responses.

To further assess the vaccine's immunogenicity, we examined antibody responses against HuNoV VP1 in the immunized mice. Specifically, we measured IgG- and IgA-specific antibody levels were assessed by ELISA, utilizing polystyrene 96-well plates coated with HuNoV VLPs. The results demonstrated that our vaccine successfully elicited a substantial level of NoV-specific antibodies through both intranasal (i.n.) and intramuscular (i.m.) administration routes. Notably, i.m. route administration resulted in a more potent IgG antibody response, surpassing the levels observed with both low and high doses of the i.n. route. This indicates that i.m.

administration route holds greater potential for inducing robust IgG antibody production in response to the vaccine. Furthermore, we explored the impact of heterologous prime-boost immunization employing the SeV /VP1 and MVA/VP1 viral vectors, comparing it to single administrations of either viral vector. The prime-boost regimen exhibited superior efficacy in inducing a higher NoV-specific antibody response when compared to the individual administrations of the viral vectors alone. This underscores the synergistic effect of combining the two viral vectors in promoting a more potent and targeted antibody response against HuNoV. Additionally, we explored the balance between two different types of immune responses, namely Th1- (IgG2a) and Th2-like (IgG1). In our viral vector vaccine study, we observed a subtle yet noteworthy shift in the IgG1/IgG2a ratio, revealing a skew towards IgG2a. This finding suggests that our viral vector vaccine elicits a Th1-biased immune response. In the context of our research, this is a positive outcome as a Th1 response, characterized by elevated IgG2a levels, is associated with potent cellular immunity. The prominence of IgG2a indicates an activation of cytotoxic T cells and enhanced phagocytic activity. These immune mechanisms are crucial for combating intracellular pathogens, such as viruses, and suggest that our viral vector vaccine holds promise in generating a robust and effective immune response. This aligns with our intended goal of developing a vaccine that can efficiently clear virally-infected cells, contributing to heightened protection against the targeted pathogen.

To assess the potential for mucosal immune responses, we examined lung and intestinal homogenates for NoV-specific IgA levels as an indicator. We observed a significant level of NoV-specific IgA response in lung homogenates, particularly with high doses of the viral vector, whereas only a minor level of secreted NoV-specific IgA was detected in intestinal homogenates of mice immunized with a high dose of the viral vector. These findings indicate that intranasal administration of recSeV GII.4 is much more effective in triggering mucosal immune responses, aligning with our expectations. This aligns with the findings of M Wiegand. et al, [165] where they demonstrated the capability of a replication-deficient SeV vector vaccine to generate substantial RSV-specific antibodies through both i.n. and i.m administration routes, with i.m. immunization resulting in a stronger IgG response. Notably, systemic vaccination appeared to trigger higher titers of neutralizing antibodies compared to mucosal vaccination, signifying a significant difference. Their results also revealed clear evidence of mucosal immune responses against RSV following i.n. immunization, whereas i.m. immunization did not result in specific mucosal IgA. A higher IgA level was observed in the nasal washes (NWs) compared to bronchoalveolar lavage (BAL) fluids, indicating the vaccine's effectiveness in creating a barrier at the site of virus entry. In contrast, mice immunized with SeV -GFP or PBS did not develop specific anti-RSV mucosal immunity.

We compared our findings with the findings of Li Guo, et. al study focusing on a different vaccine platform targeting HuNoV VP1 [86]. Our study demonstrated the ability of the replication-deficient Sendai vector, r.d-SeV-VP1, to induce robust CD8+ T cell responses specific to HuNoV VP1. These responses were characterized by the production of IFN-γ and IL2 cytokines, indicating activation of T cell-mediated immunity. Similarly, they observed strong humoral immune responses in mice following intranasal administration of a recombinant adenovirus (rvAdGGII4) targeting NV VLPs. Both studies reported significant increases in specific antibody titers, indicating effective stimulation of the humoral immune response. While our study focused on a replication-deficient Sendai vector, they utilized a recombinant adenovirus as the vaccine platform. Despite the differences in vector types, both studies achieved potent immune responses against their respective target antigens. Our findings highlight the potential of the Sendai vector in eliciting robust cellular immunity, while they showcased the adenovirus vector's ability to induce strong humoral and cellular immune responses. We investigated the influence of different routes of administration on vaccine-induced immune responses. Our results demonstrated that intramuscular injection resulted in higher CD8+ T cell responses compared to intranasal administration. This observation aligns with Li Guo, et. Al findings, which also observed strong mucosal immune responses following intranasal administration of the recombinant adenovirus. These findings underscore the importance of optimizing the route of administration to maximize vaccine immunogenicity. Both studies explored the use of heterologous prime-boost regimens to enhance vaccine efficacy. We demonstrated a synergistic effect between the replication-deficient Sendai vector and the MVA.VP1 vaccine vector, resulting in augmented CD8+ T cell responses. Similarly, they observed superior antibody and cellular immune responses following prime-boost immunization with rvAdGGII4. These results highlight the potential of heterologous prime-boost strategies in enhancing vaccine-induced immune responses. Both of our studies, contribute valuable insights into the development of effective vaccines against viral pathogens. Our study demonstrates the potential of the replication-deficient Sendai vector as a promising vaccine platform for HuNoV, while the latter underscores the efficacy of recombinant adenovirus-based vaccines against HuNoV. By elucidating the mechanisms underlying vaccine-induced immune responses, both studies provide important considerations for future vaccine design and development efforts.

Our study's results also demonstrate the vaccine's effectiveness in triggering a robust immune response against HuNoV GII.4 capsid protein. Both intranasal (i.n.) and intramuscular (i.m.) administration routes proved successful in generating specific antibodies against HuNoV . Notably, i.m. administration outperformed the i.n. route, suggesting its potential for inducing potent antibody production. The investigation of heterologous prime-boost immunization using SeV /VP1 and MVA/VP1 viral vectors indicated a synergistic effect, resulting in a more robust

and targeted antibody response against HuNoV. These findings collectively highlight the vaccine's promise as a viable candidate for the development of effective vaccines against HuNoV offering a strong foundation for further research and potential clinical applications.

These results embarked on the formidable task of developing a vaccine against the HuNoV, a pathogen responsible for a significant burden of acute gastroenteritis cases worldwide. We acknowledge the profound challenges inherent in HuNoV vaccine development, including the lack of suitable infection models, universal susceptibility across age groups, extensive viral strain diversity, and the difficulty in achieving cross-reactive immunity. These challenges emphasize the critical need for innovative vaccine platforms capable of effectively addressing this pervasive and highly transmissible pathogen. Our research introduces the SeV vector as a promising candidate in the pursuit of a HuNoV vaccine. We have meticulously elucidated the attributes that make the SeV vector an attractive choice, such as its benign nature in humans, adaptability to replicate in various mammalian cell lines, and potential for intranasal administration. These inherent features collectively position the SeV vector as a promising avenue for overcoming the fundamental limitations that have impeded progress in other vaccine platforms.

In conclusion, our meticulous analysis provides compelling evidence that the replication-deficient Sendai vector, specifically in the form of r.d-SeV -VP1, possesses substantial immunostimulatory properties. Through both similar and dissimilar vaccination approaches, we observed the induction of robust NoV-specific $CD8^+$ responses. The data obtained from our study contributes significantly to a deeper understanding of the immune response elicited by this vaccine candidate and underscores its potential as a promising approach in the development of effective vaccines against HuNoV. However, it is crucial for future research to delve into the durability and long-term effectiveness of these immune responses, an essential facet of vaccine development that requires sustained attention. In closing, our study introduces an innovative approach to tackle the formidable challenge of developing a HuNoV vaccine. The replication-deficient SeV vector platform emerges as a potent contender, eliciting robust immune responses, encompassing both cellular and humoral facets, within a preclinical model. These findings kindle optimism for the development of a much-needed HuNoV vaccine. Our methodology and comprehensive characterizations offer insights that transcend the confines of HuNoV vaccine research and extend to the broader realm of vaccine development.

3.3 Generation and Characterization of mRNA-based Vaccine Against HuNoV GII.4

The exploration of RNA vaccines as a groundbreaking alternative to traditional vaccination has evolved through a captivating historical journey. Starting with initial experiments injecting reporter gene mRNAs into mice in 1990, the success of in vitro transcribed (IVT) mRNA in animals marked a promising but cautiously approached development due to concerns like mRNA instability [166]. Recent advancements, however, have propelled mRNA to the forefront of therapeutic tools, particularly in protein replacement treatments and vaccine development. Conventional mRNA vaccines rely on the synergy between mRNA and its delivery method to trigger the production of antigens, activating adaptive immunity. This involves encoding proteins or polypeptides using T7 RNA polymerase. mRNA must possess essential elements like the 5 cap, 3 and 5 untranslated regions, nucleotide modifications, and a poly(A) tail for effective translation [167]. Advantages of mRNA vaccines include inducing both antibody and $CD8^+$ T cell responses, rapid production capabilities crucial for pandemic response, innate immune properties obviating the need for additional adjuvants, and efficient antigen production compared to DNA vaccines. However, challenges exist, including safety concerns, storage issues, and the need for mRNA and delivery system modifications. Two forms of RNA, non-replicating and self-amplifying, are under investigation for vaccine development, with careful optimization of translation and stability. Flanking UTR regions and synthetic modifications, such as introducing synthetic caps or altering poly(A) tail length, play pivotal roles in this optimization. G:C composition enrichment shows promise in elevating mRNA levels and protein expression [129]. The decision to focus on an mRNA vaccine is grounded in the dynamic landscape of nucleic acid therapies, which, despite early promising breakthroughs in the 1990s, witnessed a cautious adoption due to concerns surrounding mRNA stability, immunogenicity, and efficient in vivo transport. The reluctance to explore mRNA therapeutics was further fueled by the development of strategies centered around proteins and DNA. However, recent technological advancements and substantial research investments have reignited interest in mRNA, showcasing its potential as a versatile tool in the realms of protein replacement and vaccine development [168].

Our endeavor to create an mRNA vaccine targeting the HuNoV GII4 VP1 involved a meticulous synthesis process. The gene was cloned into a pcDNA 3.1 (-) plasmid, incorporating a T7 promoter for precise control over in-vitro mRNA synthesis. The synthesis itself was carried out using the T7 MegaScript RNA synthesis kit, where a G-(5')-ppp-(5')-A RNA Cap Structure Analog was employed for capping, ensuring the production of mRNA with a cap structure vital for effective protein translation. Furthermore, we opted for a sequence modification strategy, substituting 100% of UTP with Pseudo-UTP. This modification is crucial for optimizing the

translation process, enhancing the stability and efficiency of the synthesized mRNA. Subsequent steps, including DNase treatment and polyadenylation, were meticulously executed to ensure the purity and functionality of the synthesized mRNA. Following synthesis, the mRNA underwent purification using the Monarch RNA Cleanup kit, a critical step to eliminate impurities and confirm the integrity of the mRNA constructs. The concentration of the synthesized mRNA was accurately measured using Nanodrop, providing essential information for subsequent steps. To visualize and assess the integrity and size of the mRNA constructs, we employed denaturing agarose gel electrophoresis. This technique confirmed the purity and integrity of the synthesized mRNA, with distinct bands observed at the expected sizes, a testament to the success of our synthesis and purification processes.

The *in vitro* characterization of the mRNA constructs was a pivotal phase in our study. Transfection into HEK293T cells using Lipofectamine 2000 allowed us to evaluate the ability of the mRNA constructs to be successfully translated in eukaryotic cells. Utilizing eGFP mRNA as a positive control, we observed green fluorescence within 12-72 hours, confirming successful transfection. Building on this success, the transfection of VP1 mRNA constructs was undertaken. Post-transfection, cells were harvested, and VP1 expression was confirmed through Western blotting, providing a detailed insight into the protein expression efficiency of our mRNA constructs. The synthesis, purification, and *in vitro* characterization processes collectively laid a robust foundation for our mRNA vaccine development. The careful optimization of mRNA translation and stability, including capping, sequence modification, and polyadenylation, ensured the production of high-quality mRNA constructs. The successful transfection and subsequent protein expression underscore the potential of our mRNA constructs as a platform for vaccine development. The positive outcomes of the *in vitro* evaluations pave the way for further exploration, potentially propelling mRNA-based therapeutics into the forefront of vaccine development, offering rapid production, enhanced adaptability, and potent immune responses. In conclusion, our study represents a significant stride in the ongoing narrative of mRNA therapeutics, showcasing the viability of mRNA vaccines and their potential applications in addressing pressing healthcare challenges. The success of our synthesis and evaluation processes positions mRNA as a formidable tool, providing a robust basis for future research and development endeavors in the realm of nucleic acid-based therapies.

3.4 Generation of Lipid-based Nanoparticle for in vivo Delivery of NoV mRNA Vaccine

LNP s (LNPs) have emerged as a transformative platform in recent years, particularly in the context of RNA-based therapies and vaccine development. The unique properties of LNPs make them an attractive option for the efficient delivery of RNA molecules, addressing the inherent challenges associated with the hydrophilic and negatively charged nature of naked RNA. LNPs offer a protective and effective means of transporting RNA payloads across cellular barriers, safeguarding them against rapid degradation by ubiquitous RNases. LNPs have demonstrated remarkable potential for the delivery of various nucleic acids, including messenger RNA (mRNA), small interfering RNA (siRNA), and plasmid DNA (pDNA). These nucleic acids play pivotal roles in modern therapeutic strategies, from gene-based treatments to the development of RNA vaccines [169, 170]. By utilizing LNPs, we harnessed the capacity of these nanoparticles to encapsulate and transport this crucial therapeutic cargo. We employed meticulous methods for LNP preparation, with a focus on self-assembly based on intermolecular interactions. The core of LNP preparation hinges on the electrostatic interaction between positively charged lipids and negatively charged nucleic acids, leading to the spontaneous assembly of lipid components into nanoscale particles. Our commitment to the rigorous preparation of LNPs was driven by the necessity to provide a stable and controlled platform for RNA delivery. The self-assembly process of LNPs involves complex interactions between lipid components and RNA molecules, necessitating fine-tuning of parameters such as molar ratio and lipid composition. The choice of preparation method significantly influences the resulting LNP structure, cargo loading effectiveness, and the overall performance of these nanocarriers [171, 172].

This study employed a multifaceted approach in the development and evaluation of LNP s (LNPs) for the delivery of RNA therapeutics. Crucial elements included the precise tuning of the N:P ratio, where the positively charged amino groups in cationic lipids and negatively charged phosphate groups in nucleic acids were balanced to optimize encapsulation and prevent toxicity. LNPs were carefully prepared by selecting specific lipids, including 1,2-DSPC, cholesterol, DMG-PEG, and SM-102, which were meticulously diluted in absolute ethanol to form a critical lipid mixture. To ensure purity, the LNPs underwent purification using both filter purification and dialysis methods, tailoring the purification technique based on the specific needs of various nucleic acid constructs and sizes. Long-term stability was addressed through freezing, utilizing a solution with TRIS-HCl and sucrose as a cryoprotectant. The encapsulation efficiency of LNPs was thoroughly assessed using the Quant-it™ RiboGreen RNA Assay-Kit, allowing the secure containment of RNA molecules to be evaluated. Furthermore, potential

cytotoxicity was evaluated using the MTT assay, providing insights into the safety of LNP-RNA concerning cell viability. Together, these methods ensured a comprehensive and rigorous examination of LNPs for their potential as a versatile platform for RNA-based therapeutics.

The results of this study provide a multifaceted understanding of the physical and functional characteristics of LNP s (LNPs) as carriers for mRNA delivery, with a particular emphasis on the impact of purification methods. The use of Dynamic Light Scattering (DLS) and Transmission Electron Microscopy (TEM) allowed for a thorough examination of the physical attributes of LNPs. DLS analysis revealed a homogenous size distribution, crucial for effective delivery, with Z-Average values consistently falling within the desirable range of 50 to 120 nm. The low polydispersity index (PDI) below 0.2 underscored the uniformity of the LNPs, affirming their suitability for application in both animal and human models. TEM images further confirmed the purity and undamaged nature of the LNPs, verifying their appropriateness for mRNA delivery. *In vitro* characterization of crude mRNA-LNPs provided valuable insights into their functional performance. The gradual release of mRNA over time, reaching peak expression within 48 hours, showcased the sustained and efficient delivery capabilities of the LNPs. The transfection experiments demonstrated a high efficiency rate across varying mRNA doses, indicating the robustness of the delivery system. Notably, the investigation into encapsulation efficiency emerged as a critical aspect, shedding light on the pivotal role of purification methods in optimizing LNP functionality. Purification methods, namely filter purification and dialysis, were evaluated for their efficiency in recovering prepared mRNA-LNP particles. The choice of purification method was found to significantly impact both recovery and functionality. Encapsulation efficiency measurements revealed that dialysis outperformed filter purification. The dialyzed method exhibited almost 20% more LNP-encapsulated mRNA compared to filter purification, emphasizing its superiority in preserving the integrity of LNPs during the purification process. The meticulous comparison between these methods revealed that while both were capable of successfully purifying and recovering LNP-encapsulated mRNA, dialysis stood out as the preferred method for preparing mRNA vaccines for in-vivo study. Furthermore, freeze-thawing, included in the experimental design, showed a subtle reduction in intensity in both filter-purified and dialyzed samples, highlighting the importance of considering potential impacts on LNP quality during the purification process. The cytotoxicity assay, a crucial aspect of evaluating the safety profile of the mRNA-LNP formula, consistently demonstrated high cell viability (90-95%) across different doses, further supporting the overall safety and acceptability of the formulated LNPs. In conclusion, this detailed analysis underscores the intricate interplay between physical and functional aspects of LNPs, with a specific focus on the pivotal role of purification methods. The results advocate for the careful consideration of purification strategies to enhance LNP recovery and functionality, offering valuable insights for the ongoing optimization of LNPs as effective carriers for mRNA delivery in therapeutic applications.

3.5 Immunogenicity of NoV mRNA Vaccine in Mice

In order to develop an efficacious mRNA vaccine targeting HuNoV GII.4 VP1 antigen, a comprehensive investigation was undertaken to unravel the immunological impact of various vaccine formulations. The study comprised four distinct groups of female BALB/c mice, each receiving different mRNA formulations: naked mRNA, encapsulated unmodified mRNA, encapsulated modified mRNA, and a control group receiving PBS. The mice underwent three inoculations at two-week intervals, with sacrifice and sample collection occurring ten days after the final administration. Splenocyte cells were meticulously prepared, involving the smashing of the spleen, washing, and resuspension in ACK buffer. The subsequent steps ensured the isolation of cells for further analysis, providing a foundation for assessing the immune response. A 96-well flat plate served as the platform for T cell stimulation, utilizing HuNoV GII.4 VP1 pooled peptides. Positive control samples were included to validate the responsiveness of the cells. The subsequent incubation facilitated the assessment of the T cell-mediated responses, crucial for understanding the efficacy of the mRNA vaccine. Viability dye and specific antibodies were applied to stained cells, allowing for the identification and quantification of $CD4^+$ and $CD8^+$ T cells. The staining protocol provided insights into the cytokine production, including IFNγ, IL-2, and TNFα, indicative of the T cell activation profile.

The T cell response is a critical aspect of vaccine efficacy, and the study's results underscore the robustness of T cell activation induced by LNPs encapsulating unmodified and modified mRNA. The significant increase in virus-specific $CD4^+$ and $CD8^+$ T cells in splenocytes from vaccinated mice is indicative of a potent cellular immune response. This outcome aligns with the fundamental goal of vaccination to prime the immune system for a rapid and effective response upon encountering the target antigen. The induction of $CD8^+$-$IFN\gamma^+$ cells is a particularly noteworthy result, revealing distinct differences among the vaccine groups. Both LNP-mRNA formulations exhibited significantly higher levels of $CD8^+$-$IFNg^+$ cells compared to the naked mRNA and PBS groups. This finding suggests that the encapsulation of mRNA within LNPs enhances the generation of $CD8^+$ T cells capable of producing IFNγ, a key cytokine associated with antiviral immunity. Furthermore, the concurrent induction of $CD8^+$-$IL2^+$ cells in the LNP-mRNA groups, surpassing levels observed in the naked mRNA and PBS groups, implies an augmented development of $CD8^+$ T cell memory. The ability to stimulate long-lasting immune responses against the GII.4 HuNoV VP1 antigen is a crucial aspect for the durability of vaccine protection. The evaluation of $CD4^+$ T cell responses provides additional layers of understanding, particularly in the context of LNPs' impact. While the naked mRNA group showed marginal induction of $CD4^+$-$IFN\gamma^+$ and $CD4^+$-$IL2^+$ cells, both LNP-mRNA groups exhibited significantly higher levels. This result suggests that LNPs play a pivotal role

in enhancing $CD4^+$ T cell responses, contributing to a more comprehensive and coordinated immune reaction. The superior immunogenicity observed in the LNP-mRNA (modified) group, with even higher mean percentages of $CD4^+$-IFNγ+ and $CD4^+$-$IL2^+$ cells, indicates that mRNA modification within LNPs may act synergistically to further augment the $CD4^+$ T cell response. Comparing the results among the different groups provides a comprehensive perspective on the efficacy of mRNA vaccine formulations. LNPs consistently outperformed both the naked mRNA and PBS groups in terms of T cell response induction, showcasing their superior immunogenicity. This observation holds true for both $CD8^+$ and $CD4^+$ T cell responses, emphasizing the pivotal role of LNPs in shaping a robust and balanced immune response. Moreover, the superiority of the LNP-mRNA (modified) group in inducing $CD8^+$ and $CD4^+$ T cell responses suggests that mRNA modification within LNPs is a crucial factor in enhancing the overall immune response. The potential synergistic effects of mRNA modification in combination with LNP delivery may open new avenues for optimizing mRNA vaccine design, further enhancing their effectiveness.

The evaluation of specific antibody responses is crucial for understanding the humoral immunity generated by HuNoV GII.4-targeting mRNA vaccine. The study employed a well-established quantitative ELISA to measure IgG antibody titers in the mouse sera. The outcomes revealed compelling insights, shedding light on the effectiveness of mRNA vaccine formulation in inducing humoral immune responses. The comparison between vaccinated groups highlights notable differences in IgG antibody production. Mice immunized with naked mRNA displayed a higher IgG antibody titer compared to the PBS group, emphasizing the immunogenic potential of the mRNA vaccine. However, the groups that received LNPs loaded with unmodified and modified mRNAs exhibited substantially higher IgG antibody titers compared to both the naked mRNA and PBS groups. This substantial increase in IgG antibody production, with the mean titers of 2988 and 4215 ng/ml for unmodified mRNA- and modified mRNA loaded LNP, respectively, indicates a robust and enhanced humoral immune response against the HuNoV GII.4. The consistent outperformance of LNPs, regardless of modification status, emphasizes their role as potent mRNA delivery tools. LNPs significantly enhance the induction of IgG antibody production, surpassing the levels observed in both Naked mRNA and PBS groups. This finding underscores the superior immunogenicity of LNPs, aligning with their efficacy in promoting robust humoral immune responses. Furthermore, the higher IgG antibody titer observed in mice vaccinated with the modified mRNA-loaded LNP, compared to the unmodified mRNA-loaded LNP group, indicates that mRNA modification has the potential to further enhance the humoral immune response. This observation opens avenues for optimizing mRNA vaccine design, exploring modifications that augment antibody production and potentially contribute to heightened vaccine efficacy. Comparing IgG antibody responses among different groups provides a comprehensive perspective on the performance of vaccine

formulations. LNPs consistently outperformed naked mRNA and PBS in terms of antibody production, emphasizing the pivotal role of LNPs in shaping a robust humoral immune response. The results of the IgG antibody response analysis hold significant implications for the design and development of mRNA vaccines targeting infectious diseases, including HuNoV . The substantial increase in IgG antibody titers observed in the mice immunized with mRNA-loaded LNPs, particularly the modified mRNA group, underscores the potential of LNPs as a vaccine platform for the development of effective vaccines against the target antigen. Moreover, we measured the IgG1 to IgG2a ratio in response to the NoV capsid protein. The vaccinated mice exhibited a slight but discernible inclination towards higher IgG1 responsiveness compared to IgG2a. This finding implies a tendency towards the induction of more Th2 responses than Th1 by our mRNA vaccine. The elevated IgG1 levels are indicative of a Th2-biased immune response, which is typically associated with antibody-mediated immunity and an increased production of neutralizing antibodies. While a Th2 response can be beneficial in certain contexts, particularly for extracellular pathogens, it's crucial to consider the specific goals of our vaccine and the characteristics of the targeted virus. The observed Th2 bias suggests that our mRNA vaccine may be particularly effective in eliciting humoral immune responses, which could play a significant role in neutralizing the virus. However, the ideal balance between Th1 and Th2 responses may vary depending on the nature of the targeted pathogen. Further investigation is warranted to determine the implications of this immune profile and to assess the overall effectiveness of our mRNA vaccine in conferring protection against the NoV capsid protein.

This finding presents a striking parallel to the results of a recent study, which explored the immunogenicity of LNP-mRNA vaccines targeting rotavirus VP8 protein in rodents [164]. A remarkable convergence emerged in the T cell responses induced by LNP-mRNA vaccines in both studies. Our study documented a significant increase in NoV-specific CD4+ and CD8+ T cell populations in the spleens of vaccinated mice. Similarly, they reported substantial T cell responses in mice immunized with LNP-mRNA-VP8. This shared induction of both CD4+ and CD8+ T cells suggests that LNP-mRNA vaccines may trigger a multifaceted T cell response, potentially leading to a more comprehensive immunological attack against viral infection. The data from both studies paint a compelling picture of robust humoral immunity elicited by LNP-mRNA vaccines. Our study observed a significant elevation of IgG antibody titers in mice immunized with LNP-mRNA vaccines compared to the naked mRNA group. Similarly, they demonstrated the successful induction of virus-neutralizing antibodies against rotavirus in mice vaccinated with LNP-mRNA-VP8. Both studies provide resounding evidence for the superiority of LNP-encapsulated mRNA vaccines compared to their naked mRNA counterparts. Our data clearly showed that LNPs significantly enhanced both T cell responses and antibody titers. Likewise, they demonstrated the superior immunogenicity of LNP-mRNA vaccines encoding

VP8* in inducing antibody responses. This collective evidence strongly suggests that LNPs play a critical role in delivering and amplifying the immune response potential of mRNA vaccines.

In conclusion, the significantly higher IgG antibody titers observed in the LNP-mRNA groups, particularly the LNPs loaded with modified mRNA, highlight the potential of LNPs as a robust mRNA delivery platform. These findings contribute to the growing body of evidence supporting the effectiveness of LNPs in promoting specific antibody production, emphasizing their role in the development of potent mRNA vaccines against the HuNoV GII.4. The study serves as a valuable contribution to the field, guiding future endeavors in mRNA vaccine design and translational research.

4 Material and Methods

4.1 Materials

4.1.1 Devices and technical equipment

Centrifuge 5920R	Eppendorf
CytoFLEX S	Beckman Coulter
ELISA-Reader infinite F200	Tecan
Western Blotting device Trans Plot SD	Bio-Rad
Tecnai T12 transmission electron microscope (TEM)	FEI
Fusion Fx7	Peqlab
ECL CHEMOCAM imager	INTAS
Incubator Heracell 150	Heraeus Holding GmbH
LightCycler® 480 II	Roche Diagnostics
NanoDrop One	Thermo Scientific
Nanophotometer OD600	IMPLEN GmbH
Shaker and incubator for bacteria	INFORS AG; Heraeus Holding GmbH
Sterile hood HERA safe	Thermo Scientific
Table-top centrifuge 5417R	Eppendorf
Thermo Mixer F1.5	Eppendorf
Water bath WNB 10	Memmert GmbH

Agarose Gel electrophoresis device Bio Rad power bank basic	PegLab
Accu Jet® pro	Brand
Digital lab scale balance analytical PC440	Mettler-Toledo
FiveEasyPlusTM pH Meters	Mettler-Toledo
Fluorescence microscope DMi8	Leica
Gel chambers (agarose gel electrophoresis)	Peqlab
Heating block	Eppendorf
Ultracentrifuge Beckman SW40 rotor	Beckman Coulter

4.1.2 Consumables

Product	Supplier
Cell culture flasks, dishes, plates	TPP
Cell strainer 100 mm	Falcon
Cover glass 24 x 50 mm	VWR international
Cryo vials, Greiner Bio One	Merck
Cuvettes	Implen
ELISA 96-well plates Nunc MaxiSorb	Thermo Scientific
E-Plate (VIEW) 96	ACEA Biosciences
FACS 96-well V-bottom plates	Roth
Falcon tubes 15 ml / 50 ml	Greiner Bio One
Filter tips	Greiner Bio One
Filters 0.45 µm/0.2 µm	Sarstedt
FrameStar® 96 Well Semi-Skirted PCR Plates	4titude
FCF400-Cu Formvar 400 mesh copper grids	Electron Microscopy Sciences
Microvette 500 LH-Gel	Sarstedt
Needles	Braun
PCR tubes	Thermo Scientific

Pipette tips 10 ml – 1 ml	Biozym / Greiner Bio One / Gilson
Pipettes (disposable) 2, 5, 10, 25, 50 ml	Greiner Bio One
Reaction tubes 1.5 ml, 2 ml	Greiner Bio One, Eppendorf
Reagent reservoirs, sterile	Corning
Surgical Disposable Scalpels	Braun
Syringes	Braun
Whatman paper	GE healthcare lifesciences
Amicon Ultra 2ml Centrifugal filters 50 K	Merck
100 KDa MWCO Amicon Ultra 0.5 mL filter	Merck
25K MWCO dialysis membrane	Roth

4.1.3 Chemicals and reagents

Product	Supplier
Acetic acid	Roth
Agarose	PeqLab
Ammonium persulfade (APS)	Roth
Ampicillin	Roth
Glucose	Roth
Antibiotics/Antimycotics, 100x	ThermoFisher scientific
Biocoll separating solution (density 1.077 g/ml)	Biochrom
Blasticidin	Gibco
Bovine serum albumin (BSA)	Roth
Brefeldin A	Sigma-Aldrich
Cytofix/Cytoperm	BD Biosciences
Sodium dihydrogenic phosphate (NaH2PO4)	Roth
Sodium bicarbonate (NaHCO4)	Roth
Sodium pyruvate	Roth
Dimethyl sulfoxide (DMSO)	Sigma-Aldrich
DMEM	Gibco
DMEM/F12	Gibco
DNA ladder 1kb / 100bp	Eurogentec
EDTA	Roth
Sodium hydroxide (NaOH)	Roth
Ethanol	Roth
Methanol (MetOH)	Roth

1,2-DSPC	Biomol
Cholestrol	Biomol
DMG-PEG 2000	Biomol
SM-102	Biomol
Imidazole	Sigma-Aldrich
Fetal calf serum (FCS)	ThermoFisher scientific
Fixable Viability Dye eF780	eBioscience
Coomassie brilliant blue-R250	Roth
Glycerol	Roth
Heparin-Natrium 25000	Ratiopharm
Page RulerPlus Protein standart (SDS-PAGE)	ThermoFisher scientific
Isopropanol	Roth
Pseudouridine (Ψ)	Jena Bioscienc
L-Glutamine, 200 mM	Gibco
LDS sample Buffer non-reducing (4x)	ThermoFisher scientific
LightCycler 480 SYBR green master mix	Roche
near-infrared live/dead	ThermoFisher scientific
FuGene HD	Promega
Mounting solution	Southern Biotech
Lipofectamine 2000	Invitrogen
Tris(hydroxymethyl)-aminomethan (TRIS)	Roth
6-aminocaproic acid	Sigma-Aldrich
2-Mercaptoethanol	Roth
Sodium chloride (NaCl)	Roth
Glycine	Roth
Propidium iodid	BD bioscience
CellTiter-Blue® Cell Viability Assay	Promega
Polyethylenglycol 6000 (PEG)	Merck
Trypsine	ThermoFisher scientific
Versene	ThermoFisher scientific
Wheat germ agglutinin (Alexa Flour 488 coupled)	ThermoFisher scientific
Collagen R Solution 0,2%, (10x)	SERVA
Phosphate Buffered Saline pH 7,4 (PBS)	ThermoFisher scientific
Minimum Essential Medium Non-essential amino acids (MEM NEAA) 100x	ThermoFisher scientific
Sodiumpyruvate (NaP) 100x	ThermoFisher scientific

Amersham ECL Prime Western Blotting Detection Reagent	GE healthcare lifesciences
Magnesium chloride	Roth
Magnesium sulfade	Roth
OptiMEM	ThermoFisher scientific
Milk powder	Roth
Peptone	Roth
Yeast extract	Roth
Tween 20	Roth
Ultra Pureprotogel	National diagnostics
Tryphan blue 0.4%	Sigma-Aldrich
Temed	Roth
3,3′,5,5′-Tetramethylbenzidin (TMB)	Invitrogen
SDSultra pure	Roth
Sulfuric acid (2 N)	Roth
Potassium chloride (KCl)	Roth

4.1.4 Buffers and solutions

Buffer	Ingredients/source	
ELISA assay diluent	1% BSA in PBS	
FACS buffer	0.1% BSA in PBS	
PBS-T	0.05% Tween 20 in PBS	
MOPS Buffer (0.2 M MOPS pH 7 with NaOH, 50 mM sodium acetate, 10 mM EDTA	(0.2 M MOPS pH 7 with NaOH, 50 mM sodium acetate, 10 mM EDTA	
Triton X-100	Thermo Fisher Scientific	
Tris-acetate-EDTA buffer (50x)	Tris Acetic acid EDTA pH 8.0 in H2O	2 M 2 M 50 mM
SDS-Page running buffer (10x)	Tris Glycin SDS	250 mM 2 M 1%
Stacking gel buffer (SDS-PAGE) pH 6.8	Tris SDS In H2O	0.5 M 0.4%
Separation gel buffer (SDS-PAGE) pH 8.8	Tris SDS In H2O	1.5 M 0.4%

ACK buffer	Ammonium chloride (NH4Cl) Potassium bicarbonate (KHCO3) Ethylenediaminetetraace tic acid (EDTA)	
WB buffer A1	Tris MetOH In H2O	0.3 M 2%
WB buffer A2	Tris MetOH In H2O	25 M 2%
WB buffer cathode buffer	Tris 6-aminocaproic acid MetOH In H2O	25 M 40 mM 2%
Immunofluorescence blocking buffer	BSA PBS	5%
3x reducing loading dye (SDS PAGE)	Tris-HCL pH 6.8 Glycerine 20% SDS 2-Mercaptoethanol H2O	2.5 ml 10 ml 10 ml 5 ml 2.5 ml
ELISA assay diluent Immunofluorescence washing buffer	BSA In PBS	1%
ELISA coating buffer	PBS	
SDS Page stacking gel (5 ml)	H2O Lower buffer Acrylamide 30% Temed 10% APS	2.975 ml 1.3 ml 0.67 ml 0.005 ml 0.05 ml
SDS Page 12% separation gel (10 ml)	H2O Lower buffer Acrylamide 30% Temed 10% APS	3.2 ml 2.7 ml 4 ml 0.01 ml 0.1 ml
SDS Page 8% separation gel (10 ml)	H2O Lower buffer Acrylamide 30% Temed 10% APS	4.6 ml 2.7 ml 2.6 ml 0.01 ml 0.1 ml
10x FastDigest buffer	ThermoFisher scientific	
10x Shrimp alkaline phosphatase buffer	ThermoFisher scientific	
Coomassie staining solution	H2O MetOH Acetic acid CBB-R250/G250	50% 40% 10% 0.1%
Coomassie de-staining solution	H2O MetOH Acetic acid	50% 40% 10%
2% aqueous uranyl formate solution	25 mM sodium hydroxide	
10x T4 ligase buffer	ThermoFisher scientific	

4x non-reducing loading dye (SDS-PAGE)	ThermoFisher scientific
Ampicillin	

4.1.5 Enzymes

BssHII	New England Biolabs
EcoRI	Thermo Fisher Scientific
T4 Ligase	Qiagen, Germany

4.1.6 Proteins and virus

Recombinant SeV	
HuNoV GII.4 VP1 capsid protein	
eGFP protein	
HuNoV GII.4 VP1 pooled peptides	

4.1.7 Kits

Infusion Cloning Kit	Takara
CyQUANT™ MTT assay kit	Thermo Fisher Scientific
Monarch RNA Cleanup kit	New England Biolabs
Phusion High-fidelity PCR master mix	New England Biolabs
Gene JET Gel Extraction Kit	Thermo Fisher Scientific
T7 MegaScript RNA synthesis kit	Thermo Fisher Scientific

Monarch RNA Cleanup kit	New England Biolabs
1 kb Smart Ladder MW-1700-10	Qiagen, Germany
Gene JET Gel Extraction Kit	Qiagen, Germany
Quant-it™ RiboGreen RNA Assay-Kit	Thermosfischer

4.1.8 Cell lines and bacteria

BSR T7 cells	AG Protzer
V3.10 helper cell line	AG Protzer
E. coli strain TOP10	AG Protzer
HEK293T cells	AG Protzer

4.1.9 Antibodies

Anti_CD4 PE Antibody	eBioscience
Anti_CD8 Pacific Blue Antibody	eBioscience
Anti_INFγ FITC Antibody	eBioscience
Anti_IL2 APC Antibody	eBioscience
Anti_TNFα PeCy7 Antibody	eBioscience
HRP goat anti mouse antibody	Thermo Fisher Scientific

4.1.10 Primers

SeV-VP1 F	CTTTCACCCCAAGCGCGCGCCACCATGAAGATGGCCTC
SeV-VP1 R	CTGATGCTGATAGCGCGCTAGTTATACGGCTCGTCTTC
Fseq 1	GCACATCAACTCTGGGGACAC
Fseq 2	CAAGACAGACCAAGAGGTTAAG
Fseq 3	CTCACAGTAGAGGAGATGAC
Fseq 4	GGTATCCCAATATGGATCTCG
Fseq 5	GAGGCATGGGACTCTGTATAC
RT.Taq GII4VP1 F	TCCAGGTGAACAGCTCCTCT
RT.Taq GII4VP1 R	CCCTCCCTGTGTCTGGATTA

4.1.11 Plasmids

pTM N plasmid	AG Protzer
pTM P/C plasmid	AG Protzer
pTM L plasmid	AG Protzer
pcDNA 3.1 ( ) plasmid	AG Protzer

4.1.12 Media

Medium	Ingredients	
DMEM full medium	DMEM FCS Pen/Strep, 10,000 IU/ml L-Glutamine, 200 mM NEAA, 100x Sodium pyruvate, 100 mM	500 ml 50 ml 5.5 ml 5.5 ml 5.5 ml 5.5 ml
DMEM/F12 full medium	DMEM/F12 FCS Pen/Strep, 10,000 IU/ml L-Glutamine, 200 mM NEAA, 100x Sodium pyruvate, 100 mM	500 ml 50 ml 5.5 ml 5.5 ml 5.5 ml 5.5 ml
Freezing medium	FCS DMSO	90% 10%
RPMI full medium	RPMI FCS Pen/Strep, 10,000 IU/ml L-Glutamine, 200 mM NEAA, 100x Sodium pyruvate, 100 mM	500 ml 50 ml 5.5 ml 5.5 ml 5.5 ml 5.5 ml
Lysogen Broth (LB)-Medium	NaCl Peptone Yeast extract Agar (optional) In H20	9 g/l 10 g/l 5 g/l 14 g/l
Super optimal broth (SOB) medium	LB medium with Potassium chloride Magnesium chloride Magnesium sulfide	 2.5 mM 10 mM 10 mM

4.1.13 Mouse strains

Female BALB/c mice	

4.1.14 Software

Software	Application	Supplier
FlowJo, Version 10.4	Flow cytometry analysis	BD Biosciences
ImageJ	Purity calculation of Coomassie stains	National Institutes of Health
LightCycler 480 SW 1.5.1	qPCR analysis	Roche
RTCA software 2.0	xCELLigence viability analysis	ACEA Biosciences
Serial cloner	DNA and protein analysis	SerialBasics
GraphPad Prism	Graph design, statistical calculation	Graphpad Software inc.

4.2 Methods

4.2.1 Construction of Recombinant SeV Vector

The SeV genome is comprised of a 3' leader sequence, six structural genes (N, P, M, F, HN, L), and a 5' trailer [74]. Due to the specific replication cycle and transcription features of SeV results in a descending abundance in production of mRNA transcripts from 5’ end to 3’ end of the genome (N > P > M > F > HN > L). Consequently, the closer the foreign reporter gene is cloned into the SeV genome, the more abundant the target foreign protein is expressed. A subgenomic plasmid containing a truncated Phosphoprotein gene, Matrix gene, Fusion gene, Hemmaglutinin Neuraminidase gene, & Large Polymerase gene. The subgenomic vector has been modified by deleting the N-terminal 76 amino acids of Phosphoprotein (Pdel). This modification makes the SeV virus unable to replicate. In order to clone the VP1 capsid gene of HuNoV GII.4 into the subgenomic plasmid, the gene of interest was amplified using Polymerase Chain Reaction (PCR) method. The PCR product was loaded onto an agarose gel and electrophoresis was performed to check the quality and integrity of the amplified gene. The VP1 gene was then cut and purified using gel purification method.

The subgenomic vector was linearized with *BssH*II restriction enzyme which is located between the Pdel & M gene. The Purified VP1 gene was cloned using a specific cloning method at the *BssH*II restriction site. Then the recombinant subgenomic vector was cut by *EcoR*I and purified using gel extraction. The resulting gene segment from *EcoR*I digestion is used to be cloned to the full length SeV vector. Both the subgenomic and full-length vectors was cut by *EcoR*I and the purified target segments of each were used in a ligation mixture to perform ligation reaction that results in a recombinant replication deficient SeV vector with a truncated *p* gene and HuNoV -VP1 gene.

4.2.2 Cloning strategy

To clone the VP1 gene into the *BssH*II single restriction site of the subgenomic plasmid, we used the Infusion Cloning Kit from Takara. Based on this method, the VP1 gene was amplified with forward and reverse primers that have a 15 homologous sequence similar to the upstream and downstream of the restriction site of the subgenimoc plasmid. Once the gene of interest was amplified, a 10 µl master mix of VP1 gene, linearized subgenomic plasmid and a mix of 5× Exonucleas/polymerase/Ligation enzymes was prepared. The reaction was incubated for 15 minutes at 50 °C.

4.2.3 PCR

PCR was carried out to amplify the target genes in 50 µl reaction mixture containing ca. 250 ng of DNA template, 2.5 µl of forward and reverse primers, and the Phusion High-fidelity PCR master mix (New England Biolabs, Frankfurt, Germany) In a thermal cycler, following an initial denaturation at 98 ºC for 30 sec, the samples were subjected to 35 cycles of 10s denaturation at 98 ºC, 30s annealing temperature, 30s extension at 72 ºC, and a final extension at 72 ºC for 10 min.

4.2.4 Restriction enzyme digestion

Restriction enzyme (RE) digestion was performed using Fast Digest Restriction Enzymes (Thermo Fisher Scientific). For this purpose, approximately one µg DNA plasmid was treated at 37 ºC for 30 min with one unit RE in a reaction mixture containing 1x digestion buffer.

4.2.5 Gel electrophoresis

PCR products and digested DNA samples were analyzed on 1% agarose gel (in TAE buffer) containing Roti Safe for DNA visualization. Electrophoresis was done at 120 V for 40-60 min and DNA fragments were visualized by UV-excitation. The size of the fragments was determined by comparison with the 1 kb Smart Ladder MW-1700-10 (Qiagen, Germany).

4.2.6 DNA purification from agarose gel

After DNA gel electrophoresis, the respective band was cut out with a scalpel and DNA was purified with the Gene JET Gel Extraction Kit (Qiagen, Germany). One ml P1 resuspension buffer (Qiagen, Germany) was added to the gel and was placed at 50 ºC for 10 min until the gel liquified. The P1 containing the amplified product was added to the column and centrifuged for 2min. The flow-through was discarded. After centrifugation 650 µl wash buffer was added. The column was centrifuged at 13000 rpm for 2 mins. The process was repeated with the same conditions. The column was then added to a new tube. 50 µl elution buffer was added and left for 5min. After five min the column was centrifuged, and the DNA concentration was measured with Nanodrop-One (Thermo Scientific).

4.2.7 Ligation

In a total of 20 µl reaction mixture, 2 µl of 10x ligase buffer and 1 µl T4 Ligase (Qiagen, Germany) was mixed with linearized vector and digested PCR product. ligation was carried out at 16 ºC overnight. The reaction was stopped at 65 ºC for 10 min.

4.2.8 Transformation of E. coli competent cells

TOP10 Competent *E. coli* (50 µl) were thawed on ice and mixed with 2,5 µl of the recombination reaction mixture. After 15 min incubation on ice, the cells were heat-shocked at 42 ºC for 1 min. The cells were placed on ice for 2 min; then 500 µl of pre-warmed SOC medium was added. After 1 h incubation at 37 ºC with agitation at 180 rpm, 150 µl of the culture was spread on LB agar supplemented with 100µg/ml ampicillin. Single colonies of the transformants were selected, after overnight incubation at 37 ºC, for further analysis.

4.2.9 Plasmid extraction from E. coli—Mini-prep

Plasmid extraction was carried out based on the alkaline lysis methods using the Thermo Fisher Scientific Gene Jet Plasmid Mini-prep Kit. Briefly, single cell colonies from overnight cultures were picked and grown at 37 ºC for 16 h in 5 ml LB + antibiotics medium. The cells were harvested at 3500 rpm for 5 min and then resuspended in 250 µl of resuspending solution (25mM Tris-HCl, 10 mM EDTA, pH 8.0, 100 µg/ml RNase I). The cells were lysed by adding 250µl of lysis buffer (0.2 N NaOH, 1% (w/v) SDS) followed by 5 min incubation at RT. The lysate was then neutralized with 250 µl of neutralizing buffer (60% (v/v) 5M KHCO3, 11.5 % (v/v) glacial acetic acid, pH 4.8). The mixture was centrifuged at high speed for 10 min at 4 ºC; the supernatant containing plasmids was transferred into the spin column and after washing the pure DNA plasmids were dissolved in the elution buffer (10 mM Tris).

4.2.10 Sequencing

The constructed recombinant vectors sequences were characterized by sanger sequencing (Eurofins) to check for any possible mutation or inaccuracies. The performed sequencing covered all the length of the recombinant rd-SeV -VP1 vector and showed no mutation or sequence change after cloning.

4.2.11 Virus Rescue and Propagation

BSR-T7 cells were transfected with the recombinant rd.SeV .VP1 (4 ug), and three helper plasmids pTM-N (0.25 ug), pTM-P/C (0.15 ug) and pTM-L (0.05 ug) encoding SeV N, P and L proteins, respectively, using Lipofectamin 2000 (Invitrogen). All of the target genes in the plasmids were controlled by a T7 promoter. Transfected cells supplemented with 2% FCS DMEM were incubated at 37 ºC for 3 days. At day 3 a second transfection was performed with 1 ug of pTM-P/C plasmid (for SeV P gene). At day 6 a third transfection with 1 ug of pTM-P/C plasmid was performed again. Since the rd.SeV .VP1 vector was capable of expressing eGFP protein, the expression status of the vector was evaluated using a fluorescence microscope (Leica). The green fluorescence meaning the successful expression of the vector and generation of viral particles was visible starting from the day 8 in some single regions of the cell culture plate and was spreaded to more than 30 % of the cell population at day 10. The cells were harvested and were freeze-thawed once to release the viral particles out of the BSR-T7 cells. Then in order to propagate the viruses in bulk amounts we infected the V3.10 helper cell line to generate more viral particles. In general, a total of 80 T-125 flasks of V3.10 cells were cultured supplemented with DMEM with 10 % FCS, 4.5g/l Glucose, 3.7 g/l NaHCO4, 1x Glutamine & Sodium pyruvate. Once the confluency of the cells was about 70%, the medium was changed with a 2% FCS DMEM and infected with r.d.SeV viral particles (harvested from BSR-T7 cells). The eGFP fluorescence was checked day by day and at day 4, all the flasks were harvested.

4.2.12 Virus Purification

The harvested V3.10 cells were freeze-thawed once to release the viral particles out of the cells & then were centrifuged and washed 3 times with PBS to get rid of the cell debris. The collected supernatant was loaded onto 35 % sucrose gradient & centrifuged with a speed of 25000 rpm for 1 hour. The SeV pellet was collected and resuspended in Tris buffer.

4.2.13 Titration

To quantify the live viral particles a TCID-50 titration test was carried out. From the purified virus stock serial dilution from 10^-1 to 10^-10. V3.10 cells were cultured in a 96 well plate and infected with the 10^-6, 10^-17, 10^-8, 10^-19 & 10^-10 as depicted in picture below. The concentration was then calculated based on $TCID_{50}$ (50% tissue culture infectious dose)

4.2.14 Western blot

Western blot analysis was performed to confirm the expression of the HuNV.GII4 VP1 protein. To this end, the 10% separating SDS-PAGE gel was prepared with 2 ml 40% PAA/BisAA, 3 ml 1M Tris (PH 8.8), 80 µl 10% SDS, 3 ml H2O, 7 µl TEMED & 40 µl APS. The 5 % collection gel was prepared on top with 0.24 ml 40% PAA/BisAA, 0.5 ml 1M Tris (PH 8.8), 20 µl 10% SDS, 1.25 ml H2O, 2 µl TEMED & 15 µl APS. The infected cells with r.d.SeV -VP1 virus were harvested. WB dye was added to the sample (1:4) and boiled for 10 min at 95°C. The stained sample was loaded onto the gel and was run for 1.5 hr with 15mA in WB chamber in 1X running gel buffer (250 mM Tris, 2 M Glycin, 1% SDS). Then A sandwich with the gel, PFDV 0.2 µm membrane, Whatman paper & sponge was made and run for 1.5 hr with 200 mA in 1X transfer buffer (Tris, Glycin, H2O). The membrane was blocked with milk powder (5% in TBS-T) at RT for 1 hour. The membrane was incubated with appropriate dilutions of primary antibody in blocking buffer overnight at 4°C and washed. Then it was incubated with appropriate dilutions of secondary antibody in blocking buffer overnight at RT for 1 hr and washed. The membrane was covered with the substrate working solution by mixing equal parts of the Peroxide Solution and the Luminol Enhancer Solution (Promega) and imaged with INTAS ECL CHEMOCAM.

4.2.15 Electron Microscopy

For negative stain EM imaging FCF400-Cu Formvar 400 mesh copper grids with a collodion-supported carbon film (by Electron Microscopy Sciences) were used and glow discharged for 45s at 35mA prior to sample application. The samples were incubated on the grids for 10min and subsequently stained with 20µl of 2% aqueous uranyl formate solution including 25 mM sodium hydroxide. For imaging a FEI Tecnai T12 microscope operated at 120kV with Tietz TEMCAM-F416 camera was utilised. The images were acquired at a magnification of 30 000x using the software SerialEM.

4.2.16 Animals and immunization; SeV -based vaccine

Six study groups of four female BALB/c mice at 6–8 weeks of age consisting of two low titer and high titer intranasally and intramuscular-immunized and two PBS groups were included. In each administration the low titer and high titer groups received 3×10^{8}/ml and 3.25×10^{10}/ml viral particles, respectively. Each group was inoculated three times, two weeks apart. Mice were sacrificed, ten days after the last administration, spleen, lung and blood samples were collected.

4.2.17 Animals and immunization; mRNA-based vaccine

Four study groups of four female BALB/c mice at 6–8 weeks of age consisting of one naked mRNA group, one encapsulated unmodified mRNA group, one encapsulated modified mRNA and one PBS groups were included. In each administration the mice were injected with 15 µg of mRNA. Each group was inoculated three times, two weeks apart. Mice were sacrificed, ten days after the last administration, spleen and blood samples were collected.

4.2.18 Splenocyte cell preparation

The spleen was smashed on 100 µm cell strainer, washed by 20ml RPMI (10% FCS) and spun down at 1500rpm, 5min, 4°C. cell pellets were resuspended in 2ml ACK buffer by pipetting up and down quickly and incubate for 2 min at room temperature. Then they were diluted with 28 ml RPMI, spun down at 1500 rpm, 5 min, 4°C and resuspended in a final volume of 5 ml RPMI-10.

4.2.19 T cell stimulation

HuNoV GII.4 VP1 pooled peptides were applied for T cell stimulation. To this end, 200µl of prepared spleen samples was seeded to a 96-well flat plate and then were stimulated at 37°C overnight with the pooled peptides at a final concentration of 2 µg/ml. For the positive control samples PMA with a final concentration of 400 ng/ml and Inomycin with a final concentration of 5 µg/ml were added to the cells. The plates were incubated at 37°C for 1 hr. 1h later, BFA (Brefeldin A) was added to every well to inhibit cytokines release outside the cells.

4.2.20 Intracellular Cytokine Staining (ICS)

Overnight-stimulated cells were transferred into a V-bottom 96 well plate and centrifuged at 1400 rpm (800 ×g), 2.5 min, 4°C. The cells were then stained with the Fixable Viability Dye (FVD), αCD4-PE Ab and αCD8-Pacific Blue Ab were diluted in FACS buffer (500 ml PBS + 5 ml FCS) in dilution factor of 1:2500, 1:100 and 1:100 respectively. After incubating on ice in the dark for 20 minutes, 150 µl of FACs buffer was added, and the mixture was centrifuged at 1400 rpm for 2.5 minutes at 4°C. Cells were then re-suspended in in 75 µl of cytofix/cytoperm solution (BD Bioscience) and incubated on ice for 17 min. Thereafter, 150 µl of 1× Perm/Wash buffer was added and were spun down at 1400rpm, 5min, 4°C. Finally, intracellular cytokines were stained using anti_INFɣ-FITC Ab, anti_IL2-APC Ab, anti_TNFα-PeCy7 Ab diluted in 1×

Perm/Wash buffer in dilution factor of 1:300, 1:200 and 1:200 respectively. After 25 min incubation on ice in the dark, 150 µl of 1× Perm/Wash buffer was added and the cells were spun down at 1400rpm, 2.5min, 4°C. The cells were rinsed with 150 µl of FACs buffer, centrifuged at 1400 rpm for 2.5 min, and subsequently re-suspended in 200 µl of FACs buffer for analysis using the Cytoflex FSCs machine.

4.2.21 Enzyme-linked Immunosorbent Assay (ELISA)

HuNoV VP1-specific IgG and IgA antibody titers in vaccinated mice were measured by ELISA on polystyrene 96-well microtiter plates via overnight coating with 2µg/ml HNoV VLP protein, followed by blocking with 5% milk powder and 2 h incubation with immunized mice serum samples and 1.5 h incubation with HRP goat anti mouse antibody. The sera were prediluted at 1:100 for IgG and 1:5 for IgA. The optical density (OD) values of all the samples were subtracted from the background value recorded in the negative-control sera (from mice immunized with PBS).

4.2.22 mRNA in-vitro synthesis

In order to prepare our construct of interest, the HNoV GII4 VP1 was cloned into a pcDNA 3.1 (-) plasmid. At the 5' upstream of the gene a T7 promoter controls the in-vitro mRNA synthesis process. Two Xenopus β-globin UTRs are flanking the VP1 sequence right at the 5' & 3' ends of the gene. The plasmid was then linearized with EcoRI restriction enzyme (Thermo Scientific) for 15 min at 37°C. The linearized plasmid was purified using a PCR purification kit (Roche). The key specifications of the mRNA synthesis procedure are capping, synthesis, sequence modification, DNase treatment, poly Adenylation. The T7 MegaScript RNA synthesis kit (Thermo Scientific) was used to perform the synthesis. For capping purpose, the G-(5')-ppp-(5')-A RNA Cap Structure Analog from NEB was used. To perform the sequence modification, we decided to substitute 100% of the UTP with Pseudo-UTP (Jena Bioscienc). A 20 µl reaction mixture of the following components was first prepared: Template linearized DNA (1 µg), Cap analog (6 mM), GTP (1.5 mM), ATP (7.5 mM), CTP (7.5 mM), Pseudo-UTP (7.5 mM), T7 polymerase (2 µl), 10X buffer (2 µl). The ratios of different components are as follows: Cap: GTP → 4:1, other NTPs:GTP → 1.25:1, other NTPs:Cap → 1.25:1. The reaction was incubated for 1 hr at 37°C. The template DNA was denatured by treating the reaction with 2 µl DNase and 15 min incubation at 37°C. Poly Adenylation was performed by adding 5 µl Poly (A) polymerase and 5 ul 10X Poly (A) polymerase reaction buffer from NEB and bringing the reaction volume to 50 µl. The reaction was then incubated for 30 min at 37°C.

4.2.23 mRNA purification

Monarch RNA Cleanup kit was used to purify the synthesized mRNA. To this end, 100 µl RNA Cleanup Binding Buffer was added to the 50 µl mRNA sample. After adding 150 µl of ethanol (≥ 95%) and mixing by pipetting, the sample was loaded onto filter column and spun down. Washing was performed twice by adding 500 µl of Wash Buffer and spun down for 1 min. As the last step the mRNA was diluted by adding 50 µl RNase-free water to the filter and spinning down.

4.2.24 Characterization of the purified mRNAs

The concentration of *in-vitro* synthesized mRNA was measured by Nanodrop. In order to visualize the mRNA and check the integrity and size of the mRNA construct a denaturing agarose gel was made. 1.0 g agarose was melted in 72 ml of MiliQ water, by dispersing the agarose uniformly and heating in a microwave until all particles were dissolved. The melted agarose was brought to 60 °C. 10 ml 10× MOPS Buffer (0.2 M MOPS pH 7 with NaOH, 50 mM sodium acetate, 10 mM EDTA) and 18 ml 37% formaldehyde were added and the gel was allowed to set for 1 hour. 2 µg of mRNA was mixed with 8 µl of 2× RNA Loading Dye (NEB), incubated at 70°C for 10 minutes and placed immediately on ice for 1–2 minutes. Electrophoresis was done by running the gel in 1× MOPS Buffer at 70V for 60 min and DNA fragments were visualized by UV-excitation. The size of the fragments was determined by comparison with the ssRNA ladder (NEB).

4.2.25 mRNA Transfection

An eGFP mRNA was synthesized based on the same protocol for the VP1 mRNA as a control. HEK293T cells were cultured in a 6 well plate and transfected with 2 ug of eGFP mRNA using Lipofectamin 2000 (Invitrogen). After 4-6 hr the medium was replaced with fresh medium. Within 12-72 hr, the green fluorescence resulted from eGFP expression was screened using a fluorescence microscope (Leica DMi8). Once the positive results were detected, we proceeded with the VP1 mRNA transfection. The HEK293T cells were transfected with the same protocol for eGFP construct. After 72 hr, the cells were harvested and the VP1 expression was evaluated by Western blot.

4.2.26 mRNA - LNP formulation

The N:P ratio is a critical parameter in the formulation of LNP s (LNPs). It refers to the ratio of the positively charged amino groups in the cationic lipid to the negatively charged phosphate groups in the nucleic acid being delivered by the LNP. The optimal N:P ratio for LNP preparation can vary depending on the specific lipids and nucleic acid being used. However, in general, the N:P ratio should be high enough to ensure efficient encapsulation and protection of the nucleic acid, but not so high that the LNP becomes unstable or toxic. In this protocol we used the N:P ratio of 6:1. The provided amounts are based on the specific nucleic acid structure being used for this experiment. For each nucleic acid construct of interest in your experiments all the numbers have to be calculated and adjusted accordingly. The lipids were diluted in ETOH as follows. 25 mg 1,2-DSPC**,** 15 mg Cholestrol**,** 50 mg DMG-PEG**,** 90 µl SM-102 were diluted in 1000 µl, 1000 µl, 500 µl and 900 µl of absolute EtOH respectively. All the lipid components were purchased from Biomol. From the diluted lipids a mixture was prepared by mixing the mentioned volumes of each lipid: 21.3 µl 1,2-DSPC, 66.7 µl Cholestrol, 2.5 µl DMG-PEG, 23.9 µl SM-102, 85.6 µl EtOH. The mRNA stock was diluted with a ratio of 1:2 in 50 mM Acetate buffer (pH=5 5). Using a manual mixing method, 33.3 µl of lipid mixture was added on top of 100 ul of RNA mixture and mixed very fast by pipetting.

4.2.27 Purification of mRNA-loaded LNPs

Both filter purification and dialysis methods were performed to check and compare their purification efficiency. For filter purification the LNPs were washed with DPBS in a 100 KDa MWCO Amicon Ultra 0.5 mL filter. The sample was spun down at 13 krcf for 30 minutes, and finally washed 3 times by adding 1 mL DPBS. For dialysis 25K MWCO dialysis membrane tubes were used. The dialysis was done overnight for 17 hours in DPBS at RT. For constructs with different lengths and sizes, the right filter size has to be chosen.

4.2.28 Storage of LNPs

A Tris-sucrose mixture was used as a cryoprotectant for the purified LNPs. To this end, 10 mM Tris-HCl (pH 7.4) + 300 mM Sucrose was prepared and mixed with LNP in a 1:1 ratio. In this blend, the osmolality of the sucrose buffer is approximately 364 mOsm/kg (as per the literature, any value below 600 mOsm/kg is considered acceptable).

4.2.29 Encapsulation efficiency of mRNA in LNPs

Encapsulation efficiency was determined the using Quant-it™ RiboGreen RNA Assay-Kit: An untreated and a Triton X-100 treated version for each sample were prepared. In the untreated LNP samples, RiboGreen can only bind to free mRNA as it cannot penetrate the LNPs. In the Triton X-100 treated samples, the LNPs are destroyed by the detergent so the result here will be the total mRNA in the sample. Encapsulation efficiency is calculated by taking the ratio of untreated samples to treated samples, subtracting that result from 1 (1 - (untreated/treated)).

4.2.30 Cytotoxicity assay

Cytotoxicity assessment is a crucial step in evaluating the safety and potential adverse effects of novel therapeutics. In this study, the cytotoxicity effects of LNP-RNA were evaluated using the MTT assay, a commonly employed method to assess cell viability. The MTT assay relies on the ability of viable cells to convert a yellow tetrazolium salt (MTT) into purple formazan crystals through mitochondrial activity. The absorbance of the formazan crystals is directly proportional to the number of viable cells present in the culture. The study included six sample groups treated with different concentrations of LNP-RNA (100 – 600 ng) and three replicates for each group. Additionally, a negative control group (untreated cells) and a blank control (medium only) were included to establish baselines for cell viability measurements. 10^4 HEK293T cells were seeded in each well of a 96-well plate format. The cells in the sample groups were treated with LNP-RNA at concentrations ranging from 100 to 600 ng. The negative control group remained untreated, while the blank control contained only cell culture medium. After the designated incubation period, the medium was aspirated from each well. 10 µl of MTT solution from the CyQUANT MTT Cell Viability Assay kit was added to each well. The plate was covered and incubated for 4 hours at 37°C to allow the cells to convert the MTT reagent into formazan crystals. Following the incubation period, the MTT solution was carefully removed from each well. 100 µl of SDS-HCl solution from the CyQUANT MTT Cell Viability Assay kit was added to each well. The plate was covered and incubated for an additional 4 hours at 37°C to solubilize the formazan crystals. After the solubilization step, the absorbance of the formazan solution was measured using a microplate reader. The wavelength used for measurement was 570 nm, as specified in the CyQUANT MTT Cell Viability Assay kit instructions. Each well was read individually, and the absorbance values were recorded. The recorded absorbance values were used to calculate the cell viability percentage and cytotoxicity effects of LNP-RNA.

5 References

1. Zahorsky, J., *Hyperemesis hiemis or the winter vomiting disease.* Arch Pediatr, 1929. **46**: p. 391-395.
2. Ahmed, S.M., et al., *Global prevalence of norovirus in cases of gastroenteritis: a systematic review and meta-analysis.* The Lancet infectious diseases, 2014. **14**(8): p. 725-730.
3. Scallan, E., et al., *Foodborne illness acquired in the United States—major pathogens.* Emerg Infect Dis, 2011. **17**(1): p. 7-15.
4. Hall, A.J., et al., *Norovirus disease in the United States.* Emerging infectious diseases, 2013. **19**(8): p. 1198.
5. Hall, A.J., et al., *The roles of Clostridium difficile and norovirus among gastroenteritis-associated deaths in the United States, 1999–2007.* Clinical Infectious Diseases, 2012. **55**(2): p. 216-223.
6. Debbink, K., L.C. Lindesmith, and R.S. Baric, *The state of norovirus vaccines.* Clinical Infectious Diseases, 2014. **58**(12): p. 1746-1752.
7. Bartsch, S.M., et al., *The potential economic value of a human norovirus vaccine for the United States.* Vaccine, 2012. **30**(49): p. 7097-7104.
8. Zhang, X., et al., *Global burden and trends of norovirus-associated diseases from 1990 to 2019: an observational trend study.* Frontiers in public health, 2022. **10**: p. 905172.
9. Jones, M. and S.M. Karst, *Foodborne Infections and Intoxications: Chapter 17. Noroviruses*. 2013: Elsevier Inc. Chapters.
10. Daniels, N.A., et al., *A foodborne outbreak of gastroenteritis associated with Norwalk-like viruses: first molecular traceback to deli sandwiches contaminated during preparation.* The Journal of infectious diseases, 2000. **181**(4): p. 1467-1470.
11. Seitz, S.R., et al., *Norovirus infectivity in humans and persistence in water.* Applied and environmental microbiology, 2011. **77**(19): p. 6884-6888.
12. Hall, A.J., *Noroviruses: the perfect human pathogens?* 2012, Oxford University Press. p. 1622-1624.
13. Cáceres, V.M., et al., *A viral gastroenteritis outbreak associated with person-to-person spread among hospital staff.* Infection Control & Hospital Epidemiology, 1998. **19**(3): p. 162-167.
14. Alfano-Sobsey, E., et al., *Norovirus outbreak associated with undercooked oysters and secondary household transmission.* Epidemiology & Infection, 2012. **140**(2): p. 276-282.
15. O'Neill, P.D. and P.J. Marks, *Bayesian model choice and infection route modelling in an outbreak of Norovirus.* Statistics in Medicine, 2005. **24**(13): p. 2011-2024.
16. Atmar, R.L., et al., *Norwalk virus shedding after experimental human infection.* Emerging infectious diseases, 2008. **14**(10): p. 1553.
17. Sakai, Y., et al., *Clinical severity of Norwalk virus and Sapporo virus gastroenteritis in children in Hokkaido, Japan.* The Pediatric infectious disease journal, 2001. **20**(9): p. 849-853.
18. Lopman, B.A., et al., *Clinical manifestation of norovirus gastroenteritis in health care settings.* Clinical Infectious Diseases, 2004. **39**(3): p. 318-324.
19. Ahn, J.Y., et al., *Clinical characteristics and etiology of travelers' diarrhea among Korean travelers visiting South-East Asia.* Journal of Korean medical science, 2011. **26**(2): p. 196-200.
20. Dolin, R., et al., *Viral gastroenteritis induced by the Hawaii agent: jejunal histopathology and serologic response.* The American journal of medicine, 1975. **59**(6): p. 761-768.
21. Troeger, H., et al., *Structural and functional changes of the duodenum in human norovirus infection.* Gut, 2009. **58**(8): p. 1070-1077.
22. Matthews, J., et al., *The epidemiology of published norovirus outbreaks: a review of risk factors associated with attack rate and genogroup.* Epidemiology & Infection, 2012. **140**(7): p. 1161-1172.

23. Takanashi, S., et al., *Failure of propagation of human norovirus in intestinal epithelial cells with microvilli grown in three-dimensional cultures.* Archives of virology, 2014. **159**: p. 257-266.
24. Agus, S.G., et al., *Acute infectious nonbacterial gastroenteritis: intestinal histopathology: histologic and enzymatic alterations during illness produced by the Norwalk agent in man.* Annals of internal medicine, 1973. **79**(1): p. 18-25.
25. Jones, M.K., et al., *Enteric bacteria promote human and mouse norovirus infection of B cells.* Science, 2014. **346**(6210): p. 755-759.
26. Wobus, C.E., et al., *Replication of Norovirus in cell culture reveals a tropism for dendritic cells and macrophages.* PLoS biology, 2004. **2**(12): p. e432.
27. Lay, M.K., et al., *Norwalk virus does not replicate in human macrophages or dendritic cells derived from the peripheral blood of susceptible humans.* Virology, 2010. **406**(1): p. 1-11.
28. Chan, M.C.-W., W.-S. Ho, and J.J.-Y. Sung, *In vitro whole-virus binding of a norovirus genogroup II genotype 4 strain to cells of the lamina propria and Brunner's glands in the human duodenum.* Journal of virology, 2011. **85**(16): p. 8427-8430.
29. Bok, K., et al., *Chimpanzees as an animal model for human norovirus infection and vaccine development.* Proceedings of the National Academy of Sciences, 2011. **108**(1): p. 325-330.
30. Taube, S., et al., *A mouse model for human norovirus.* MBio, 2013. **4**(4): p. e00450-13.
31. Miura, T., et al., *Histo-blood group antigen-like substances of human enteric bacteria as specific adsorbents for human noroviruses.* Journal of virology, 2013. **87**(17): p. 9441-9451.
32. Kuss, S.K., et al., *Intestinal microbiota promote enteric virus replication and systemic pathogenesis.* Science, 2011. **334**(6053): p. 249-252.
33. Takanashi, S., et al., *Detection, genetic characterization, and quantification of norovirus RNA from sera of children with gastroenteritis.* Journal of clinical virology, 2009. **44**(2): p. 161-163.
34. Obinata, K., et al., *Norovirus encephalopathy in a previously healthy child.* The Pediatric infectious disease journal, 2010. **29**(11): p. 1057-1059.
35. Cheetham, S., et al., *Pathogenesis of a genogroup II human norovirus in gnotobiotic pigs.* Journal of virology, 2006. **80**(21): p. 10372-10381.
36. Duizer, E., et al., *Laboratory efforts to cultivate noroviruses.* Journal of General Virology, 2004. **85**(1): p. 79-87.
37. McFadden, N., et al., *Norovirus regulation of the innate immune response and apoptosis occurs via the product of the alternative open reading frame 4.* PLoS pathogens, 2011. **7**(12): p. e1002413.
38. Gutiérrez-Escolano, A.L., et al., *Interaction of cellular proteins with the 5' end of Norwalk virus genomic RNA.* Journal of virology, 2000. **74**(18): p. 8558-8562.
39. Hyde, J.L. and J.M. Mackenzie, *Subcellular localization of the MNV-1 ORF1 proteins and their potential roles in the formation of the MNV-1 replication complex.* Virology, 2010. **406**(1): p. 138-148.
40. Sosnovtsev, S.V., et al., *Cleavage map and proteolytic processing of the murine norovirus nonstructural polyprotein in infected cells.* Journal of virology, 2006. **80**(16): p. 7816-7831.
41. Fields, B.N., *Fields' virology*. Vol. 1. 2007: Lippincott Williams & Wilkins.
42. Karst, S.M., et al., *STAT1-dependent innate immunity to a Norwalk-like virus.* Science, 2003. **299**(5612): p. 1575-1578.
43. Mumphrey, S.M., et al., *Murine norovirus 1 infection is associated with histopathological changes in immunocompetent hosts, but clinical disease is prevented by STAT1-dependent interferon responses.* Journal of virology, 2007. **81**(7): p. 3251-3263.
44. Chang, K.-O. and D.W. George, *Interferons and ribavirin effectively inhibit Norwalk virus replication in replicon-bearing cells.* Journal of virology, 2007. **81**(22): p. 12111-12118.
45. Changotra, H., et al., *Type I and type II interferons inhibit the translation of murine norovirus proteins.* Journal of virology, 2009. **83**(11): p. 5683-5692.
46. Chachu, K.A., et al., *Antibody is critical for the clearance of murine norovirus infection.* Journal of virology, 2008. **82**(13): p. 6610-6617.

47. Tomov, V.T., et al., *Persistent enteric murine norovirus infection is associated with functionally suboptimal virus-specific CD8 T cell responses.* Journal of virology, 2013. **87**(12): p. 7015-7031.
48. Zhu, S., et al., *Identification of immune and viral correlates of norovirus protective immunity through comparative study of intra-cluster norovirus strains.* PLoS pathogens, 2013. **9**(9): p. e1003592.
49. Lindesmith, L., et al., *Human susceptibility and resistance to Norwalk virus infection.* Nature medicine, 2003. **9**(5): p. 548-553.
50. Chachu, K.A., et al., *Immune mechanisms responsible for vaccination against and clearance of mucosal and lymphatic norovirus infection.* PLoS pathogens, 2008. **4**(12): p. e1000236.
51. Parrino, T.A., et al., *Clinical immunity in acute gastroenteritis caused by Norwalk agent.* New England Journal of Medicine, 1977. **297**(2): p. 86-89.
52. Johnson, P.C., et al., *Multiple-challenge study of host susceptibility to Norwalk gastroenteritis in US adults.* Journal of Infectious Diseases, 1990. **161**(1): p. 18-21.
53. Wyatt, R.G., et al., *Comparison of three agents of acute infectious nonbacterial gastroenteritis by cross-challenge in volunteers.* Journal of Infectious Diseases, 1974. **129**(6): p. 709-714.
54. Bull, R.A. and P.A. White, *Mechanisms of GII. 4 norovirus evolution.* Trends in microbiology, 2011. **19**(5): p. 233-240.
55. Estes, M.K., B.V. Prasad, and R.L. Atmar, *Noroviruses everywhere: has something changed?* Current opinion in infectious diseases, 2006. **19**(5): p. 467-474.
56. Debbink, K., et al., *Emergence of new pandemic GII. 4 Sydney norovirus strain correlates with escape from herd immunity.* The Journal of infectious diseases, 2013. **208**(11): p. 1877-1887.
57. Lindesmith, L.C., et al., *Heterotypic humoral and cellular immune responses following Norwalk virus infection.* Journal of virology, 2010. **84**(4): p. 1800-1815.
58. Swanstrom, J., et al., *Characterization of blockade antibody responses in GII. 2.1976 Snow Mountain virus-infected subjects.* Journal of Virology, 2014. **88**(2): p. 829-837.
59. Karst, S.M., *Pathogenesis of noroviruses, emerging RNA viruses.* Viruses, 2010. **2**(3): p. 748-781.
60. Simmons, K., et al., *Duration of immunity to norovirus gastroenteritis.* Emerging infectious diseases, 2013. **19**(8): p. 1260.
61. Ettayebi, K., et al., *Replication of human noroviruses in stem cell–derived human enteroids.* Science, 2016. **353**(6306): p. 1387-1393.
62. Karst, S.M., *Identification of a novel cellular target and a co-factor for norovirus infection–B cells & commensal bacteria.* Gut microbes, 2015. **6**(4): p. 266-271.
63. Jones, M.K., et al., *Human norovirus culture in B cells.* Nature protocols, 2015. **10**(12): p. 1939-1947.
64. Jiang, X., et al., *Expression, self-assembly, and antigenicity of the Norwalk virus capsid protein.* Journal of virology, 1992. **66**(11): p. 6527-6532.
65. Ball, J.M., et al., *Recombinant Norwalk virus–like particles given orally to volunteers: phase I study.* Gastroenterology, 1999. **117**(1): p. 40-48.
66. El-Kamary, S.S., et al., *Adjuvanted intranasal Norwalk virus-like particle vaccine elicits antibodies and antibody-secreting cells that express homing receptors for mucosal and peripheral lymphoid tissues.* The Journal of infectious diseases, 2010. **202**(11): p. 1649-1658.
67. Ramirez, K., et al., *Intranasal vaccination with an adjuvanted Norwalk virus-like particle vaccine elicits antigen-specific B memory responses in human adult volunteers.* Clinical immunology, 2012. **144**(2): p. 98-108.
68. Atmar, R.L., et al., *Norovirus vaccine against experimental human Norwalk Virus illness.* N Engl J Med, 2011. **365**: p. 2178-2187.
69. Parra, G.I., et al., *Immunogenicity and specificity of norovirus Consensus GII. 4 virus-like particles in monovalent and bivalent vaccine formulations.* Vaccine, 2012. **30**(24): p. 3580-3586.

70. Treanor, J.J., et al., *A novel intramuscular bivalent norovirus virus-like particle vaccine candidate—reactogenicity, safety, and immunogenicity in a phase 1 trial in healthy adults.* The Journal of infectious diseases, 2014. **210**(11): p. 1763-1771.
71. Sundararajan, A., et al., *Robust mucosal-homing antibody-secreting B cell responses induced by intramuscular administration of adjuvanted bivalent human norovirus-like particle vaccine.* Vaccine, 2015. **33**(4): p. 568-576.
72. Ramani, S., et al., *B-cell responses to intramuscular administration of a bivalent virus-like particle human norovirus vaccine.* Clinical and Vaccine Immunology, 2017. **24**(5): p. e00571-16.
73. Lindesmith, L.C., et al., *Broad blockade antibody responses in human volunteers after immunization with a multivalent norovirus VLP candidate vaccine: immunological analyses from a phase I clinical trial.* PLoS medicine, 2015. **12**(3): p. e1001807.
74. Bernstein, D.I., et al., *Norovirus vaccine against experimental human GII. 4 virus illness: a challenge study in healthy adults.* The Journal of infectious diseases, 2015. **211**(6): p. 870-878.
75. Huang, Z., et al., *A DNA replicon system for rapid high-level production of virus-like particles in plants.* Biotechnology and bioengineering, 2009. **103**(4): p. 706-714.
76. Tacket, C.O., et al., *Human immune responses to a novel Norwalk virus vaccine delivered in transgenic potatoes.* The journal of infectious diseases, 2000. **182**(1): p. 302-305.
77. Santi, L., et al., *An efficient plant viral expression system generating orally immunogenic Norwalk virus-like particles.* Vaccine, 2008. **26**(15): p. 1846-1854.
78. Mathew, L.G., M.M. Herbst-Kralovetz, and H.S. Mason, *Norovirus Narita 104 virus-like particles expressed in Nicotiana benthamiana induce serum and mucosal immune responses.* BioMed Research International, 2014. **2014**.
79. Prasad, B.V., et al., *X-ray crystallographic structure of the Norwalk virus capsid.* Science, 1999. **286**(5438): p. 287-290.
80. Tan, M. and X. Jiang, *The p domain of norovirus capsid protein forms a subviral particle that binds to histo-blood group antigen receptors.* Journal of virology, 2005. **79**(22): p. 14017-14030.
81. Tan, M., et al., *Noroviral P particle: structure, function and applications in virus–host interaction.* Virology, 2008. **382**(1): p. 115-123.
82. Kocher, J., et al., *Intranasal P particle vaccine provided partial cross-variant protection against human GII. 4 norovirus diarrhea in gnotobiotic pigs.* Journal of virology, 2014. **88**(17): p. 9728-9743.
83. Xia, M., et al., *A candidate dual vaccine against influenza and noroviruses.* Vaccine, 2011. **29**(44): p. 7670-7677.
84. Dai, Y.-C., et al., *A dual chicken IgY against rotavirus and norovirus.* Antiviral research, 2013. **97**(3): p. 293-300.
85. Wang, L., et al., *Polyvalent complexes for vaccine development.* Biomaterials, 2013. **34**(18): p. 4480-4492.
86. Guo, L., et al., *Intranasal administration of a recombinant adenovirus expressing the norovirus capsid protein stimulates specific humoral, mucosal, and cellular immune responses in mice.* Vaccine, 2008. **26**(4): p. 460-468.
87. Kim, L., et al., *Safety and immunogenicity of an oral tablet norovirus vaccine, a phase I randomized, placebo-controlled trial.* JCI insight, 2018. **3**(13).
88. Baehner, F., H. Bogaerts, and R. Goodwin, *Vaccines against norovirus: state of the art trials in children and adults.* Clinical microbiology and infection, 2016. **22**: p. S136-S139.
89. Lopman, B.A., et al., *The vast and varied global burden of norovirus: prospects for prevention and control.* PLoS medicine, 2016. **13**(4): p. e1001999.
90. Atmar, R.L., et al., *Rapid responses to 2 virus-like particle norovirus vaccine candidate formulations in healthy adults: a randomized controlled trial.* The Journal of infectious diseases, 2016. **214**(6): p. 845-853.

91. Leroux-Roels, G., et al., *Safety and immunogenicity of different formulations of norovirus vaccine candidate in healthy adults: a randomized, controlled, double-blind clinical trial.* The Journal of infectious diseases, 2018. **217**(4): p. 597-607.
92. Atmar, R.L., et al., *Persistence of antibodies to 2 virus-like particle norovirus vaccine candidate formulations in healthy adults: 1-year follow-up with memory probe vaccination.* The Journal of Infectious Diseases, 2019. **220**(4): p. 603-614.
93. Available, A.V.A.F.S.E.i.P.b.N.D.-R.T.i.E.A. and o.h.i.v.c.n.-r.n.-r.-d.v.-a.-f.-s.-e.-p.-b.-d.a.o.D. 2021).
94. Scallan, C.D., et al., *An adenovirus-based vaccine with a double-stranded RNA adjuvant protects mice and ferrets against H5N1 avian influenza in oral delivery models.* Clinical and vaccine immunology, 2013. **20**(1): p. 85-94.
95. Ishida, N. and M. Homma, *Sendai virus.* Advances in virus research, 1978. **23**: p. 349-383.
96. Kuroya, M., N. Ishida, and T. Shiratori, *Newborn Virus Pneumonitis (Type Sendai). II. Report: The Isolation of a New Virus possessing Hemagglutinin Activity.* Yokohama medical bulletin, 1953. **4**(4): p. 217-33.
97. FUKUMI, H., F. NISHIKAWA, and T. KITAYAMA, *A pneumotropic virus from mice causing hemagglutination.* Japanese Journal of Medical Science and Biology, 1954. **7**(4): p. 345-363.
98. Parker, J., M. Whiteman, and C. Richter, *Susceptibility of inbred and outbred mouse strains to Sendai virus and prevalence of infection in laboratory rodents.* Infection and Immunity, 1978. **19**(1): p. 123-130.
99. Bousse, T., et al., *Human parainfluenza virus type 1 but not Sendai virus replicates in human respiratory cells despite IFN treatment.* Virus research, 2006. **121**(1): p. 23-32.
100. Lamb, R.A., *Paramyxoviridae: the viruses and their replication.* Fields virology, 2001: p. 1305-1340.
101. Giorgi, C., B.M. Blumberg, and D. Kolakofsky, *Sendai virus contains overlapping genes expressed from a single mRNA.* Cell, 1983. **35**(3): p. 829-836.
102. Curran, J. and D. Kolakofsky, *Ribosomal initiation from an ACG codon in the Sendai virus P/C mRNA.* The EMBO journal, 1988. **7**(1): p. 245-251.
103. Vidal, S., J. Curran, and D. Kolakofsky, *Editing of the Sendai virus P/C mRNA by G insertion occurs during mRNA synthesis via a virus-encoded activity.* Journal of virology, 1990. **64**(1): p. 239-246.
104. Hausmann, S., et al., *Two nucleotides immediately upstream of the essential A6G3 slippery sequence modulate the pattern of G insertions during Sendai virus mRNA editing.* Journal of virology, 1999. **73**(1): p. 343-351.
105. Samal, S.K. and P.L. Collins, *RNA replication by a respiratory syncytial virus RNA analog does not obey the rule of six and retains a nonviral trinucleotide extension at the leader end.* Journal of Virology, 1996. **70**(8): p. 5075-5082.
106. Calain, P. and L. Roux, *The rule of six, a basic feature for efficient replication of Sendai virus defective interfering RNA.* Journal of virology, 1993. **67**(8): p. 4822-4830.
107. Kolakofsky, D., et al., *Paramyxovirus RNA synthesis and the requirement for hexamer genome length: the rule of six revisited.* Journal of virology, 1998. **72**(2): p. 891-899.
108. Sanderson, C., N. McQueen, and D. Nayak, *Sendai virus assembly: M protein binds to viral glycoproteins in transit through the secretory pathway.* Journal of virology, 1993. **67**(2): p. 651-663.
109. Scheid, A. and P.W. Choppin, *Identification of biological activities of paramyxovirus glycoproteins. Activation of cell fusion, hemolysis, and infectivity by proteolytic cleavage of an inactive precursor protein of Sendai virus.* virology, 1974. **57**(2): p. 475-490.
110. Vidal, S. and D. Kolakofsky, *Modified model for the switch from Sendai virus transcription to replication.* Journal of virology, 1989. **63**(5): p. 1951-1958.
111. Kato, A., et al., *Sendai virus gene start signals are not equivalent in reinitiation capacity: moderation at the fusion protein gene.* Journal of virology, 1999. **73**(11): p. 9237-9246.
112. Tokusumi, T., et al., *Recombinant Sendai viruses expressing different levels of a foreign reporter gene.* Virus research, 2002. **86**(1-2): p. 33-38.

113. Burke, C.W., et al., *Illumination of parainfluenza virus infection and transmission in living animals reveals a tissue-specific dichotomy.* PLoS pathogens, 2011. **7**(7): p. e1002134.
114. Russell, C.J. and J.L. Hurwitz, *Sendai virus as a backbone for vaccines against RSV and other human paramyxoviruses.* Expert review of vaccines, 2016. **15**(2): p. 189-200.
115. Luongo, C., et al., *Codon stabilization analysis of the "248" temperature sensitive mutation for increased phenotypic stability of respiratory syncytial virus vaccine candidates.* Vaccine, 2009. **27**(41): p. 5667-5676.
116. Schickli, J.H., J. Kaur, and R.S. Tang, *Nonclinical phenotypic and genotypic analyses of a Phase 1 pediatric respiratory syncytial virus vaccine candidate MEDI-559 (rA2cp248/404/1030ΔSH) at permissive and non-permissive temperatures.* Virus research, 2012. **169**(1): p. 38-47.
117. Henrickson, K.J., et al., *Neutralizing epitopes of human parainfluenza virus type 3 are conformational and cannot be imitated by synthetic peptides.* Vaccine, 1991. **9**(4): p. 243-249.
118. York, I.A. and K.L. Rock, *Antigen processing and presentation by the class I major histocompatibility complex.* Annual review of immunology, 1996. **14**(1): p. 369-396.
119. Ehrenfeld, E., J. Modlin, and K. Chumakov, *Future of polio vaccines.* Expert review of vaccines, 2009. **8**(7): p. 899-905.
120. Salk, D. and J. Salk, *Vaccinology of poliomyelitis.* Vaccine, 1984. **2**(1): p. 59-74.
121. Kew, O.M., et al., *Vaccine-derived polioviruses and the endgame strategy for global polio eradication.* Annu. Rev. Microbiol., 2005. **59**: p. 587-635.
122. Abdulhaqq, S.A. and D.B. Weiner, *DNA vaccines: developing new strategies to enhance immune responses.* Immunologic research, 2008. **42**: p. 219-232.
123. Wiegand, M., et al., *Evaluation of a novel immunogenic vaccine platform based on a genome replication-deficient Sendai vector.* Vaccine, 2013. **31**(37): p. 3888-3893.
124. Wolff, J.A., et al., *Direct gene transfer into mouse muscle in vivo.* Science, 1990. **247**(4949): p. 1465-1468.
125. Jirikowski, G.F., et al., *Reversal of diabetes insipidus in Brattleboro rats: intrahypothalamic injection of vasopressin mRNA.* Science, 1992. **255**(5047): p. 996-998.
126. Suschak, J.J., J.A. Williams, and C.S. Schmaljohn, *Advancements in DNA vaccine vectors, non-mechanical delivery methods, and molecular adjuvants to increase immunogenicity.* Human vaccines & immunotherapeutics, 2017. **13**(12): p. 2837-2848.
127. Tandrup Schmidt, S., et al., *Liposome-based adjuvants for subunit vaccines: formulation strategies for subunit antigens and immunostimulators.* Pharmaceutics, 2016. **8**(1): p. 7.
128. Xu, S., et al., *mRNA vaccine era—mechanisms, drug platform and clinical prospection.* International journal of molecular sciences, 2020. **21**(18): p. 6582.
129. Jackson, N.A., et al., *The promise of mRNA vaccines: a biotech and industrial perspective.* npj Vaccines, 2020. **5**(1): p. 11.
130. Iavarone, C., et al., *Mechanism of action of mRNA-based vaccines.* Expert review of vaccines, 2017. **16**(9): p. 871-881.
131. Crommelin, D.J., et al., *Addressing the cold reality of mRNA vaccine stability.* Journal of Pharmaceutical Sciences, 2021. **110**(3): p. 997-1001.
132. Weissman, D., *mRNA transcript therapy.* Expert review of vaccines, 2015. **14**(2): p. 265-281.
133. Sahin, U., K. Karikó, and Ö. Türeci, *mRNA-based therapeutics—developing a new class of drugs.* Nature reviews Drug discovery, 2014. **13**(10): p. 759-780.
134. Tsui, N.B., E.K. Ng, and Y.D. Lo, *Stability of endogenous and added RNA in blood specimens, serum, and plasma.* Clinical chemistry, 2002. **48**(10): p. 1647-1653.
135. Pardi, N., et al., *mRNA vaccines—a new era in vaccinology.* Nature reviews Drug discovery, 2018. **17**(4): p. 261-279.
136. Ross, J. and T.D. Sullivan, *Half-lives of beta and gamma globin messenger RNAs and of protein synthetic capacity in cultured human reticulocytes.* Blood, 1985. **66**(5): p. 1149-1154.
137. Holtkamp, S., et al., *Modification of antigen-encoding RNA increases stability, translational efficacy, and T-cell stimulatory capacity of dendritic cells.* Blood, 2006. **108**(13): p. 4009-4017.

138. Gallie, D., *The cap and poly (A) tail function synergistically to regulate mRNA translational efficiency.* Genes & development, 1991. **5**(11): p. 2108-2116.
139. Martin, S., E. Paoletti, and B. Moss, *Purification of mRNA guanylyltransferase and mRNA (guanine-7-) methyltransferase from vaccinia virions.* Journal of Biological Chemistry, 1975. **250**(24): p. 9322-9329.
140. STEPINSKI, J., et al., *Synthesis and properties of mRNAs containing the novel "anti-reverse" cap analogs 7-methyl (3'-O-methyl) GpppG and 7-methyl (3'-deoxy) GpppG.* Rna, 2001. **7**(10): p. 1486-1495.
141. Malone, R.W., P.L. Felgner, and I.M. Verma, *Cationic liposome-mediated RNA transfection.* Proceedings of the National Academy of Sciences, 1989. **86**(16): p. 6077-6081.
142. Thess, A., et al., *Sequence-engineered mRNA without chemical nucleoside modifications enables an effective protein therapy in large animals.* Molecular Therapy, 2015. **23**(9): p. 1456-1464.
143. Kudla, G., et al., *High guanine and cytosine content increases mRNA levels in mammalian cells.* PLoS biology, 2006. **4**(6): p. e180.
144. Verbeke, R., et al., *Three decades of messenger RNA vaccine development.* Nano Today, 2019. **28**: p. 100766.
145. Wang, F., T. Zuroske, and J.K. Watts, *RNA therapeutics on the rise.* Nat Rev Drug Discov, 2020. **19**(7): p. 441-442.
146. Eygeris, Y., et al., *Chemistry of lipid nanoparticles for RNA delivery.* Accounts of Chemical Research, 2021. **55**(1): p. 2-12.
147. Han, X., et al., *An ionizable lipid toolbox for RNA delivery.* Nature Communications, 2021. **12**(1): p. 7233.
148. Witzigmann, D., et al., *Lipid nanoparticle technology for therapeutic gene regulation in the liver.* Advanced drug delivery reviews, 2020. **159**: p. 344-363.
149. Kulkarni, J.A., et al., *On the role of helper lipids in lipid nanoparticle formulations of siRNA.* Nanoscale, 2019. **11**(45): p. 21733-21739.
150. Ambegia, E., et al., *Stabilized plasmid–lipid particles containing PEG-diacylglycerols exhibit extended circulation lifetimes and tumor selective gene expression.* Biochimica et Biophysica Acta (BBA)-Biomembranes, 2005. **1669**(2): p. 155-163.
151. Dai, Q., C. Walkey, and W.C. Chan, *Polyethylene glycol backfilling mitigates the negative impact of the protein corona on nanoparticle cell targeting.* Angewandte Chemie International Edition, 2014. **53**(20): p. 5093-5096.
152. Belliveau, N.M., et al., *Microfluidic synthesis of highly potent limit-size lipid nanoparticles for in vivo delivery of siRNA.* Molecular Therapy-Nucleic Acids, 2012. **1**: p. e37.
153. Kowalski, P.S., et al., *Delivering the messenger: advances in technologies for therapeutic mRNA delivery.* Molecular Therapy, 2019. **27**(4): p. 710-728.
154. Kauffman, K.J., et al., *Optimization of lipid nanoparticle formulations for mRNA delivery in vivo with fractional factorial and definitive screening designs.* Nano letters, 2015. **15**(11): p. 7300-7306.
155. Żak, M.M. and L. Zangi, *Lipid nanoparticles for organ-specific mRNA therapeutic delivery.* Pharmaceutics, 2021. **13**(10): p. 1675.
156. Kim, J., et al., *Self-assembled mRNA vaccines.* Advanced drug delivery reviews, 2021. **170**: p. 83-112.
157. Evers, M.J., et al., *State-of-the-art design and rapid-mixing production techniques of lipid nanoparticles for nucleic acid delivery.* Small Methods, 2018. **2**(9): p. 1700375.
158. Leung, A.K., et al., *Microfluidic mixing: a general method for encapsulating macromolecules in lipid nanoparticle systems.* The Journal of Physical Chemistry B, 2015. **119**(28): p. 8698-8706.
159. Chen, D., et al., *Rapid discovery of potent siRNA-containing lipid nanoparticles enabled by controlled microfluidic formulation.* Journal of the American Chemical Society, 2012. **134**(16): p. 6948-6951.

160. Shepherd, S.J., et al., *Scalable mRNA and siRNA lipid nanoparticle production using a parallelized microfluidic device.* Nano Letters, 2021. **21**(13): p. 5671-5680.
161. Fan, Y., et al., *Automated high-throughput preparation and characterization of oligonucleotide-loaded lipid nanoparticles.* International Journal of Pharmaceutics, 2021. **599**: p. 120392.
162. Kulkarni, J.A., et al., *Fusion-dependent formation of lipid nanoparticles containing macromolecular payloads.* Nanoscale, 2019. **11**(18): p. 9023-9031.
163. Gindy, M.E., et al., *Mechanism of macromolecular structure evolution in self-assembled lipid nanoparticles for siRNA delivery.* Langmuir, 2014. **30**(16): p. 4613-4622.
164. Roier, S., et al., *mRNA-based VP8* nanoparticle vaccines against rotavirus are highly immunogenic in rodents.* npj Vaccines, 2023. **8**(1): p. 190.
165. Wiegand, M.A., et al., *A respiratory syncytial virus vaccine vectored by a stable chimeric and replication-deficient Sendai virus protects mice without inducing enhanced disease.* Journal of Virology, 2017. **91**(10): p. 10.1128/jvi. 02298-16.
166. Dolgin, E., *The tangled history of mRNA vaccines.* Nature, 2021: p. 318-324.
167. Cheng, F., et al., *Research advances on the stability of mRNA vaccines.* Viruses, 2023. **15**(3): p. 668.
168. Rzymski, P., et al., *mRNA vaccines: The future of prevention of viral infections?* Journal of Medical Virology, 2023. **95**(2): p. e28572.
169. Eygeris, Y., et al., *Deconvoluting lipid nanoparticle structure for messenger RNA delivery.* Nano letters, 2020. **20**(6): p. 4543-4549.
170. Jeong, M., et al., *Lipid nanoparticles (LNPs) for in vivo RNA delivery and their breakthrough technology for future applications.* Advanced drug delivery reviews, 2023: p. 114990.
171. Xu, L., et al., *Lipid nanoparticles for drug delivery.* Advanced NanoBiomed Research, 2022. **2**(2): p. 2100109.
172. Khairnar, S.V., et al., *Review on the scale-up methods for the preparation of solid lipid nanoparticles.* Pharmaceutics, 2022. **14**(9): p. 1886.